NASA CONTRACTOR
REPORT

NASA CR-129007

USE OF 4-D ATMOSPHERIC MODELS IN THE SIMULATION OF RADIOMETRIC MEASUREMENTS

By David T. Chang, and Mary Grace Fowler
Environmental Research and Technology, Inc.
429 Marrett Road
Lexington, Massachusetts 02173

July 1973

Prepared for

NASA-GEORGE C. MARSHALL SPACE FLIGHT CENTER
Marshall Space Flight Center, Alabama 35812

TECHNICAL REPORT STANDARD TITLE PAGE

1. REPORT NO.	2. GOVERNMENT ACCESSION NO.	3. RECIPIENT'S CATALOG NO.
NASA CR-129007		

4. TITLE AND SUBTITLE
USE OF 4-D ATMOSPHERIC MODELS IN THE SIMULATION OF RADIOMETRIC MEASUREMENTS

5. REPORT DATE
July 1973

6. PERFORMING ORGANIZATION CODE

7. AUTHOR(S)
David T. Chang and Mary Grace Fowler

8. PERFORMING ORGANIZATION REPORT #
P-417

9. PERFORMING ORGANIZATION NAME AND ADDRESS
Environmental Research and Technology, Inc.
429 Marrett Road
Lexington, Massachusetts 02173

10. WORK UNIT NO.

11. CONTRACT OR GRANT NO.
NAS 8-28720

12. SPONSORING AGENCY NAME AND ADDRESS
National Aeronautics and Space Administration
Washington, D. C. 20546

13. TYPE OF REPORT & PERIOD COVERED
Contractor Report

14. SPONSORING AGENCY CODE

15. SUPPLEMENTARY NOTES
Technical Coordinator: Dale Johnson, Aerospace Environment Division, Aero-Astrodynamics Laboratory, Marshall Space Flight Center, Alabama 35812

16. ABSTRACT

Atmospheric moisture data contained in the Global 4-D Atmospheric Models developed in previous studies were analyzed to establish regional differences. The regional values of precipitable water along latitudinal belts were compared with values derived from the corresponding atmospheric models defined in the U. S. Standard Atmosphere Supplement. The effects of the differences between the 4-D Models and the Standard Atmosphere Models on radiometric computations in the infrared window and water vapor absorption band regions were evaluated using a standard computation model of radiation transfer through a cloudless atmosphere. The significance of these differences in simulation is discussed.

17. KEY WORDS
4-D Atmospheric Model
Global Precipitable Water
Radiative Transfer
Atmospheric Absorption of Infrared Radiation

18. DISTRIBUTION STATEMENT
Unclassified - unlimited

E. D. Geissler
Director, Aero-Astrodynamics Laboratory

19. SECURITY CLASSIF. (of this report)	20. SECURITY CLASSIF. (of this page)	21. NO. OF PAGES	22. PRICE
Unclassified	Unclassified	114	NTIS

FOREWORD

The objective of the four-dimensional atmospheric modeling task is to provide world-wide profiles of pressure, temperature, density, and moisture from the surface to 25 km altitude. The model gives mean monthly values and daily variations of the four parameters for any input of latitude, longitude, and month. This model can then serve as input for attenuation models that predict the degree of atmospheric attenuation likely to be encountered by satellite or air-borne electromagnetic sensors engaged in earth resources observations. It can also be used as mean model atmospheres in trajectory and vehicle heating analyses.

This report gives a comparison study between the 4-D model versus standard model atmospheres. Also radiometric computations using these two models are given and discussed.

The 4-D computer program can be obtained, upon request, from the Aerospace Environment Division, NASA, Marshall Space Flight Center, Alabama 35812.

Associated work has been and is still being done in this field. For example, work reported on, thus far, includes the world-wide cloud cover model (NASA CR-61226, NASA CR-61345, and NASA CR-61389, and the interaction model involving microwave energy and atmospheric variables (NASA CR-61348). The four-dimensional atmospheric model is being improved to ultimately present pressure, temperature, density, moisture, and cloud cover as one attenuation model for earth resources problem.

TABLE OF CONTENTS

LIST OF ILLUSTRATIONS

LIST OF ILLUSTRATIONS (Cont'd)

LIST OF ILLUSTRATIONS (Cont'd)

LIST OF TABLES

1. INTRODUCTION

The Aerospace Environment Division (Aero-Astrodynamics Laboratory) of the Marshall Space Flight Center has sponsored the development of a global atmospheric model, known as the MSFC 4-D Atmospheric Model. This Model consists of 45 "homogeneous" moisture regions; for each region, pressure, temperature, density, and water vapor are given at kilometer levels up to 25 km. Previous studies (Spiegler and Greaves, 1971; Spiegler and Fowler, 1972) have processed the necessary global data and refined the atmospheric statistics; this study has attempted to analyze the meteorological and radiometric differences indicated by the region values.

Regions in the 4-D atmospheric model were defined on the basis of atmospheric moisture; each region is homogeneous with respect to its moisture mean and seasonal variability. As water vapor amounts are dependent on atmospheric temperature and reflect general climatic patterns, these moisture regions are also presumed relatively homogeneous with respect to the temperature, pressure and density. The atmospheric statistics given for these regions consist of monthly means and variances for each meteorological parameter; these values are derived from similar statistics given for 3470 points spanning the globe. The grid point values form a more detailed version of the 4-D atmospheric model; a brief description of these models, and of the data used to derive them, is given in Table 1-1. The U.S. Standard Atmosphere Supplement, 1966, defines representative atmospheric profiles on the basis of "latitudinal homogeneity"; the first part of this study was devoted to a comparison of these two atmospheric models, and to an analysis of the meteorological aspects of this "latitudinal homogeneity."

The second part of this study investigated the differences in the two atmospheric models in their simulation of remote sensing measurements. The increased use of remote sensing data by individuals not skilled in the interpretation of atmospheric effects necessitates tables which provide easily accessible correction values. To date, such tables have been based on the Standard Atmospheres; in this study, the value of tables computed from more detailed atmospheric data was investigated. This analysis paralleled the study of atmospheric latitudinal homogeneity, and was summarized by two simulated orbital paths.

To perform the above studies, certain minor investigations were necessary. First, conversion was needed from the 4-D atmospheric model's moisture parameter of absolute humidity, to the more common parameters of mixing ratio and dew point. Appendix A summarizes the technique used. Second, no new radiometric model was developed for this study; rather, the programs developed by Dr. David Anding were adapted to analyze the Standard Atmosphere and the 4-D atmospheric model. Appendix B reviews these modifications. The third appendix, Appendix C, presents an evaluation of the effects of clouds on the moisture statistics to permit an estimation of the applicability of these models to clear day situations.

TABLE 1-1

SUMMARY OF THE 4-D ATMOSPHERIC MODELS

INPUT DATA TO 4-D MODELS

Parameters	Form	Levels	Grid	Number of Points
Height Temperature Dew Point	Daily Values (Eight Years)	1000 - 300mb 1000 - 300mb 850 - 500mb	The National Meteorological Center (NMC) Grid	1977
Height Temperature	Daily Values (Seven Years)	100 - 10mb 100 - 10mb	NMC Grid	1977
Height Temperature Dew Point	Monthly Means & Variances	Surface - 100mb Surface - 100mb Surface - 500mb	5° Latitude - Longitude Grid Northern Hemisphere	1368
Height Temperature Dew Point	Monthly Means & Variances	Surface - 100mb Surface - 100mb Surface - 500mb	5° Latitude - Longitude Grid Southern Hemisphere	1368
Height Temperature Dew Point	Daily Variances	850 - 100mb 850 - 100mb 850 - 500mb	5° Latitude - Longitude Grid 0° - 15° North	288

FINAL 4-D MODELS

MODEL A: Global Grid Point Data				
Parameters	Form	Levels	Grid	Number of Points
Pressure Temperature Absolute Humidity Density	Means & Daily Variances for Each Month	Surface - 25 km	NMC Grid	1977
Pressure Temperature Absolute Humidity Density	Means & Daily Variances for Each Month	Surface - 25 km	5° Latitude - Longitude 5° - 90° South	288
MODEL B: Global Moisture Regions				
Pressure Temperature Absolute Humidity Density	Region Means & Daily Variances for Each Month	Surface - 25 km	"Homogeneous" Moisture Regions Entire Globe	45

2. REGIONAL DIFFERENCE IN THE 4-D MODELS

Previous studies have established the homogeneity within each region of the 4-D atmospheric model. This section will investigate the homogeneity within each latitudinal belt of the U. S. Standard Atmosphere Model. The analysis will be based primarily upon regional differences in precipitable water amounts, but will also investigate differences in the vertical structure of temperature and dew point.

2.1 Region Definition

It is customary to describe the atmosphere over a given location by its latitude. Thus Washington, D.C. has a mid-latitude atmosphere, Trinidad a tropical one, and Thule, Greenland is considered subarctic. These descriptions assume that each latitudinal belt is homogeneous with respect to temperature, moisture and pressure, and that a knowledge of the atmospheric parameters for any point on a given latitude implies a knowledge of conditions for all points on that latitude. As this homogeneity is approximately true, the Handbook of Geophysics provides atmospheric profiles representative of given latitudes and seasons. These will be referred to below as the standard atmospheres.

In reality, latitudinal homogeneity is affected by the underlying surface. This surface is not homogeneous since oceans and continents are irregularly spaced and the topography of the continents varies markedly. Furthermore, the vast currents of the atmosphere and the oceans are not entirely zonal in character. To permit a study of the effects of these factors on atmospheric moisture, homogeneous water vapor regions (Table 2-1 and Figure 2-1) were defined based on the total amount of precipitable water (Figures 2-2 and 2-3) and its seasonal variability (Spiegler and Greaves, 1971).

As the table and figures show, there are 45 regions in all, in contrast to the five given by the U.S. Standard Atmosphere Supplement, 1966. Some of these regions are zonal, such as the maritime ones, but others are meridional (reflecting major mountain ranges), and others are applicable only to small areas of the globe such as the Sahara or the Australian Desert. Each region differs from all other regions, either in its mean value of

TABLE 2-1

HOMOGENEOUS MOISTURE REGIONS

Region Number	Annual Average Moisture	Seasonal Changes	Variability Across Region	Location	Remarks
1	Extremely low	Small	Small	Arctic	
2	Very low	Small to moderate	Small, except moderate in summer	Subarctic and Arctic - continent	
3	Low	Small	Small, except moderate in summer	Subarctic ocean	Very low moisture late fall to early spring
4	Low	Moderate to large	Small, except large in summer	Polar - continent	Moderate moisture summer
5	Low	Moderate to large	Small, except moderate in summer	Subpolar	Very low moisture winter
6	Low	Small	Small, except large in summer	Polar ocean	
7	Low to moderate	Moderate	Small fall, winter and early spring, large in summer	High mid-latitude - continent	Summer maximum higher, and winter minimum lower than Regions 8, 9 and 10
8	Low to moderate	Small to moderate	Small to moderate	High mid-latitude - ocean	
9	Low to moderate	Small to moderate	Small, except moderate summer	High mid-latitude - ocean	Winter maximum lower than Region 8
10	Low to moderate	Small	Small	High mid-latitude - ocean	Moisture higher than Regions 8 & 9
11	Moderate	Small to moderate	Moderate, except large in summer	Mid-latitude - ocean	
12	Moderate	Small to moderate	Small to moderate	Eastern low mid-latitude oceans	Higher winter moisture than Region 11
13	Moderate	Large	Moderate, except small in winter and large early fall	Mid-latitude continent	
14	Moderate	Large	Moderate, except large in fall	Lower mid-latitude continent	Somewhat higher average than Regions 11-13.
15	Moderate	Moderate to large	Moderate, except large in fall	Lower mid-latitude oceans	Very high summer and early fall moisture; winter moisture higher than Region 14 (lowest 2 km)
16	Moderate	Small to moderate	Moderate	Subtropical eastern portion of oceans	
17	Moderate to high	Moderate	Moderate to large	Subtropics including western 2/3 of oceans	
18	Moderate to high	Small	Small, except small to moderate in summer and fall	Eastern subtropical and tropical oceans	Winter moisture higher than Region 17
19	High	Small to moderate	Moderate, except large in spring and fall	Subtropical-tropical border	
20	High	Small	Small, except moderate in summer and fall	Tropical eastern portion of oceans	
21	Very high	Small to moderate	Moderate, except large in spring	Tropical	
22	Very high	Small	Moderate	Tropical oceans except near Eq. in E. oceans	
23	Moderate	Moderate	Moderate, except small in spring	Tropical interior continent region	
24	Extremely high	Very small	Small	Equatorial oceans for parts of globe	
25	Moderate to high	Small to moderate	Small, except moderate in winter and spring	Equatorial continent	Lower winter moisture than Region 24
26	Low	Small to moderate	Small to moderate	Major mountain ranges average elev. > 2-4 km	
27	Very low	Small	Small to moderate	Major mountain ranges average elev. > 4-7 km	
28	Low	Small	Small	Border of mountains mid and high latitudes	
29	Low to moderate	Moderate to large	Moderate, except large in summer	Border of mountains subtropics and tropics	
30	Low	Small	Small, except moderate in summer	Deserts	
31	Low	Small to moderate	Small	Border of desert	
32	Low to moderate	Moderate	Small to moderate	Border of desert	
33	Low to moderate	Moderate	Moderate, except large in fall	Border of desert (tropical and equatorial)	Average moisture similar to Region 29
34	Moderate	Very large	Very large, except small in summer	Mid-latitude - E. coast Asia	
35	Moderate to high	Small to moderate	Moderate to large, except small in fall	Tropics - near continents	Similar to Region 19, except lower moisture in spring
36	Moderate to high	Large	Moderate, except small in summer	India and Indian Ocean	Extremely high late spring and summer moisture

TABLE 2-1 Continued

Region	Average Annual Moisture	Seasonal Change	Variability Across Region	Location	Remarks
37(1)	Very low	Very small	Small	Antarctic continent	Higher annual average moisture than arctic N. H. (Region 1) except lower in summer.
38(2)	Very low	Very small	Small	Northern Antarctic Ocean	Higher annual average moisture than subarctic and arctic continent N. H. (Region 2) winter and spring; lower in summer.
39(6)	Low	Very small	Small	S. H. polar ocean	Higher annual average moisture than N. H. polar oceans (Region 6) except in summer.
40(7)	Low-to-moderate	Very small	Very small	Southern one-third South America	Lower annual average moisture than high midlatitude continent (Region 7), except in winter.
41(15)	Moderate	Small-to-moderate	Small	S. H. lower midlatitude oceans.	
42(26)	Low-to-moderate	Small-to-moderate	Small-to-moderate	S. H. mountain ranges.	
43(30)	Low	Very small	Small	Australian Desert	Moisture lower than average of N. H. deserts (Region 30) in summer.
44(31)	Low	Small	Small	Border of Australian Desert.	Temperature much lower than N. H. border of desert (Region 31).
45(33)	Low-to-moderate	Moderate	Moderate except large in fall.	Tropical border of Australian Desert.	Lower moisture than N. H. tropical and equatorial desert borders (Region 33).

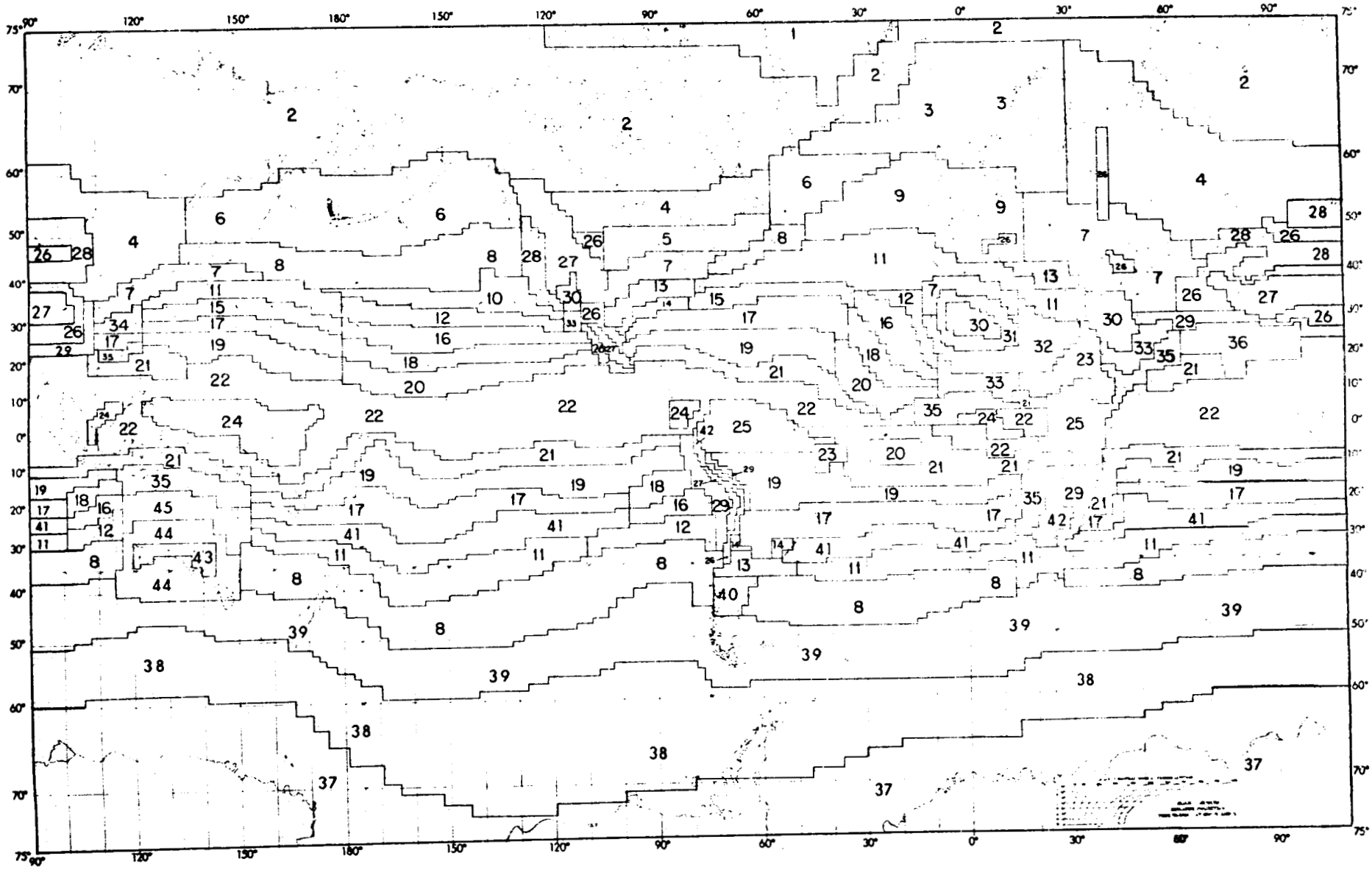

Figure 2-1 Homogeneous Moisture Regions

moisture or in its variability. While such detailed differences are reflections of actual climatic differences, it is not immediately clear that such precise region definitions are required for the intended application. There is, therefore, a need to investigate the degree of variability in the moisture data for all regions falling within the latitudinal belt of one of the standard atmospheres. Such a study was performed using the January and July data from the 4-D models; the following paragraphs present the results.

2.2 Comparative Analysis of Moisture Data

For this analysis, the nine atmospheres applicable to 15°N, 30°N, 45°N, 60°N, and 75°N were selected for January and July* from the Handbook of Geophysics. The 15°N atmosphere is assumed applicable to the latitudes from 0°-22.5°, the 30°N, to 22.5°-37.5°, the 45°N, to 37.5°-50.25°, the 60°N, to 50.25°-60.75°, and the 75°N from 60.75° to the pole. These latitudinal belts are considered appropriate for both hemispheres although the seasonal reversal between hemispheres necessitates the use of January data for the Southern Hemisphere in July, and the use of July data for January. These atmospheres are shown in Figures 2-4 to 2-13 as temperature-dew point profiles; with them are presented similar profiles of the region parameters to allow a comparison of the data at various latitudes. Total precipitable water was also computed for the standard atmospheres, and for all regions, and the resulting values were plotted for each latitudinal belt as shown in Figures 2-14 to 2-23.

2.3 Discussion

2.3.1 Latitudinal Belt from 60.75° to the Pole

Examination of the standard atmospheres and regions applicable to latitudes greater than 60.75° (Figures 2-4, 2-5, 2-14, 2-15) makes several facts immediately clear. The most obvious is the marked difference between the two hemispheres. The Antarctic winter is so much more moist than the Arctic winter, and the Antarctic summer so much drier, that the standard atmospheres for 75°N (or any other atmospheres applicable to the Northern Hemisphere) are not representative for either Region 37 or 38.

*Only an annual profile is given for 15°N because of the limited seasonal variability.

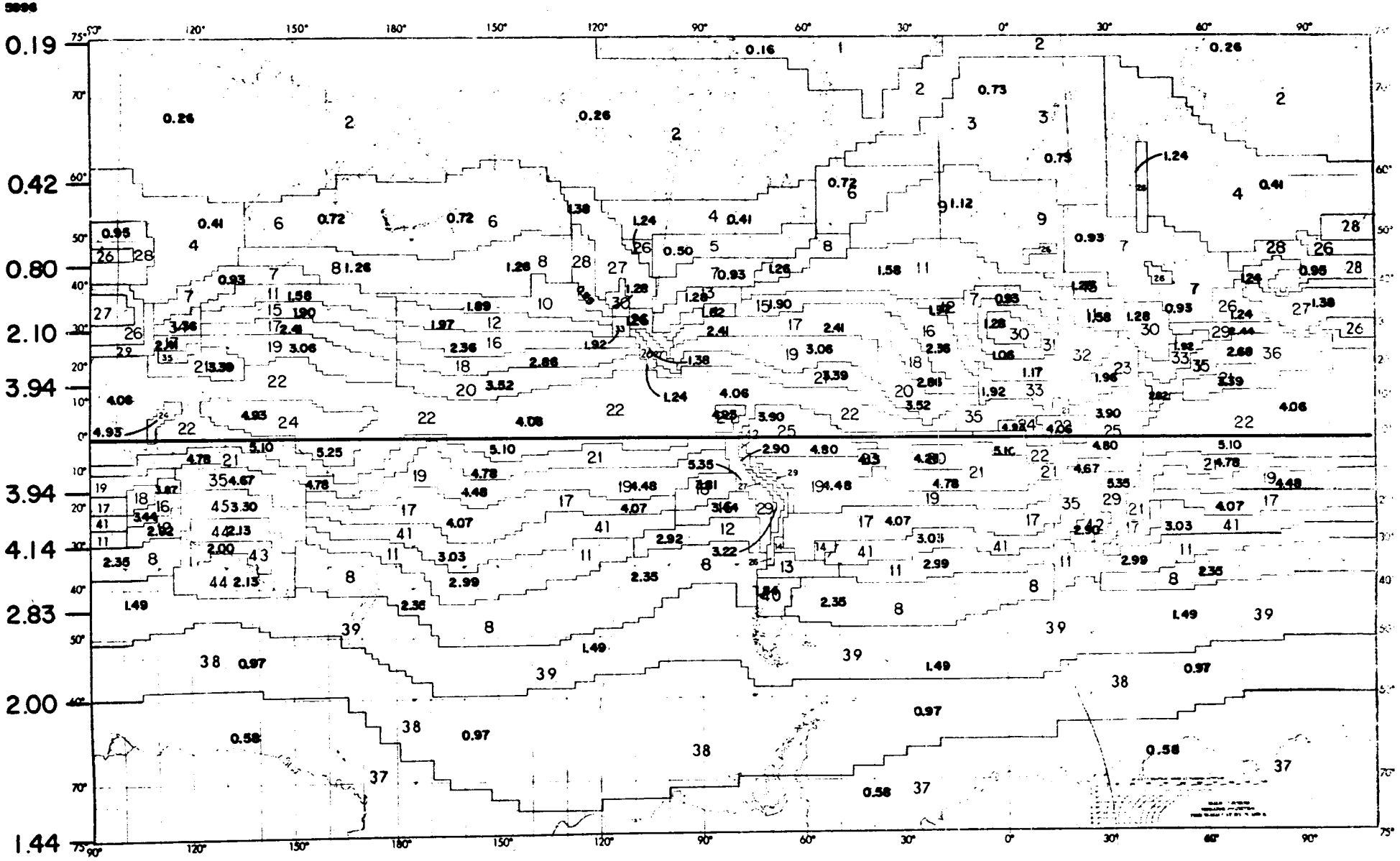

Figure 2-2 Global Precipitable Water (g cm^{-2}) January

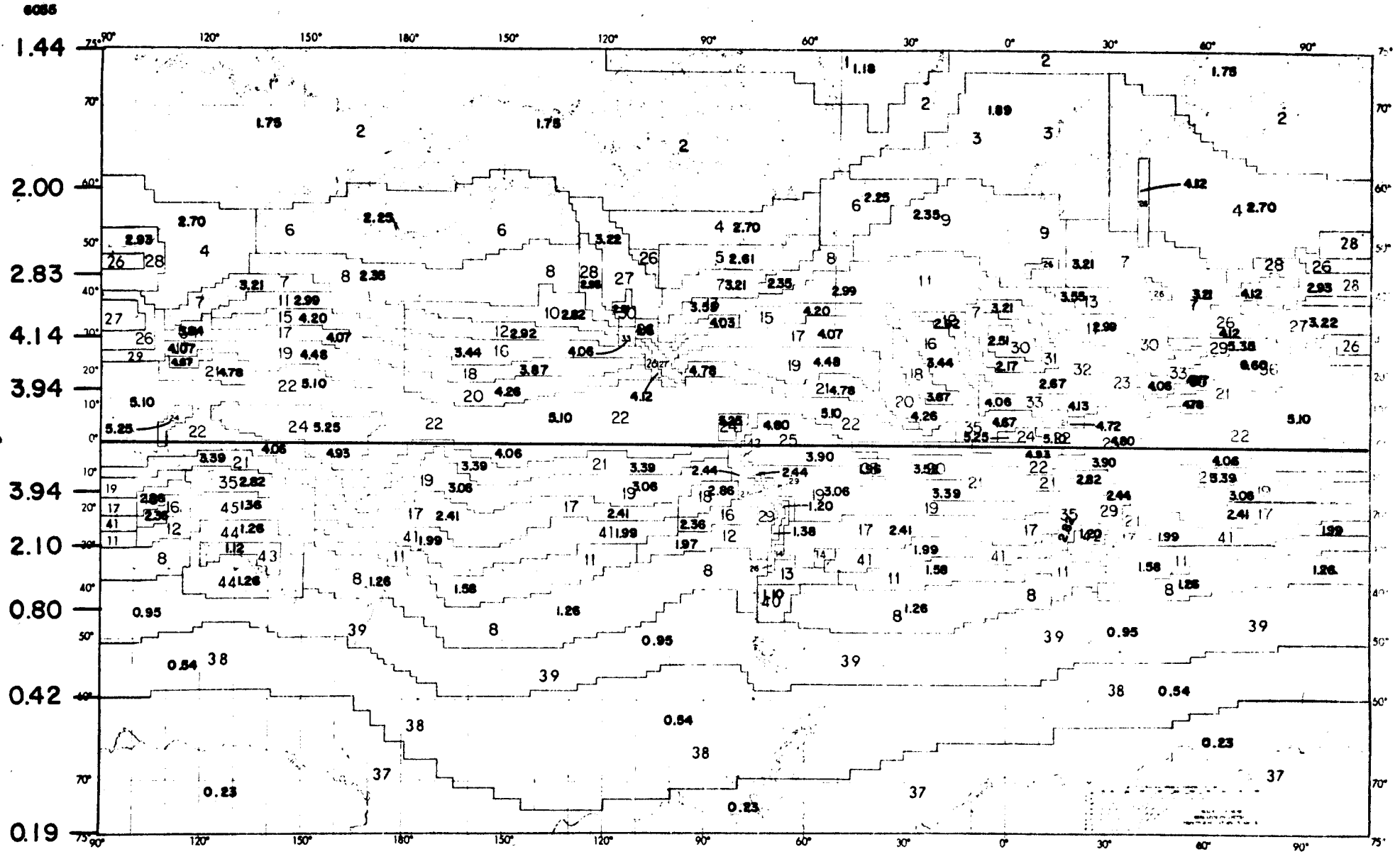

Figure 2-3 Global Precipitable Water (g cm^{-2}) July

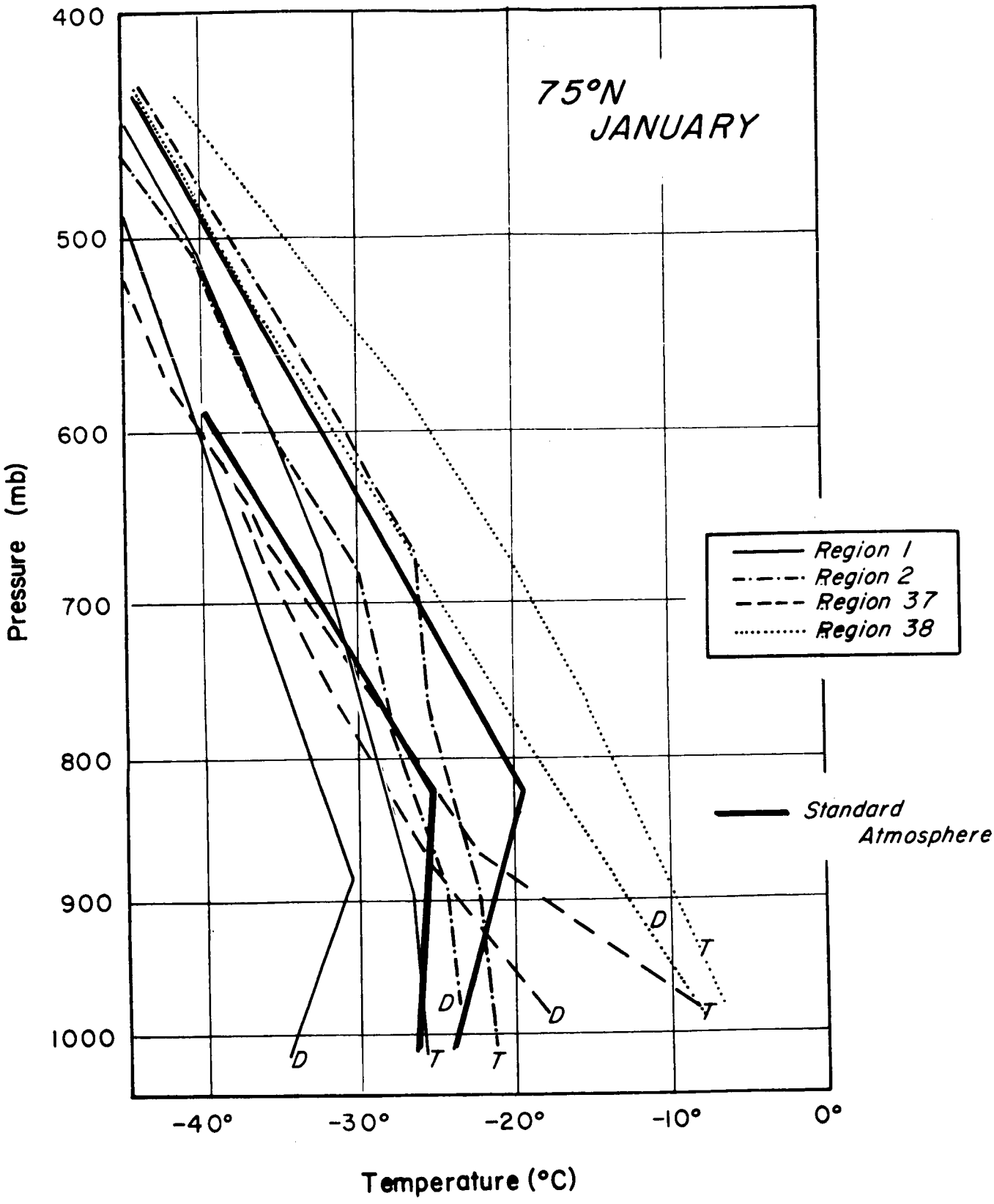

Figure 2-4 Temperature and Dew Point Profiles 60.75° - 90°N January, 60.75°- 90°S July

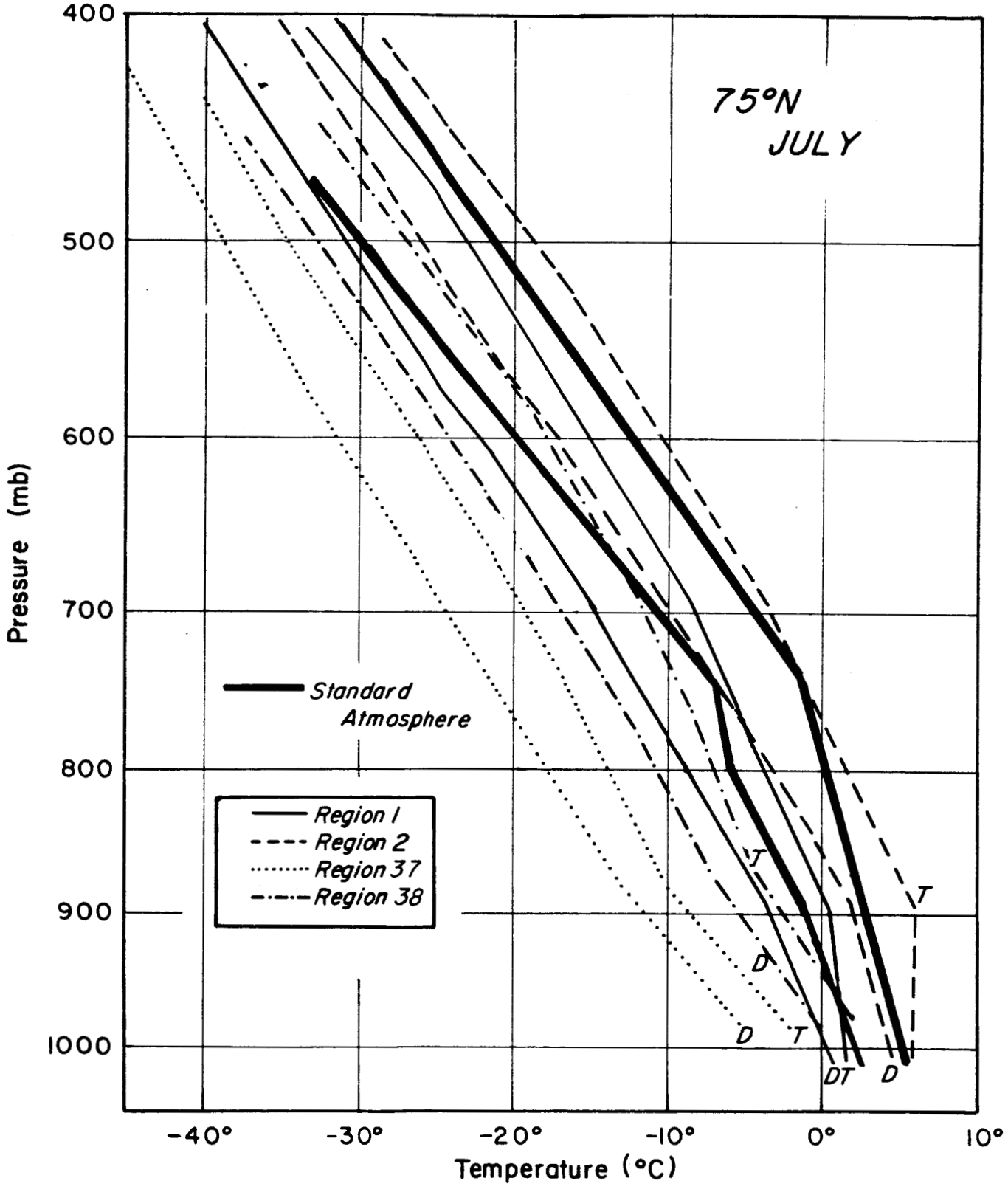

Figure 2-5 Temperature and Dew Point Profiles 60.75° -90°N July, 60.75° -90°S January

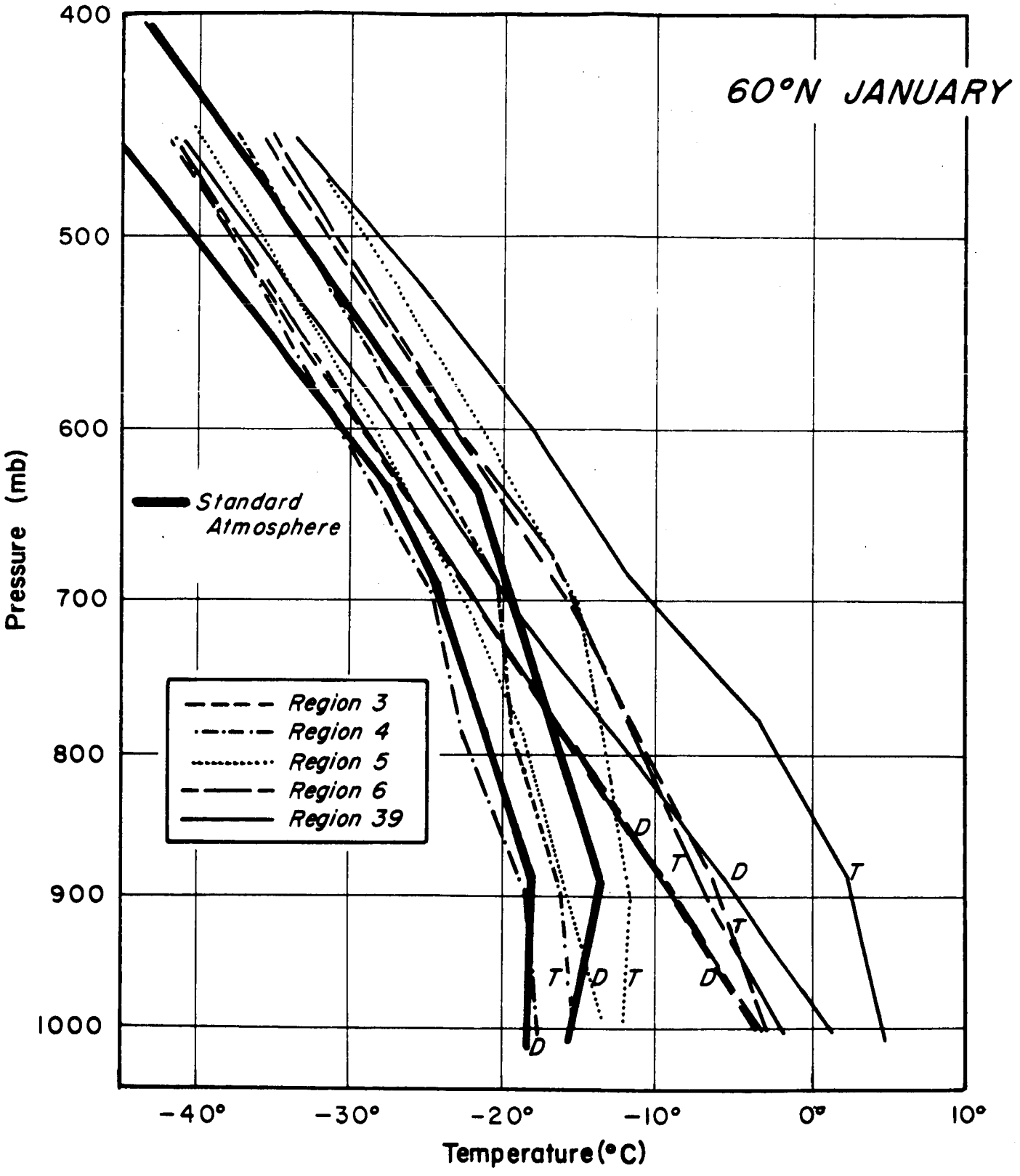

6074

Figure 2-6 Temperature and Dew Point Profiles 50.25° - 60.75°N January, 50.25° - 60.75°S July

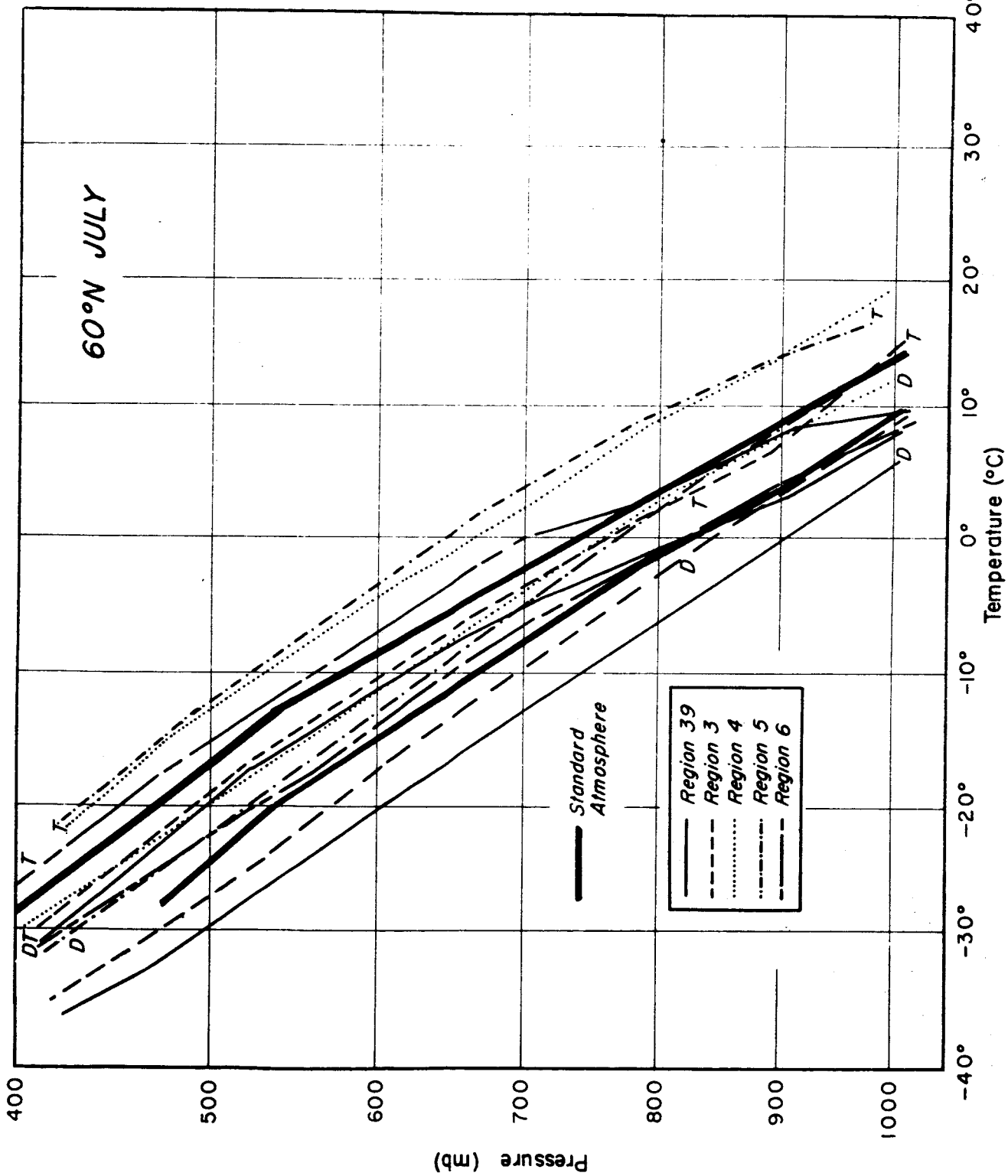

Figure 2-7 Temperature and Dew Point Profiles 50.25° -60.75°N July, 50.25° -60.75°S January

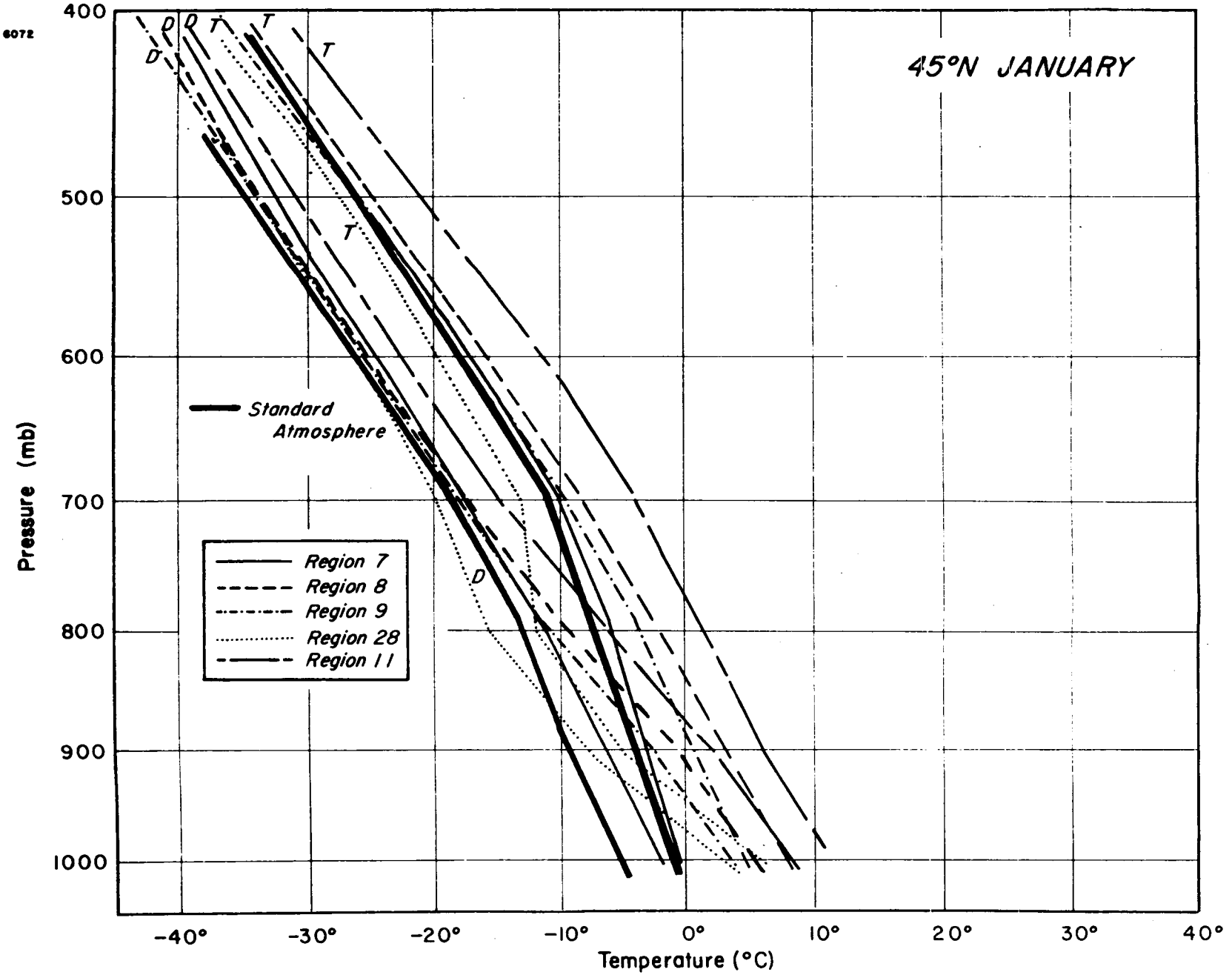

Figure 2-8 Temperature and Dew Point Profiles 37.5° -50.25°N January, 37.5° -50.25°S July

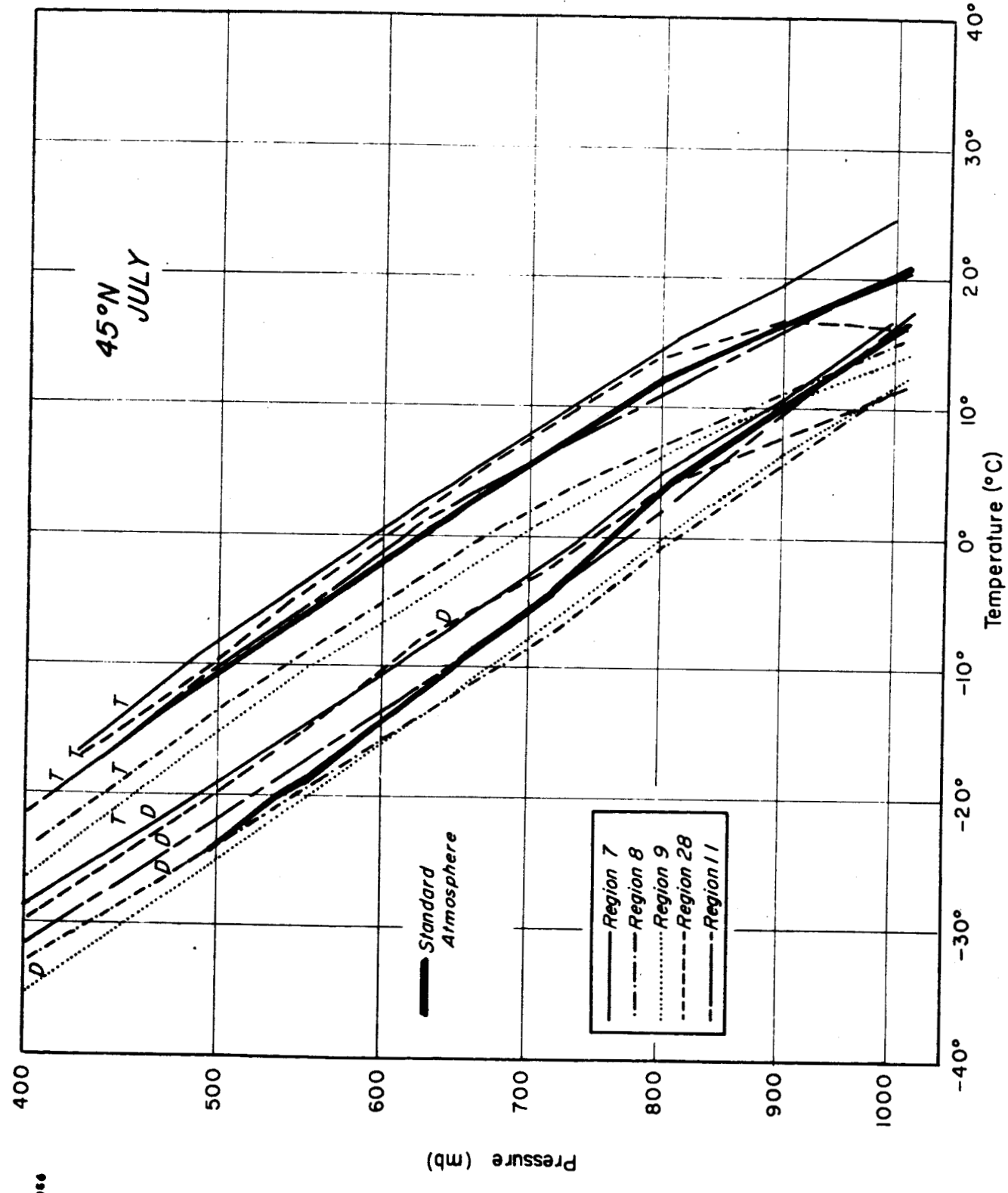

Figure 2-9 Temperature and Dew Point Profiles 37.5^{o} -50.25^{o}N July, 37.5^{o} -50.25^{o}S January

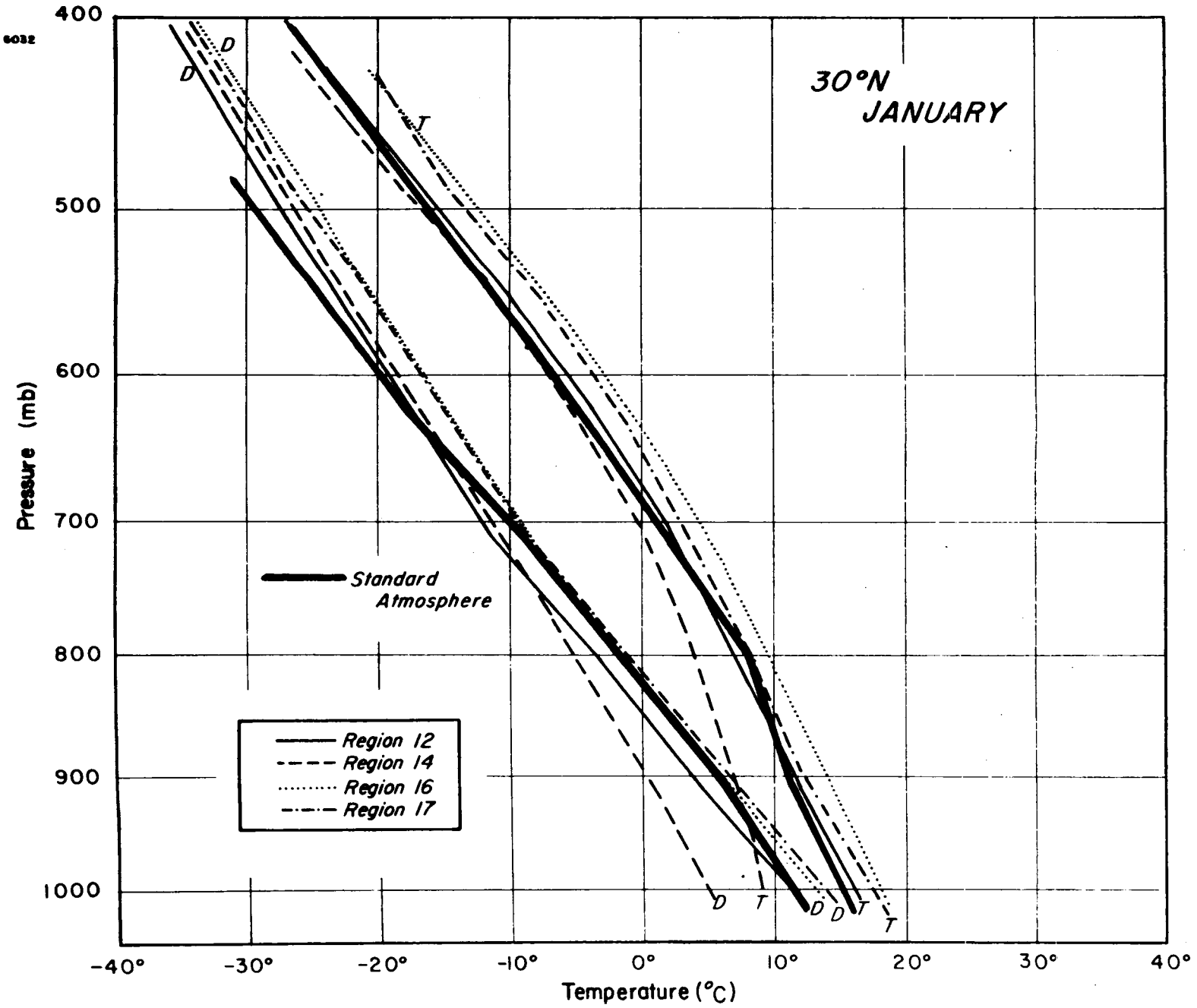

Figure 2-10(a) Temperature and Dew Point Profiles 22.5° -37.5°N January, 22.5° -37.5°S July

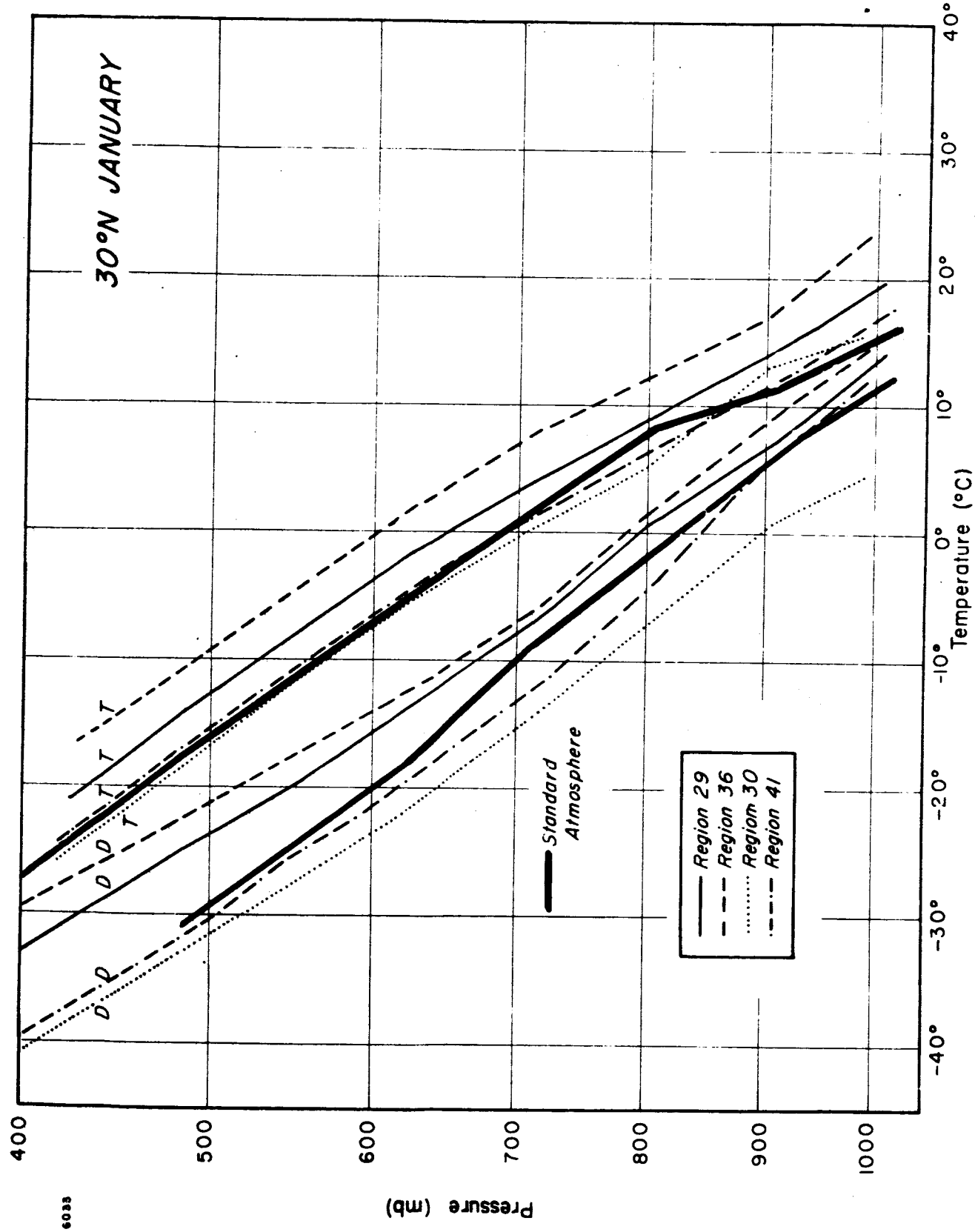
30°N JANUARY
Standard Atmosphere
Region 29
Region 36
Region 30
Region 41
T
T
T
D
D
D
Pressure (mb)
400
500
600
700
800
900
1000
Temperature (°C)
40°
30°
20°
10°
0°
-10°
-20°
-30°
-40°
6033

Figure 2-10(b)

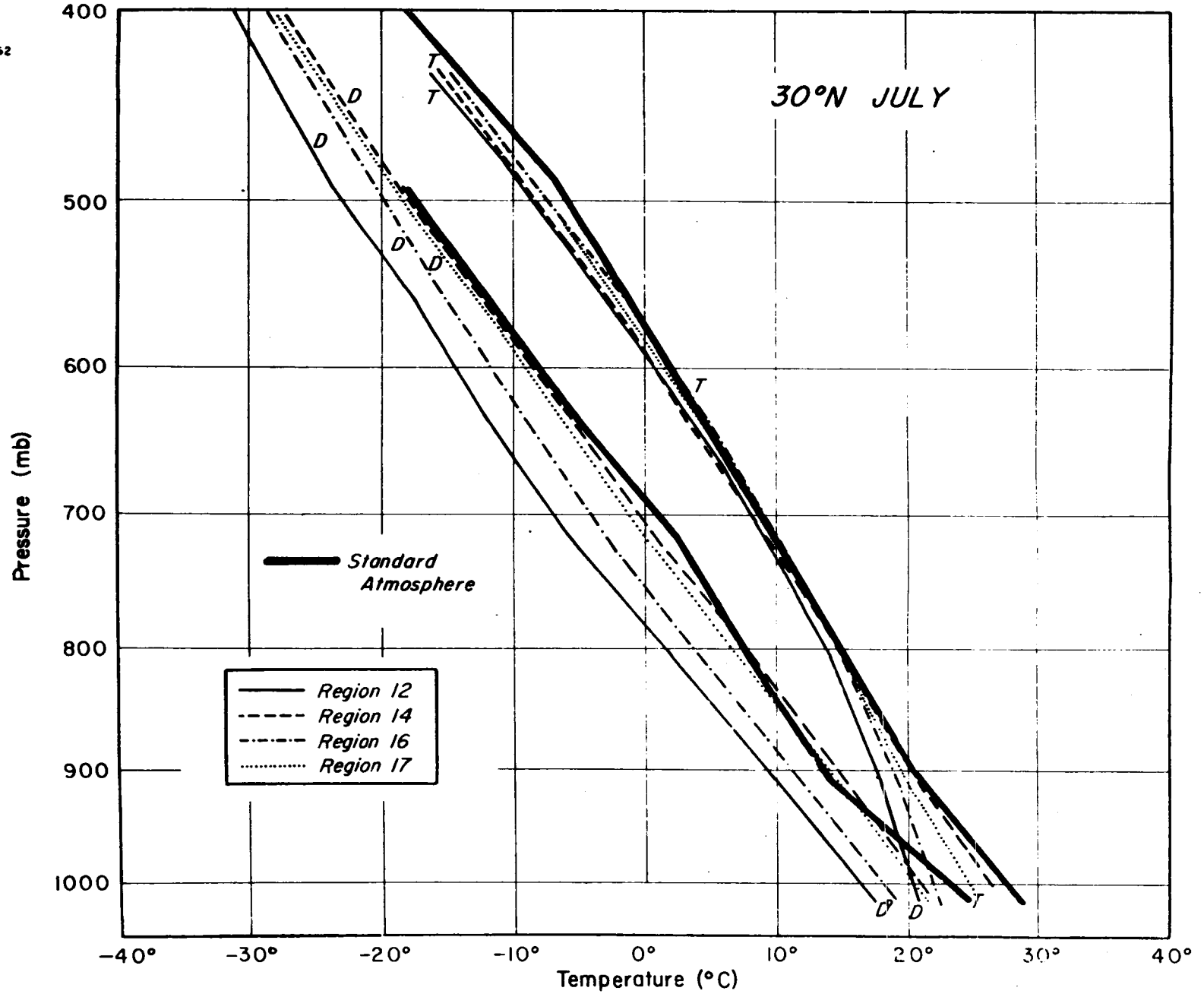

Figure 2-11(a) Temperature and Dew Point Profiles 22.5° -37.5°N July, 22.5° -37.5°S January

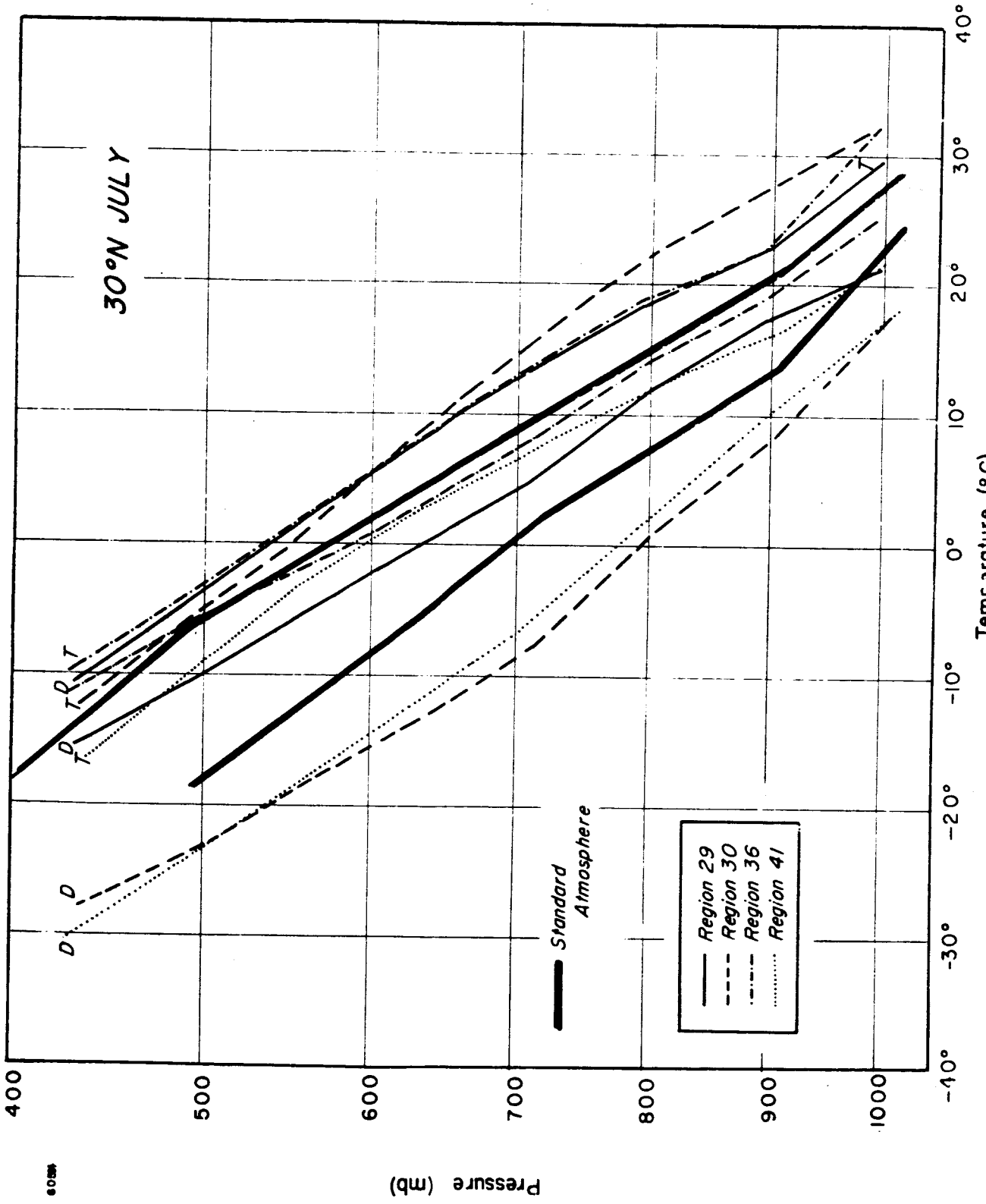
30°N JULY
Region 29
Region 30
Region 36
Region 41
Standard Atmosphere
Pressure (mb)
Temperature (°C)
400
500
600
700
800
900
1000
-40°
-30°
-20°
-10°
0°
10°
20°
30°
40°

Figure 2-11(b)

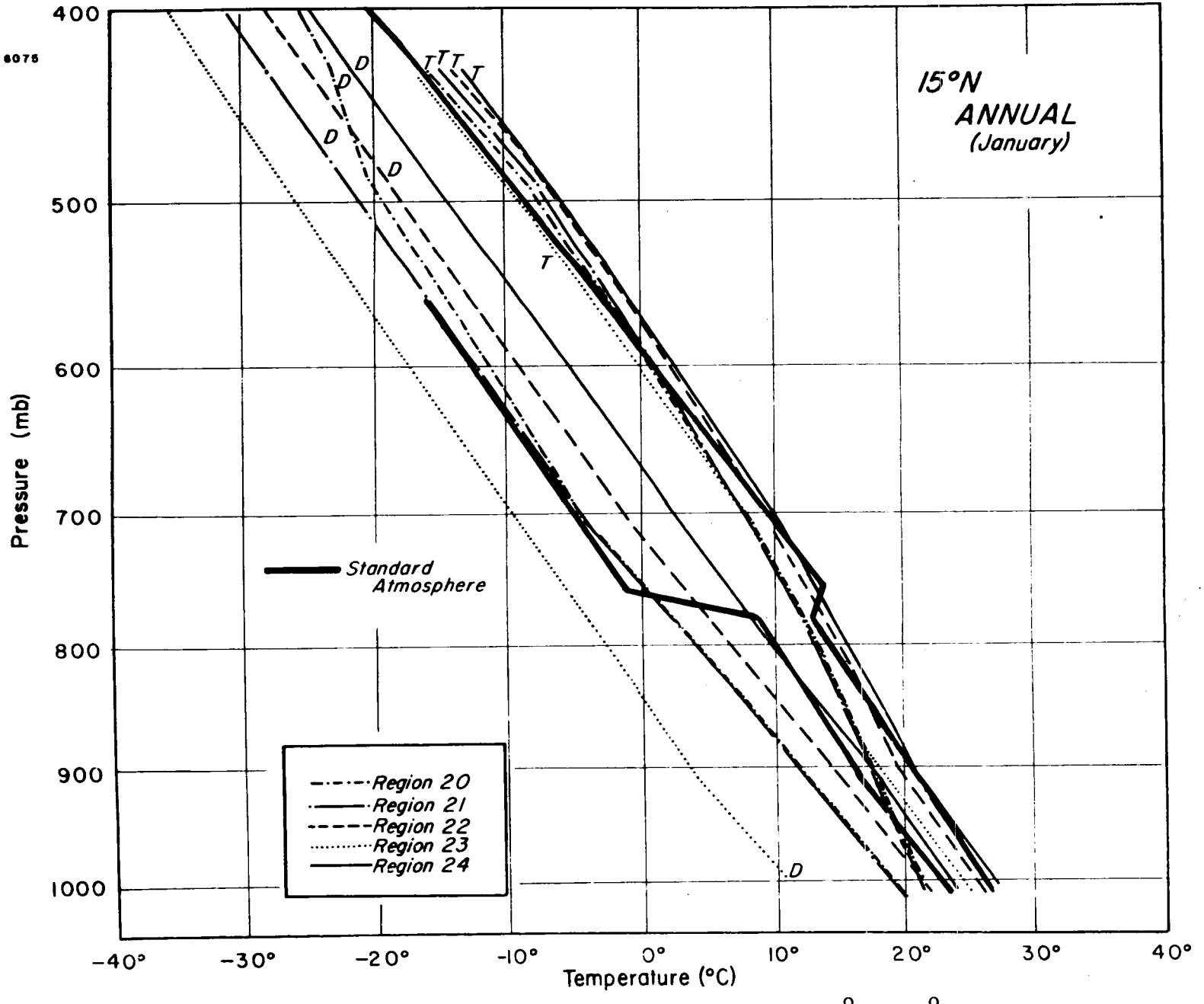

Figure 2-12 Temperature and Dew Point Profiles 0^{o} -22.5^{o}N January, 0^{o} -22.5^{o}S July

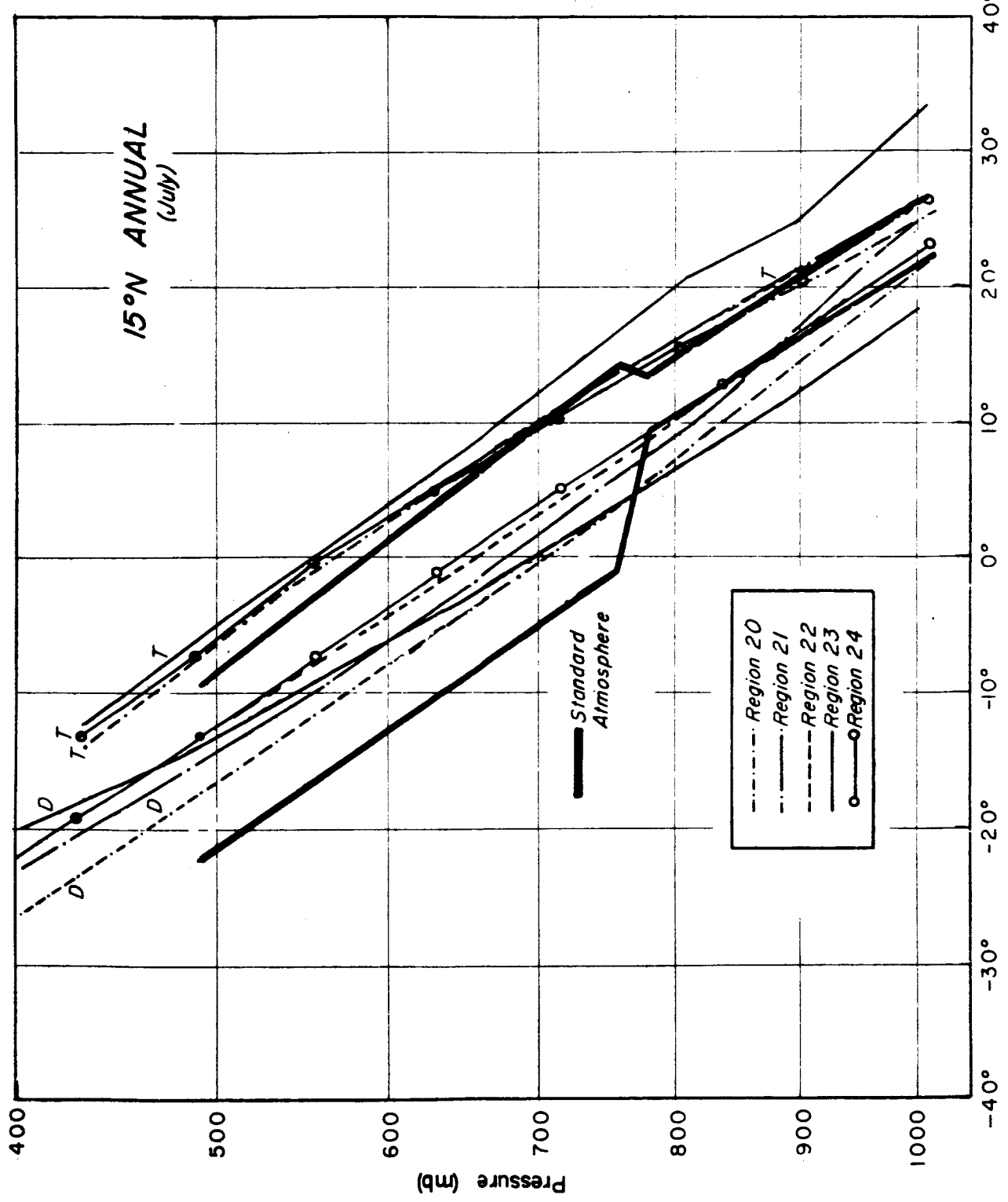

Figure 2-13 Temperature and Dew Point Profiles 0^{o} -22.5^{o}N July, 0^{o} -22.5^{o}S January

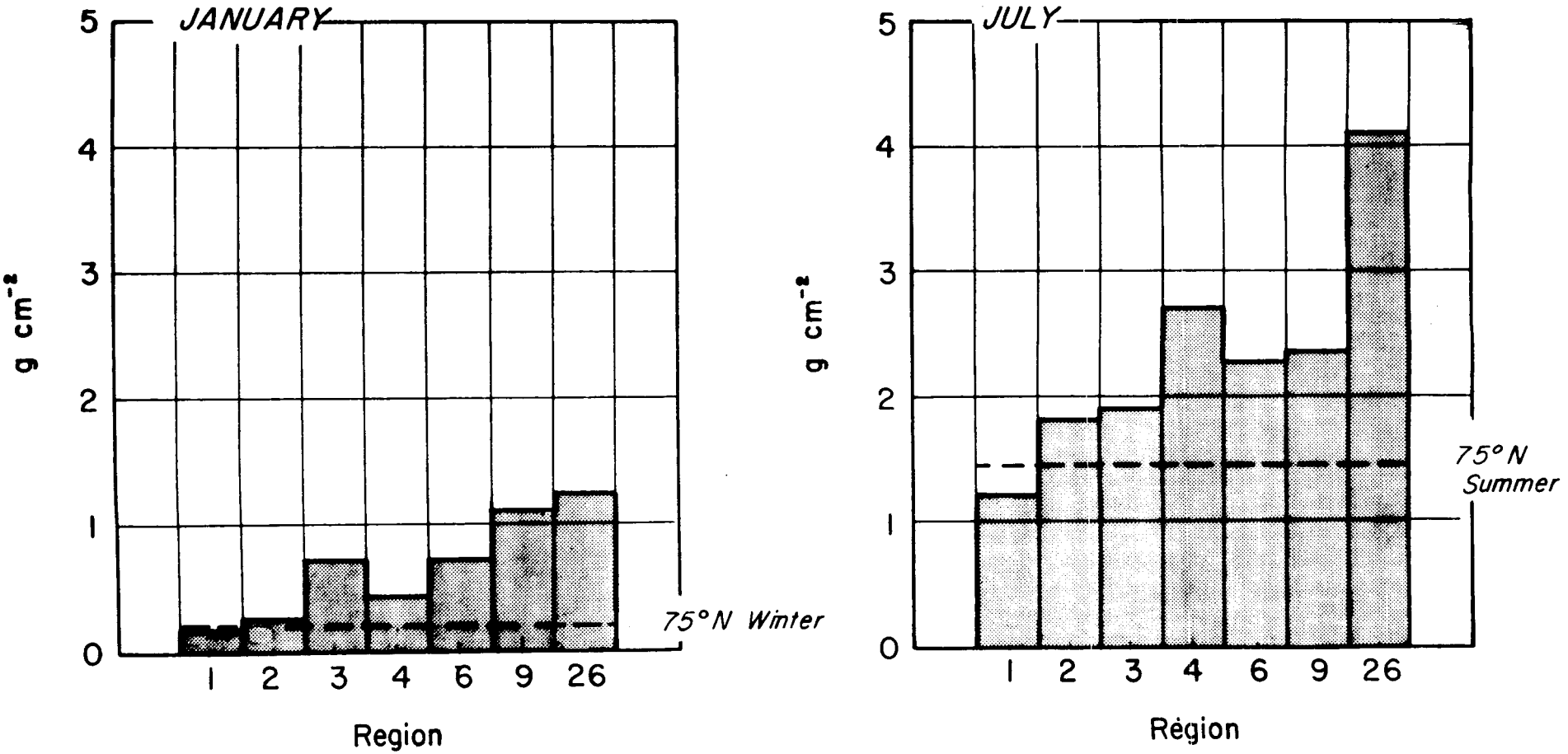

Figure 2-14 Precipitable Water 60.75° -90°N

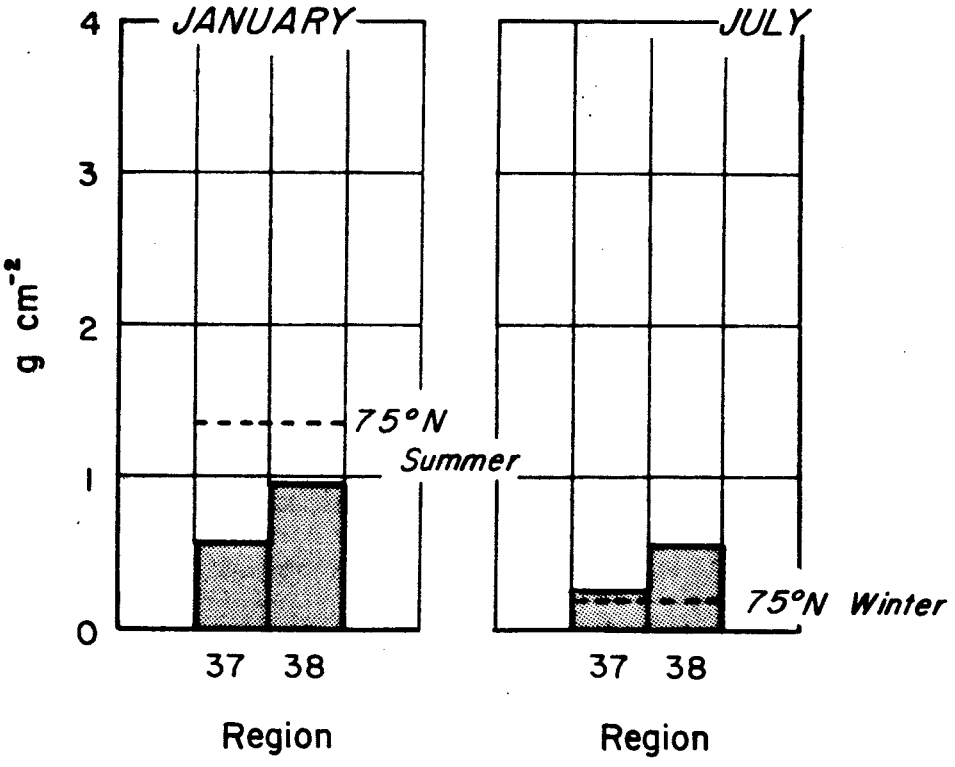

Figure 2-15 Precipitable Water 60.75° -90°S

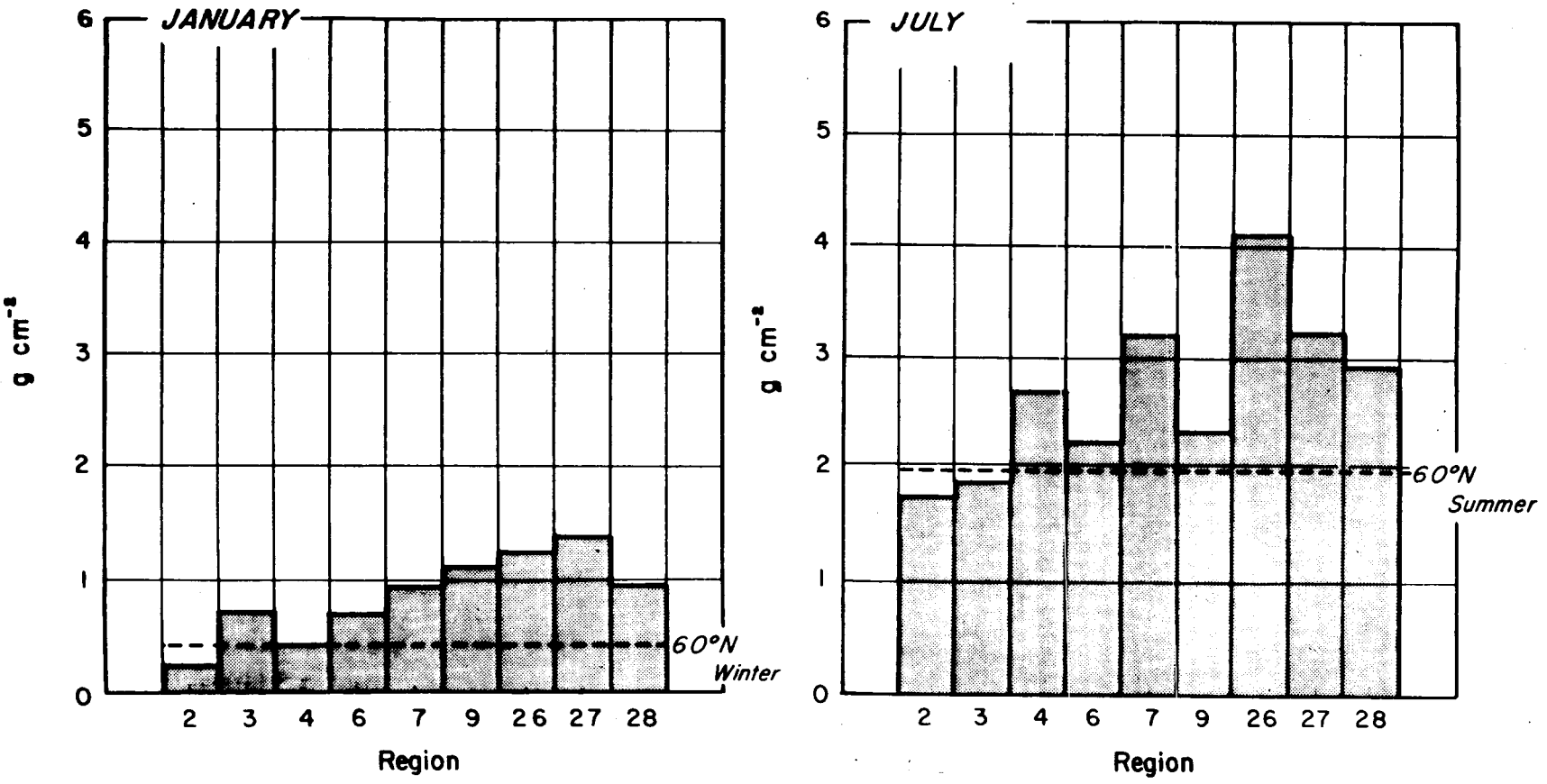

Figure 2-16 Precipitable Water 50.25° -60.75°N

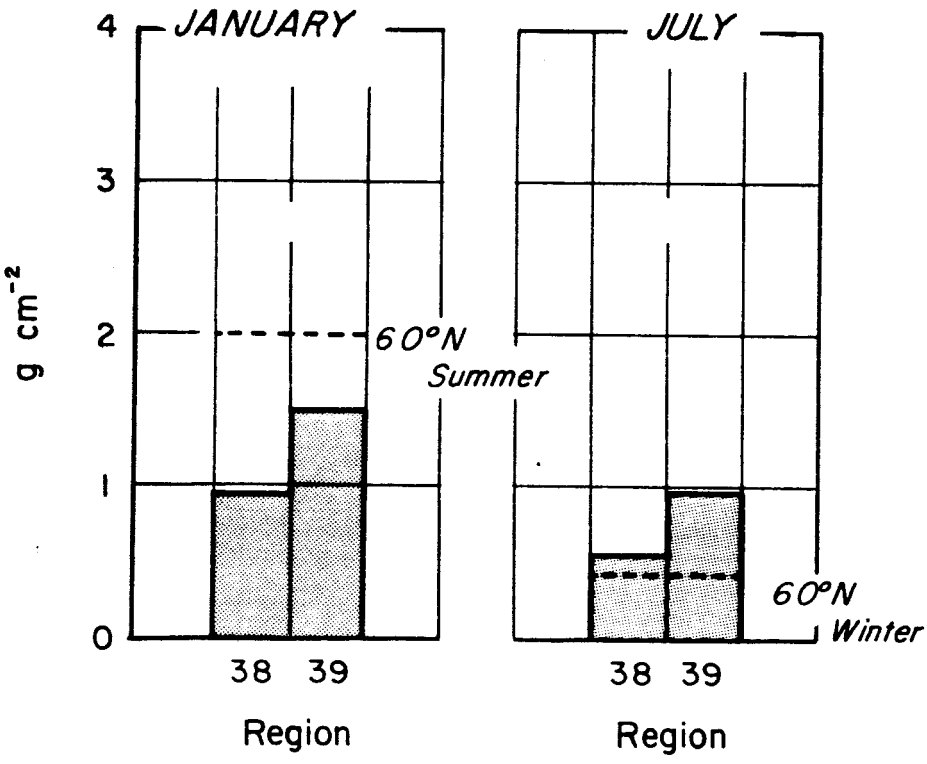

Figure 2-17 Precipitable Water 50.25° -60.75°S

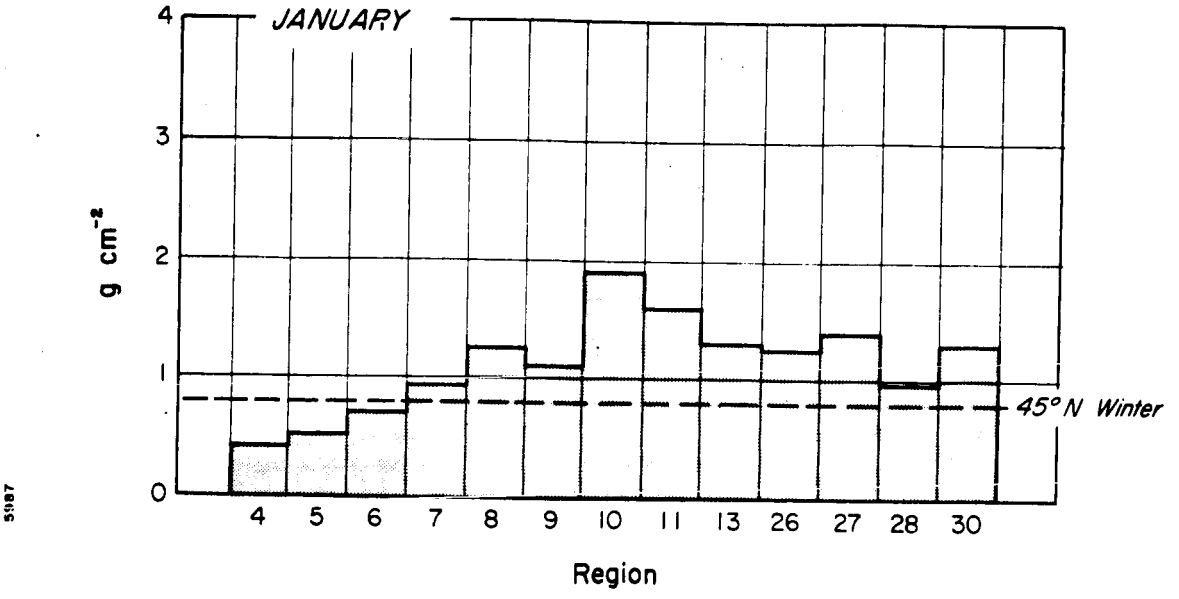

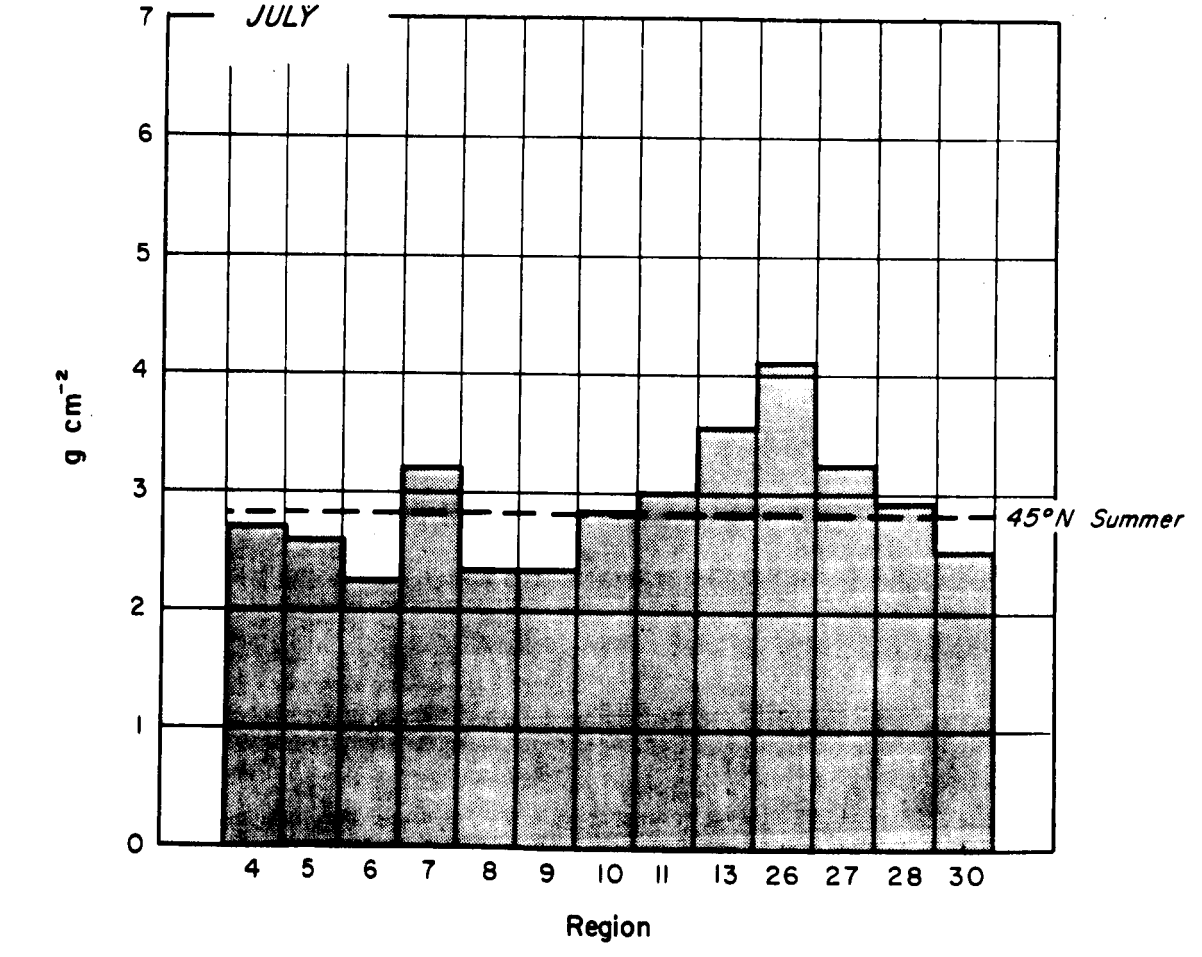

Figure 2-18 Precipitable Water 37.5° -50.25°N

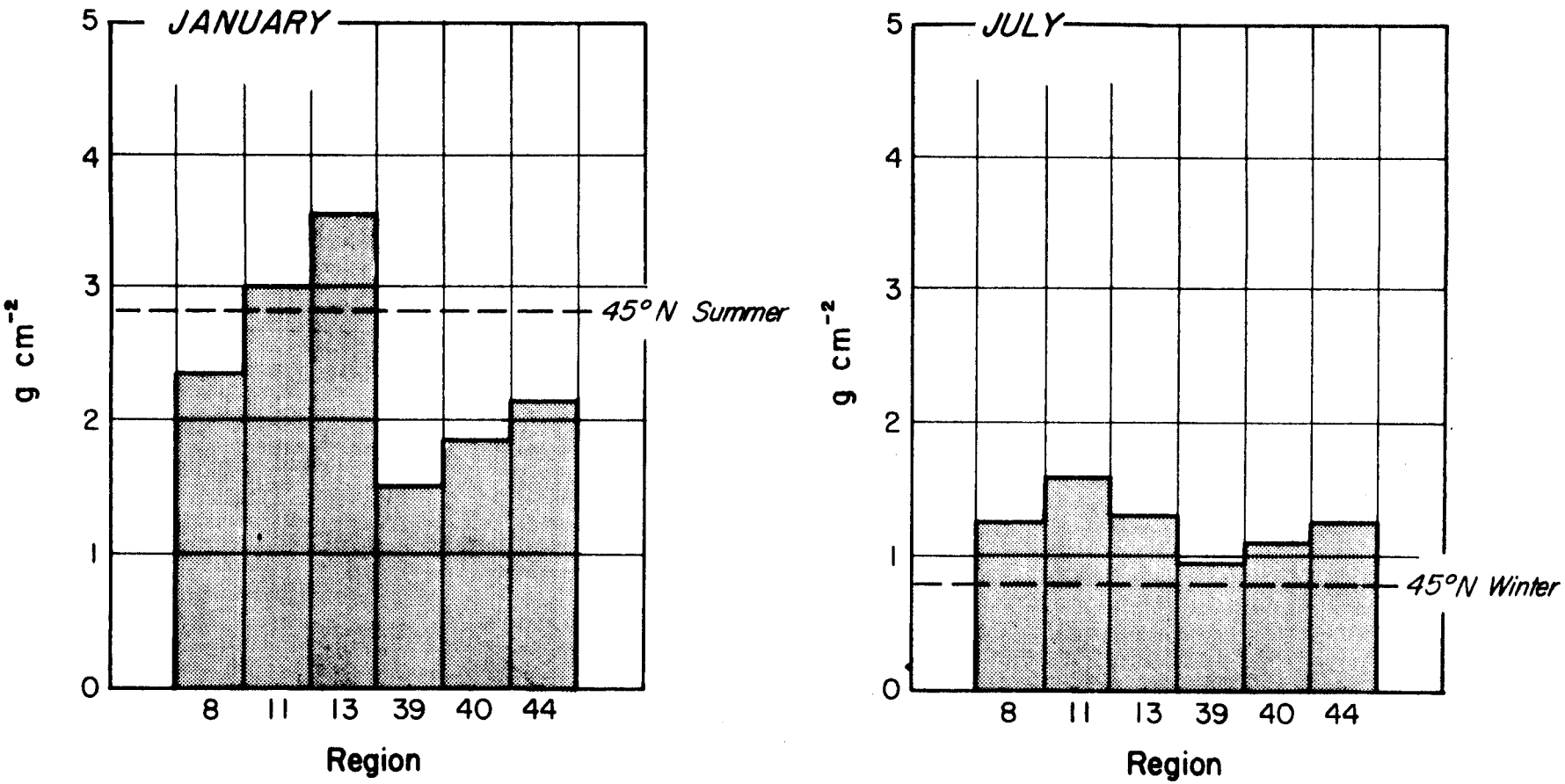

Figure 2-19 Precipitable Water 37.5° -50.25°S

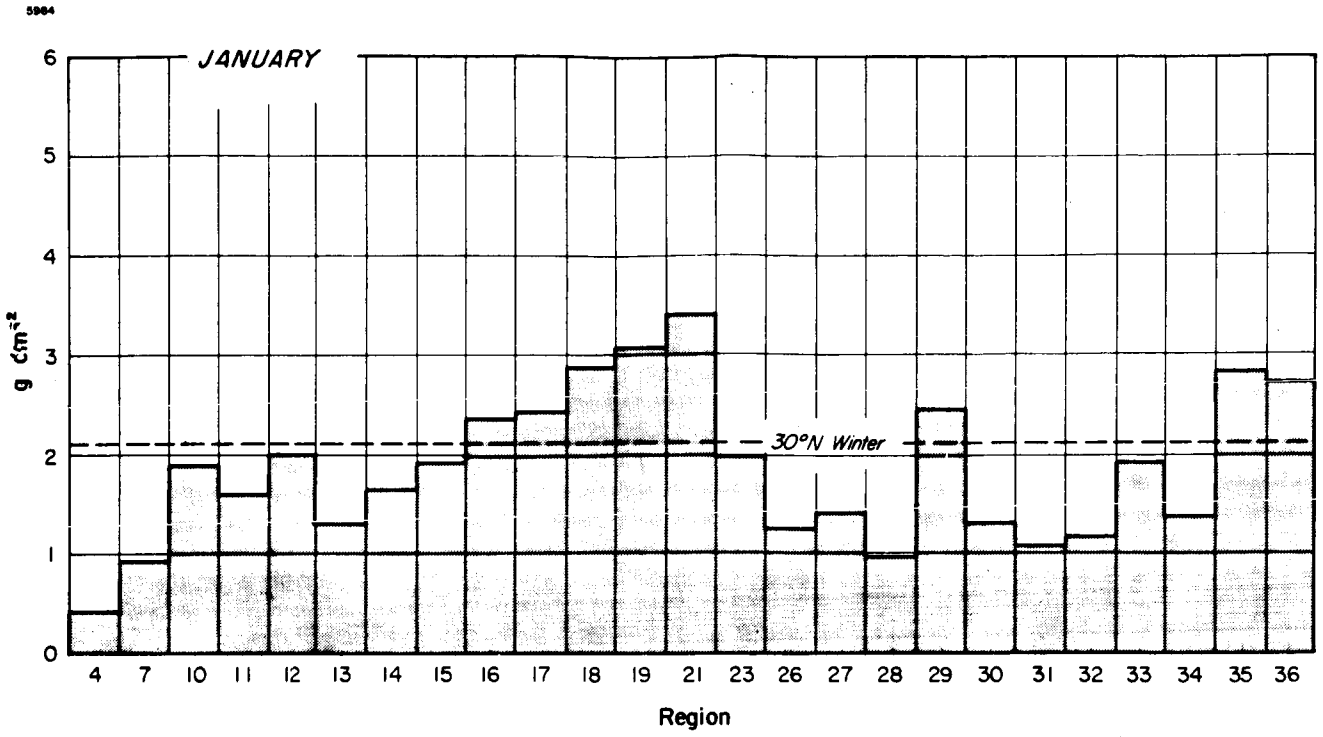

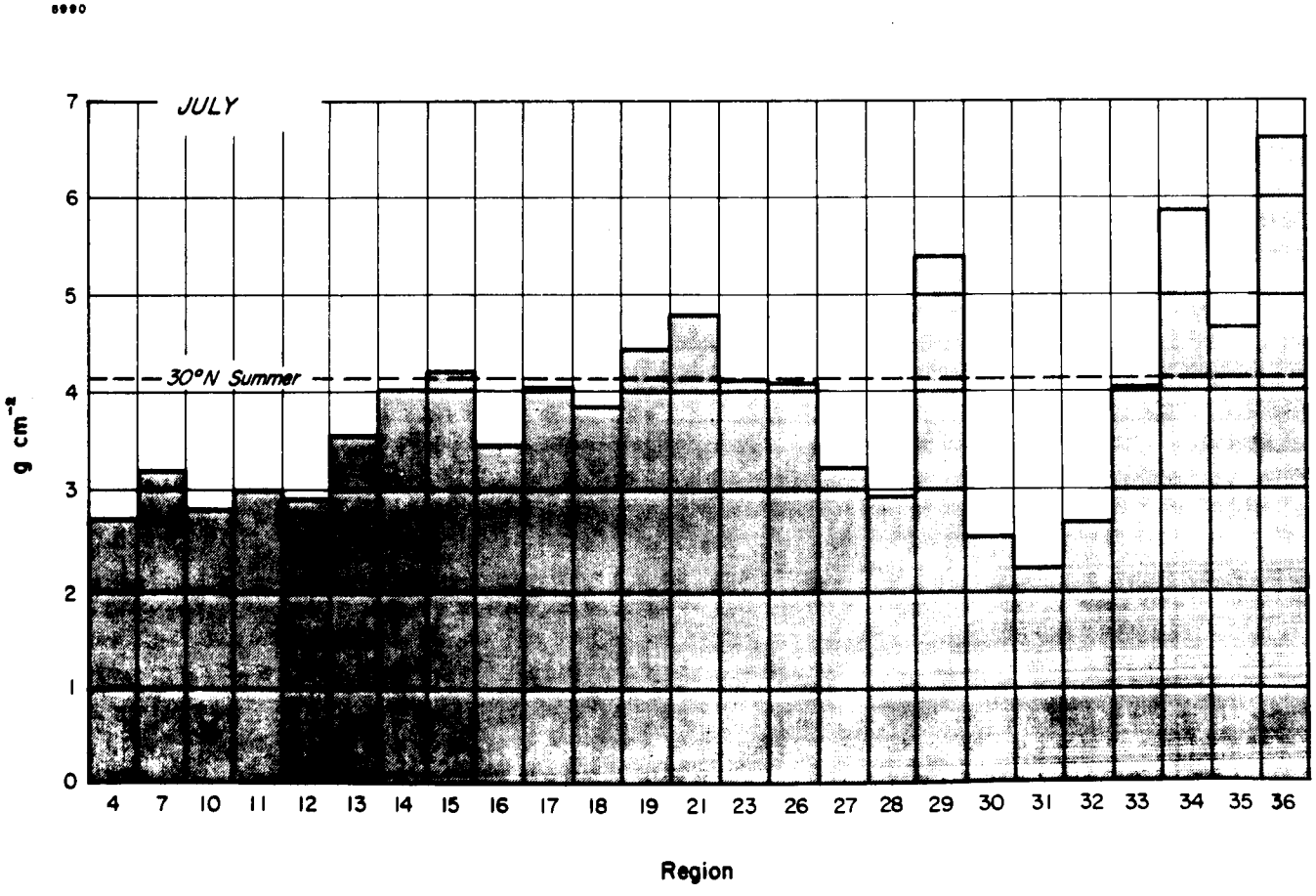

Figure 2-20 Precipitable Water 22.5° -37.5°N

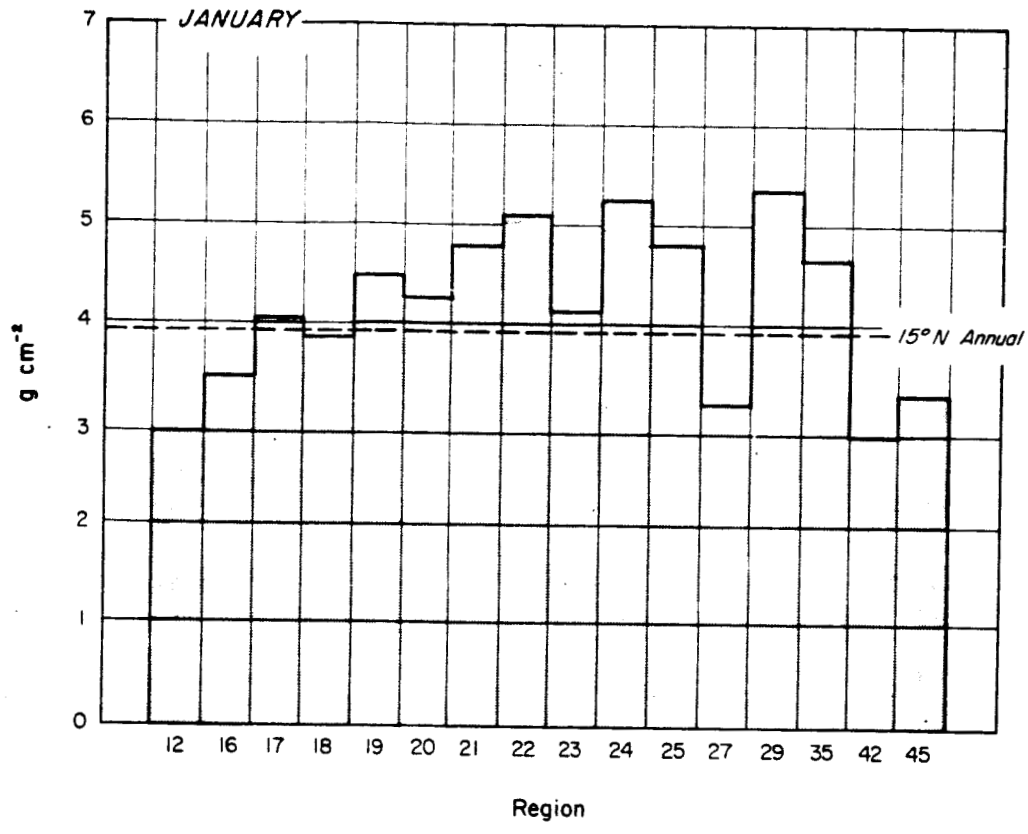

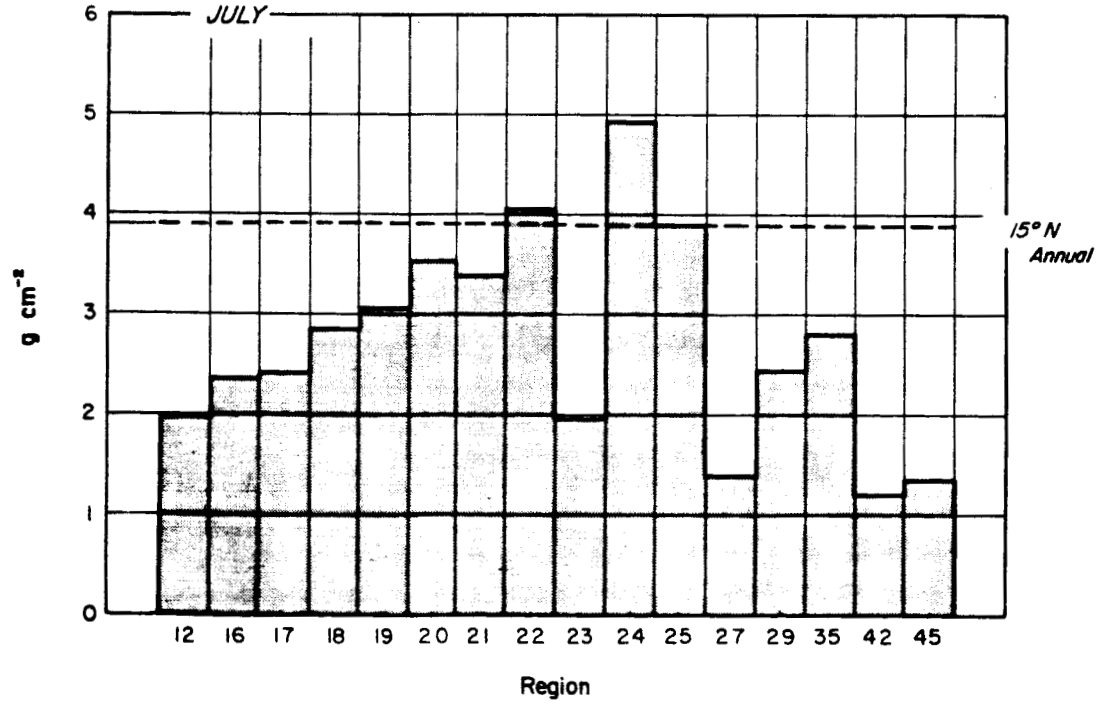

Figure 2-23 Precipitable Water 0^{o} -22.5^{o}S

A temperature inversion appears in the January standard atmosphere corresponding well to data recorded in the high latitudes. The inversion is caused by the radiational cooling of the snow-covered surface below, but averaging across time and space results in its disappearance in the region data. The dew point inversion, however, is retained in Regions 1 and 2 (the Arctic regions), and the standard atmosphere's precipitable water (0.19 g cm^{-2}) falls about halfway between Region 1's 0.15 g cm^{-2} and Region 2's 0.25 g cm^{-2}. The July standard atmosphere's profile is unlike the region profiles for both temperature and dew point, yet the temperatures, and precipitable water, again fall about halfway between those of the two regions.

Region 3, the subarctic ocean, is also located predominantly north of 60.75°N. It is, however, much warmer and more moist (Figures 2-6, 2-7 and 2-8 than either of the Arctic regions or the standard atmosphere at 75°N. Thus the latitudes between 60.75° and the poles would be best represented by the region data, although use of the 75°N standard atmosphere for the Arctic regions would not cause large errors.

2.3.2 Latitudinal Belt Between 50.25° and 60.75°

The region between 50.25°N and 60.75°N is a transition zone from the high mid-latitudes to the subarctic ocean; the most appropriate standard atmospheres would be those at 60°N. The Southern Hemisphere at these latitudes is almost entirely ocean, implying that the variation around the globe in this zone is limited. However, the same hemispheric moisture differences mentioned for the Antarctic are evident in Region 39 (Figures 2-6, 2-7, 2-16, 2-17), making the standard atmosphere for 60°N clearly inappropriate.

The Northern Hemisphere presents a more diverse picture with precipitable water values in this belt ranging from 0.25 to 1.1 g cm^{-2} in the winter and from 1.75 to 3.22 g cm^{-2} in the summer. The January standard atmosphere is most representative of land conditions at this latitude, with the temperature and dew point values corresponding well to Region 4 (polar-continent) and the precipitable water value of 0.42 g cm^{-2} matching Region 4's 0.41 g cm^{-2}. Although slightly lower in temperature and water vapor

content, it is also quite similar to Region 5. However, the standard atmosphere greatly underestimates the temperatures and moistures found in subarctic and polar oceans (Regions 3 and 6). The standard atmosphere profile also shows a slight inversion at 1 km; this is a characteristic of land or ice-capped regions only.

The July standard atmosphere resembles land conditions only in the shape of its temperature profile since its temperatures run 5°C colder than those above Regions 4 and 5 and its dew point values are almost as low below 700 mb. In this season, the temperature values are much more similar to those in the subarctic regions, and are not unlike those of Region 6 except at the surface. The dew point profile, however, has a much smaller lapse rate than is found for any related region; it also underestimates the moisture for all but the subarctic regions (2 and 3). Clearly, the variability around this latitudinal belt recommends use of regional data, rather than one standard atmosphere.

2.3.3 Latitudinal Belt Between 37.5° and 50.25°

The standard atmosphere for 45° is again most closely allied to land (Figures 2-8, 2-9, 2-18, 2-19). Like the atmospheres for higher latitudes, it underestimates the winter moisture, and overestimates the summer moisture throughout the Southern Hemisphere regions from 37.5° to 50.25°S, and should never be used there. However, its temperatures and summer dew points well represent Region 7 (high mid-latitude continent) and Region 28 (border of mid- and high-latitude mountains), and the precipitable water, though a little low, would not provide a bad estimate of the values in those two regions. The same cannot be said of the high mid-latitude oceanic regions 8 and 9. In these areas the winter temperatures run higher than the standard atmosphere's and the summer temperatures run lower. Likewise the precipitable water values are much higher in January and much lower in July. The mid-latitude ocean region, Region 11, represents a cross between these land and ocean climates. In the winter, its climate resembles those of Regions 8 and 9 with somewhat higher temperatures and moisture; in the summer, its temperatures coincide with the 45°N standard atmosphere's, and its precipitable water almost equals that of Region 7 (3.0 g cm^{-2} vs 3.2 g cm^{-2}). This drastic change in climate is not surprising; in January this region

is under the influence of the Icelandic low (as are Regions 8 and 9), in July it is subjected to warm, moist air drawn north by the circulation of the Bermuda high (as is Region 7). But it underlines not only the variability of moisture within this latitudinal belt, but also the seasonal variability of that zonal variability.

2.3.4 Latitudinal Belt Between 22.5° to 37.5°

The latitudinal belts from 22.5° to 37.5°N and from 22.5° to 37.5°S are characterized by great variability in geography. In the Northern Hemisphere these latitudes include the Sierra Madres, the subtropical oceans, the Sahara Desert, and the Himalayas. In the Southern Hemisphere these latitudes include the southern half of Australia, the mountain ranges of Chile, the plains of Argentina and the Union of South Africa. Almost every type of climate is represented from the arid, to the tropical wet, to the highland, to the continental temperate. Clearly no one atmosphere, such as the standard atmosphere for 30°N, could be representative of the entire zone (Figures 2-10, 2-11, 2-20, 2-21).

Precipitable water in the Northern Hemisphere ranges from 0.4 to 3.4 g cm^{-2} in January, and from 2.15 to 6.6 g cm^{-2} in July. The Southern Hemisphere is slightly less variable; its values range from 1.1 to 3.4 g cm^{-2} in July, and from 2.0 to 5.35 g cm^{-2} in January. The limited amount of land in this hemisphere is probably responsible for the somewhat smaller range of values. The winter value of 2.1 g cm^{-2}, given by the standard atmosphere, is obviously a midpoint value; however, it is really only representative of Regions 10, 12, 15 and 41, the lower mid-latitude oceans, and of Region 33, the border of Northern Hemisphere deserts. The standard atmosphere underestimates the moisture above the subtropical and tropical oceans, and above the continental tropics and subtropics (Regions 29, 35 and 36). On the other hand, it overestimates the moisture over all other land regions located in that latitudinal belt.

The 30°N standard atmosphere for July contains 4.1 g cm^{-2} of precipitable water, placing it with the most moist of the regions between 22.5° and 37.5°. Again it approximates the moisture in Regions 15 and 33, but it greatly overestimates the moisture in Regions 10, 12, and 41. The value is also representative of the moisture in Region 14 (lower mid-latitude continent)

and in Region 26 (major mountain ranges), both regions that the January's standard atmosphere overestimates, and it matches well with the value for Region 17 (subtropic ocean) which the winter value underestimates. The only regions whose moisture values exceed the standard atmosphere's are Regions 19, 21, 29, 34, 35, and 36. Region 36 is composed of India and the Indian Ocean; in July it is in the midst of its monsoon season and has the highest precipitable water (6.6 g cm^{-2}) recorded for any season at any location. Nor surprisingly, the driest atmospheres in the subtropics are associated with the desert borders and the mountain ranges.

The temperature profile given by the standard atmosphere for January seems to be a cross between that above the "eastern low mid-latitude ocean" (Region 12) and that over the deserts (Region 30). Below 2 km it runs warmer than the temperature over the lower mid-latitude continent (Regions 14) yet it is consistently colder than the atmosphere over the subtropical oceans (Regions 16 and 17) and over the subtropical mountain borders (Region 29). In the summer the standard atmosphere's temperatures match those of Region 14 near the surface, those of Regions 16 and 17 between 2 and 5 km, and are too warm above that level for any values but those of Region 29. Below 2 km the standard atmosphere temperatures exceed those over all the oceanic regions and fall short of those recorded in the deserts.

2.3.5 Tropical Regions

The tropical latitudes from 22.5°N to 22.5°S (Figures 2-12, 2-13, 2-22, 2-23) (the Tropic of Cancer to the Tropic of Capricorn) share many moisture regions with the subtropics. In general, however, the latitudes do not show extreme seasonal variabilities; a fact which caused only an annual standard atmosphere to be computed for 15°N. Except for a slight inversion between 2 and 2.5 km, the temperature profile is quite similar to that given for 30°N July; thus the above comments about its applicability to the deserts and mountain regions still hold. No inversion appears in any region profile, presumably because of the temporal and spatial averaging, but the standard atmosphere temperatures below 4 km agree well with those of Region 22 (the tropical oceans) for both seasons. The other tropical regions (20, 21, and 23) are colder in January near the surface; all four tropical regions are warmer above 5 km than the standard atmosphere would indicate.

The dew point profile is totally nonrepresentative, especially as it shows a sudden, sharp drop in moisture between 2 and 2.5 km that is not even suggested by the region data. The total precipitable water given by the standard atmosphere, 3.9 g cm^{-2}, overestimates all winter region values except those of Regions 22, 24 and 25. On the other hand, it underestimates all the summer values except for those of the subtropical oceans (Regions 12 and 16), the mountain ranges (Region 27), and the deserts (Regions 30, 31, 32, 42, and 45).

Despite the inapplicability of the standard atmosphere as the representative of this latitudinal belt, the spatial variability of moisture over most of this zone is not large. The amount of land found in the Northern Hemisphere south of 22.5°N is quite limited since Africa is the only continent that does not lie mainly to the north; probably two-thirds of this area is ocean. Oceans, of course, dominate the Southern Hemisphere, and though this belt contains much of South America and a good piece of Africa, less than one-fourth of these latitudes is occupied by land. Thus the winter precipitable water range of 1.05 to 4.8 g cm^{-2} can be reduced to 3.0 to 4.8 g cm^{-2} merely by concentrating on the regions which are predominate at those latitudes, Region 19 through 22, and Region 24. Likewise the summer range of 2.15 to 6.6 g cm^{-2} can be, without much error, regarded as 4.25 to 5.25 g cm^{-2}.

2.4 Summary of Comparison of Moisture Regions with U. S. Standard Atmospheres

Although the significance of the regional atmospheric difference can only be evaluated in light of particular applications, the above analyses can be summarized as follows:

- The greatest spatial variability within any latitudinal belt occurs between 22.5°N and 37.5°N where 36 of the 45 regions are represented. This area has July values of precipitable water ranging from 2.15 to 6.6 g cm^{-2} and many areas are seriously misrepresented by the 30°N standard atmosphere.
- North of 37.5°N, the standard atmosphere is much more representative of land conditions than of ocean conditions. Generally, continental areas can be approximated by the standard atmospheres; the ocean regions are warmer and wetter in the winter, colder and drier in the summer.

- The U. S. Standard Atmospheres are not applicable to Southern Hemisphere latitudes south of 40°S.
- The tropics show the least seasonal variability; however, the annual value given for 15°N does not adequately represent these climates. It overestimates the winter moisture in most of the regions and usually underestimates the summer moisture. Separate atmospheres for January and July would better represent this area.

3. THE 4-D MODELS AND RADIATION TRANSFER

In this section, the use of atmospheric models in remote sensing studies is discussed in terms of a simple model of the transfer of infrared radiation. This is followed by a short description of the computation technique actually used to convert the atmospheric data into the radiometric parameters that will be discussed in Section 4.

3.1 Elements of Radiation Transfer

In remote sensing by electromagnetic means, measurements are made of the radiation emitted, reflected, or transmitted by a target using a receiver located at some distance from the target. Properties of the target are then inferred from the radiometric measurements using known target signatures. Such signatures may include the intensity of the signal at one wavelength; it may include multispectral properties in which the relative intensities at a number of wavelengths are important; or it may extend into the angular domain in which the relative intensities measured at a number of angles provide the clue for target identification. The success of remote sensing techniques, whether to obtain an absolute measurement of a physical property of a target such as its temperature, or to simply identify the target, requires a consistent and known relationship between the measured signal and the properties of the target.

With few exceptions, remote sensing measurements are made through the atmosphere. In the case of remote sensing of earth resources from an orbiting spacecraft, the sensors on the spacecraft measure the radiation from the target after the radiation has traveled through the entire atmosphere. This atmosphere, its gaseous and particulate constituents, are "radiometrically active". They absorb, emit and scatter radiation. In so doing, they interact with the radiation propagating from the target to the sensor. If this effect is so strong that inherent relationships between target and emitted (or reflected) radiance is totally destroyed or masked, then the radiation energy measured at the sensor cannot provide any information about the target. On the other hand, if the interaction is weak, the remotely measured radiation energy contains useful information concerning the target, and the measured signal can be used to infer information about the target. The degree of success in this inference is then dependent on the degree

to which the atmospheric effects on the measured signals is known and can be accounted for.

More specifically the above discussion may be expressed in terms of a simplified equation applicable to the transfer of infrared radiation through an absorbing (and emitting) atmosphere as

$$\bar{N}_\lambda = E_\lambda(s)\ \tau_\lambda(A)\ N_\lambda[T(s)] + \int_0^\infty N_\lambda[T(z)]\ \frac{\partial \tau_\lambda(z)}{\partial z}\ dz \qquad (3\text{-}1)$$

$\bar{N}_\lambda$ is the effective spectral radiance measured by a spacecraft borne sensor at wavelength λ; $E_\lambda(s)$ and $T(s)$ are respectively the spectral emissivity and the temperature of the surface; and $\tau_\lambda(A)$ is the spectral transmissivity of the entire atmospheric layer between the target surface and the sensor along the optical path. $N_\lambda[T(s)]$ is then the blackbody spectral radiance at temperature $[T(s)]$. $T(z)$ and $\tau(z)$ are respectively the temperature and spectral transmissivity of the atmosphere at level z.

Given the above definitions, Equation 3-1 may be simply interpreted as follows: the radiance measured at a satellite sensor consists of two parts. The first part is that which is emitted by the surface and attenuated by the atmosphere. This contribution is expressed by the first term in the right hand side of Equation (3-1). The second contribution, expressed by the second terms in the equation, is made by the atmosphere. The total effects of the atmosphere on the measured radiance are through the terms of $\tau_\lambda(A)$, $\tau_\lambda(z)$ and $T(z)$. It is in the evaluation of these terms that model atmospheres, such as the 4-D Models, are used.

From Equation (3-1) it is clear that in radiation transfer studies the temperature profile of the model atmospheres is used implicitly through the blackbody Planck Radiance function. This same atmospheric parameter is also used in the evaluation of $\tau_\lambda(z)$ and therefore $\tau_\lambda(a)$ which is the integrated effect of the entire atmospheric path. Other parameters of the atmospheric models are also used in the evaluations of this term.

Absorption or transmission of radiation by the atmosphere is spectrally dependent. Given the gaseous makeup of the atmosphere, at certain

wavelengths the atmosphere is approximately transparent while at other wavelengths, the atmosphere absorbs. The absorption by the different species of gases and the magnitude of the absorption is dependent on the amount of gas through which the radiation must propagate. In the infrared region, two gases are of primary importance. The first is water vapor and the second is carbon dioxide. It is clear, therefore, that to obtain values of $\tau_\lambda(z)$, and of $\tau_\lambda(A)$, it is necessary to use appropriate values of the mixing ratio profile W(z) or some other water vapor profile parameter. For a well-mixed gas such as carbon dioxide (or oxygen), only the pressure-height (or density-height) data from the appropriate atmospheric model are required to completely specify its mixing ratio profile (at least within the region of the atmosphere in which the gas is well-mixed). Yet a third atmospheric parameter is used in the evaluation of $\tau_\lambda(z)$. This is the pressure profile, P(z). Due to pressure broadening effects on individual absorption lines, the degree of atmospheric absorption is dependent on altitude not just because absorber concentrations generally decrease with height, but also because pressure is a function of height.

From the purely heuristic discussion given above, it should be clear that simulation of expected radiometric signals is possible, and often used, to evaluate potential problems in data interpretation of remote sensing measurements. More importantly, such simulations require representative values of detailed structures of the atmosphere such as might be obtained through standard atmosphere models or from the more detailed 4-D model atmospheres discussed in Section 2.

3.2 Spectral Region Selection

This study has addressed itself to the evaluation of the use of the 4-D models in the infrared. The infrared region was selected because of its extensive use in quantitative measurements of surface and atmospheric properties in aircraft and satellite programs. More importantly, this region has significant water vapor absorption bands. Water vapor is the most variable of the atmospheric parameters. It is in fact the variability, spatial and temporal, of this parameter which has resulted in the definition of the large numbers of "homogeneous" regions in the 4-D atmospheres.

By confining the analysis to the infrared, it is hoped that validity or usefulness of the detailed 4-D models can be evaluated with a minimum number of computations.

Computations were made in the following four spectral intervals: (1) 3-4.5 μm; (2) 6-8 μm; (3) 9-13 μm; and (4) 13-18 μm.

The first and third of the spectral intervals are located in the so-called atmospheric windows where atmospheric effects are minimal, and have, therefore, been used for surface measurements, including surface temperatures. However, residual absorption by water vapor and carbon dioxide is still present. The first wavelength interval corresponds to the spectral region of the High Resolution Infrared Radiometer (HRIR) of the Nimbus II satellite while the third spectral region corresponds to the spectral region of one of the channels of the Medium Resolution Infrared Radiometer (MRIR) of Nimbus II and III, and to the window channels of the temperature humidity infrared radiometer (THIR) of Nimbus IV and V.

The 6-8 μm region is located in a water vapor absorption band. It is in this spectral region that a number of sensors have been designated to obtain measurements from which atmospheric water vapor quantities are inferred. These radiometers have included the water vapor channel of the MRIR of Nimbus II and III and the water vapor channel of the THIR of Nimbus IV and V.

The last spectral region covers a carbon dioxide band. This region has been used to obtain measurements of lower stratospheric water vapor as in the MRIR of Nimbus II. More recently, it has been used to obtain vertical profiles of atmospheric temperature. No analysis of this spectral band was performed here.

3.3 Computations

3.3.1 Procedure

The computation program developed by Dr. David Anding was modified and used to evaluate the radiation transfer process through a cloudless non-scattering atmosphere. Details of the program may be found in the referenced document. Modifications to the program are given in Appendix B. Basically, the program uses a library of absorption coefficients for the various gaseous species and, with specifications of atmospheric profiles of temperature, absorber

concentration, and pressure-height, it uses a layered geometry model of the atmosphere to compute a number of radiation quantities at fixed wavelengths for specified wavelength intervals. Since the absorption coefficients are based on empirical data, the spacing of the wavelengths at which computations are performed changes with the wavelength region. Tables 3-1 and 3-2 show two examples of this spacing. The first is a print-out of the spectral radiance and atmospheric transmissivity computed for the 4 μm water vapor window region using a specific atmosphere. The second table, Table 3-2, shows similar results for the 10-12 μm window region. It is clear that the computations are made at much closer spectral spacing in the 4 μm region than in the 10-12 μm region.

3.3.2 Parameters

The Anding program was used to compute directly the following terms:

Spectral radiance, N_λ	watts/cm^{-2} sr-μm
Blackbody temperature, T	(°K)
Atmospheric transmissivity, $\tau_\lambda(A)$	

and, in the case of the absorption band regions, computations were also made, at selected wavelengths, of

Weighting function: $\frac{\partial \tau_\lambda (z)}{\partial z}$ (km^{-1})

This term describes the relative contribution to the received radiance made by each level of the atmosphere. Figure 3-1 shows two examples of the weighting function computed for a wavelength in the 6.3 μm water vapor absorption band. In Figure 3-1a, the computations were made for a very dry atmosphere. The weighting function shows that the atmosphere is nearly transparent with major contributions being made by and near the surface. The weighting function shown in Figure 3-1b was computed for a relatively moist atmosphere. The peak of the weighting, i.e., the level of maximum contribution, is shown located in the middle troposphere. It is clear therefore that the weighting function is useful in an analysis of the source of the radiant energy received by a satellite radiometer.

Table 3-1

Example of Computer Printout for the 4 μm Region

ATMOSPHERE = REGION 6 JAN SENSOR ALTITUDE = 80000. SURFACE TEMPERATURE = 271.39

RUN NUMBER 16 HAS 221 WAVELENGTHS

LAMDA	DELTA	RADIANCE	TRANSMISSION
3,831	0,0075	1,3549448E-05	0,93529
3,839	0,0075	1,3867337E-05	0,95002
3,846	0,0075	1,4085807E-05	0,94895
3,854	0,0075	1,4290687E-05	0,93798
3,861	0,0070	1,4539764E-05	0,94224
3,868	0,0075	1,4792082E-05	0,94696
3,876	0,0075	1,5040014E-05	0,94338
3,883	0,0075	1,5242826E-05	0,93717
3,891	0,0080	1,5525700E-05	0,93994
3,899	0,0075	1,5797428E-05	0,94031
3,906	0,0075	1,6018588E-05	0,93667
3,914	0,0080	1,6277947E-05	0,93378
3,922	0,0075	1,6531034E-05	0,92904
3,929	0,0075	1,6771432E-05	0,92940
3,937	0,0080	1,7019425E-05	0,92411
3,945	0,0080	1,7274797E-05	0,92023
3,953	0,0080	1,7524551E-05	0,91482
3,960	0,0075	1,7743048E-05	0,91084
3,968	0,0075	1,7982195E-05	0,90406
3,976	0,0080	1,8222927E-05	0,89821
3,984	0,0080	1,8448816E-05	0,88955
3,992	0,0080	1,8665523E-05	0,88100
4,000	0,0080	1,8862091E-05	0,86981
4,008	0,0080	1,9088300E-05	0,86269
4,016	0,0080	1,9299987E-05	0,85375
4,024	0,0080	1,9477811E-05	0,84151
4,032	0,0080	1,9607542E-05	0,82302
4,040	0,0080	1,9821251E-05	0,81582
4,049	0,0085	2,0048421E-05	0,80573
4,057	0,0085	2,0159336E-05	0,78872
4,065	0,0080	2,0268024E-05	0,77223
4,073	0,0080	2,0353740E-05	0,74777
4,082	0,0085	2,0569685E-05	0,74122
4,089	0,0075	2,0725711E-05	0,73385
4,098	0,0080	2,0869178E-05	0,71715
4,107	0,0090	2,0987121E-05	0,69584
4,115	0,0085	2,1015803E-05	0,66933
4,124	0,0085	2,1502536E-05	0,68757
4,132	0,0085	2,1737869E-05	0,68146
4,141	0,0085	2,2005406E-05	0,67291
4,149	0,0085	2,2293636E-05	0,67051
4,158	0,0085	2,2592591E-05	0,66685
4,167	0,0090	2,2351058E-05	0,63768
4,175	0,0085	9,2450200E-06	0,10863
4,184	0,0085	2,0995240E-06	0,00001
4,193	0,0090	1,6622134E-06	0,0
4,202	0,0090	1,6953536E-06	0,0
4,211	0,0090	1,7400271E-06	0,0
4,219	0,0085	1,7757966E-06	0,0
4,228	0,0085	1,8156425E-06	0,0
4,237	0,0090	1,8561605E-06	0,0
4,246	0,0090	1,8973587E-06	0,0
4,255	0,0090	1,9391946E-06	0,0
4,264	0,0090	1,9818435E-06	0,0
4,274	0,0095	2,0299876E-06	0,0
4,283	0,0095	2,0740772E-06	0,0
4,292	0,0090	2,1188544E-06	0,0
4,301	0,0090	2,1643773E-06	0,0

Table 3-2

Example of Computer Printout for the 10 μm Region

ATMOSPHERE = REGION 5 JAN SENSOR ALTITUDE = 80000. SURFACE TEMPERATURE = 261.30

RUN NUMBER 15 HAS 122 WAVELENGTHS

LAMDA	DELTA	RADIANCE	TRANSMISSION
9.070	0.0700	4.4758711E-04	0.97115
9.130	0.0750	4.5065070E-04	0.97173
9.220	0.0900	4.5522093E-04	0.97205
9.310	0.0570	4.5939954E-04	0.96537
9.335	0.0450	4.6055624E-04	0.96544
9.398	0.0630	4.0852954E-04	0.80145
9.463	0.0490	2.0892701E-04	0.18701
9.494	0.0310	1.9092811E-04	0.13574
9.526	0.0480	2.1002495E-04	0.18164
9.590	0.0630	2.8232974E-04	0.38869
9.652	0.0620	2.1668543E-04	0.19585
9.713	0.0600	2.3922163E-04	0.25062
9.773	0.0610	2.4798373E-04	0.26763
9.834	0.0600	2.6567653E-04	0.31000
9.893	0.0590	2.9089162E-04	0.38332
9.953	0.0890	3.2988843E-04	0.49282
10.070	0.1180	3.9333478E-04	0.68054
10.190	0.1100	4.4072187E-04	0.82580
10.290	0.1250	4.9006124E-04	0.95872
10.440	0.1300	4.9245940E-04	0.96235
10.550	0.2300	4.9369480E-04	0.95385
10.900	0.2500	4.9511157E-04	0.94864
11.050	0.1370	4.9433950E-04	0.94117
11.173	0.1090	4.9284729E-04	0.93314
11.268	0.0950	4.9284683E-04	0.93042
11.364	0.1160	4.9218955E-04	0.92606
11.500	0.1530	4.9168360E-04	0.92073
11.670	0.1450	4.9101491E-04	0.91623
11.790	0.1150	4.8997952E-04	0.91461
11.900	0.1300	4.8792826E-04	0.90829
12.050	0.1500	4.8408192E-04	0.89388
12.200	0.1500	4.7898805E-04	0.87182
12.350	0.1500	4.7328277E-04	0.84749
12.500	0.0900	4.6689063E-04	0.81786
12.530	0.0300	4.6601868E-04	0.81464
12.560	0.0300	4.6475185E-04	0.80796
12.590	0.0	4.5453501E-04	0.71172
12.630	0.0	4.5170682E-04	0.69446
12.660	0.0300	4.4826674E-04	0.68198
12.690	0.0300	4.6077464E-04	0.80231
12.720	0.0450	4.5861979E-04	0.79056
12.760	0.0350	4.5700860E-04	0.78257
12.790	0.0300	4.5541720E-04	0.77519
12.820	0.0300	4.5373221E-04	0.76681
12.850	0.0350	4.5177829E-04	0.75427
12.890	0.0350	4.5011449E-04	0.74813
12.920	0.0300	4.4812215E-04	0.73571
12.950	0.0350	4.4582412E-04	0.72049
12.990	0.0350	4.4349954E-04	0.70811
13.020	0.0350	4.4096960E-04	0.69182
13.050	0.0350	4.3839798E-04	0.67682

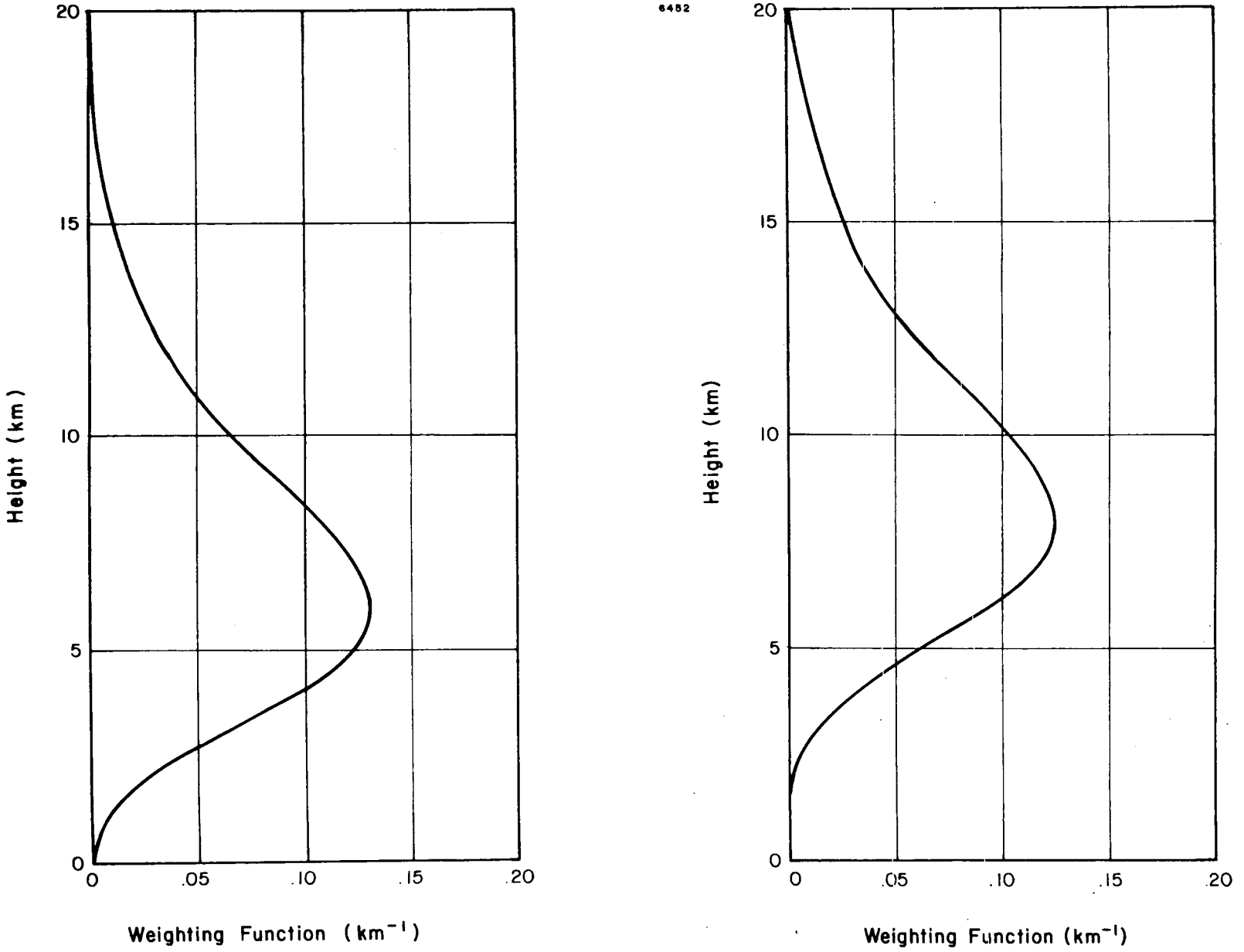

Figure 3-1 **Examples of Weighting Functions Computed for the 6.3 μm Water Vapor Absorption Band**

Spectrally weighted values of the radiance were then computed using the results of Anding's programs. The spectral weighting consists of the following procedure:

$$\overline{N} = \sum_{\lambda} \phi_{\lambda} N_{\lambda} \, d\lambda \qquad (3\text{-}2)$$

where ϕ_{λ} is a spectral response function which essentially describes the relative efficiency of a real sensor to detect and measure incident radiation at various wavelengths. In this formulation, ϕ_{λ} has values between 0 and 1. The spectral response function of the specific satellite radiometer channels selected for analysis are shown in Figure 3-2a to 3-2d.

An additional parameter evaluated was the effective blackbody temperature T_{bb} (°K) corresponding to the computed effective radiance. These values were obtained by using the calibration charts for each of the radiometers as given in the Data User's Guides. Figure 3-3 shows examples of calibration curves for the HRIR of Nimbus II and the water vapor channel of the THIR for Nimbus IV.

3.3.3 Atmospheres

The atmospheres used in the data analysis include the following:

1. Standard Atmospheres at 15°N, 30°N, 45°N, 60°N and 75°N for the months of January and July (with the exception of the 15°N model which is described by a single set of annual values). The data for these models were obtained from the Handbook of Geophysics and Space Environments and the U.S. Standard Atmosphere Supplements, 1966.
2. 4-D atmospheres from each of the 45 regions for the months of January and July.

The results of these computations are presented in Section 4 of this report.

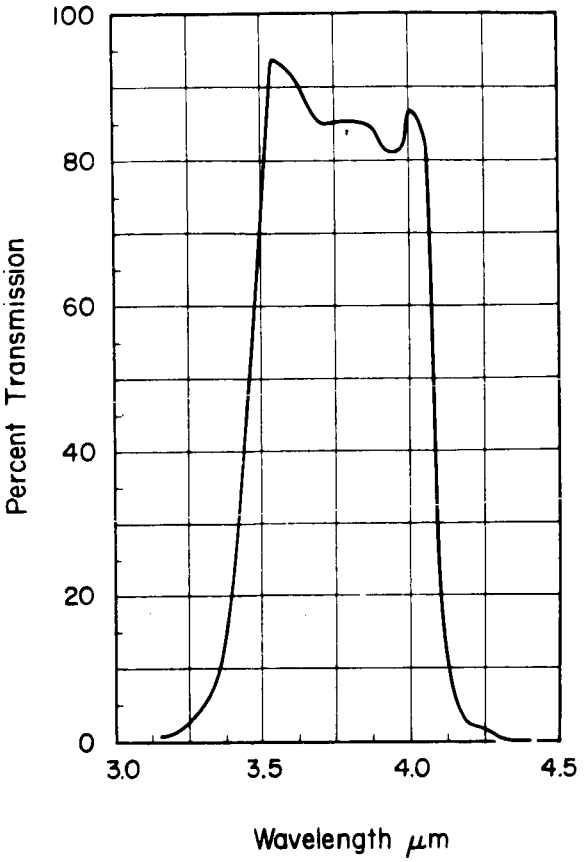

(a) Relative Spectral Response of 3-4 μm Channel on NIMBUS II

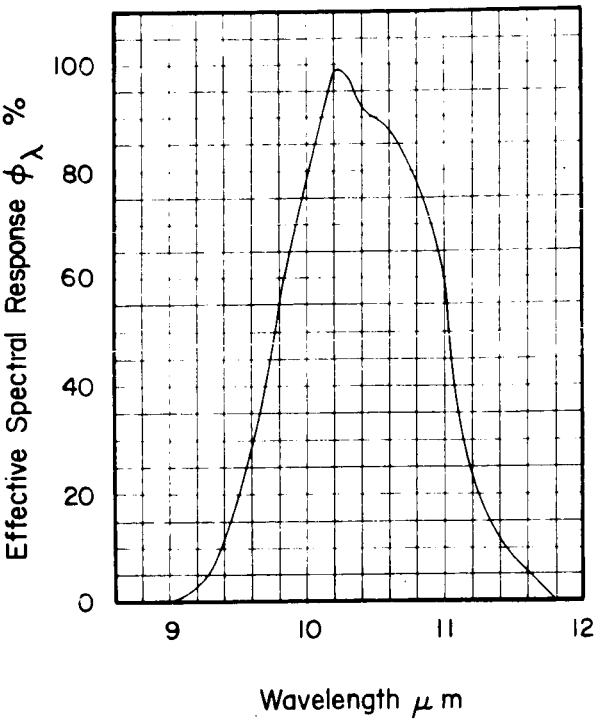

(b) Relative Spectral Response of 10-11 μm Channel on NIMBUS II

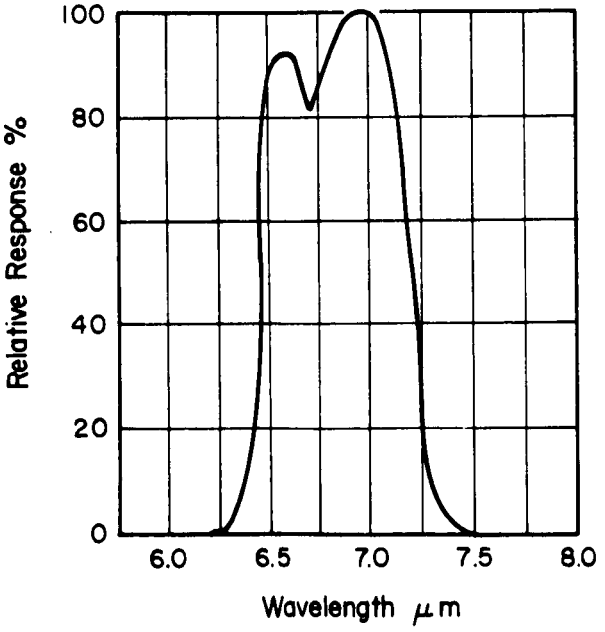

(c) Relative Spectral Response of 6.7 μm Channel on NIMBUS IV

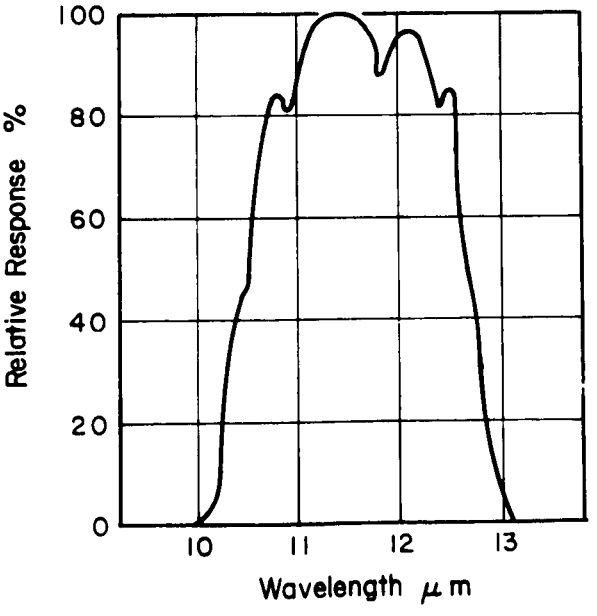

(d) Relative Spectral Response of 11.5 μm Channel on NIMBUS IV

Figure 3-2 Examples of Effective Spectral Response Functions from NIMBUS II and NIMBUS IV (from NIMBUS II and IV User's Guide)

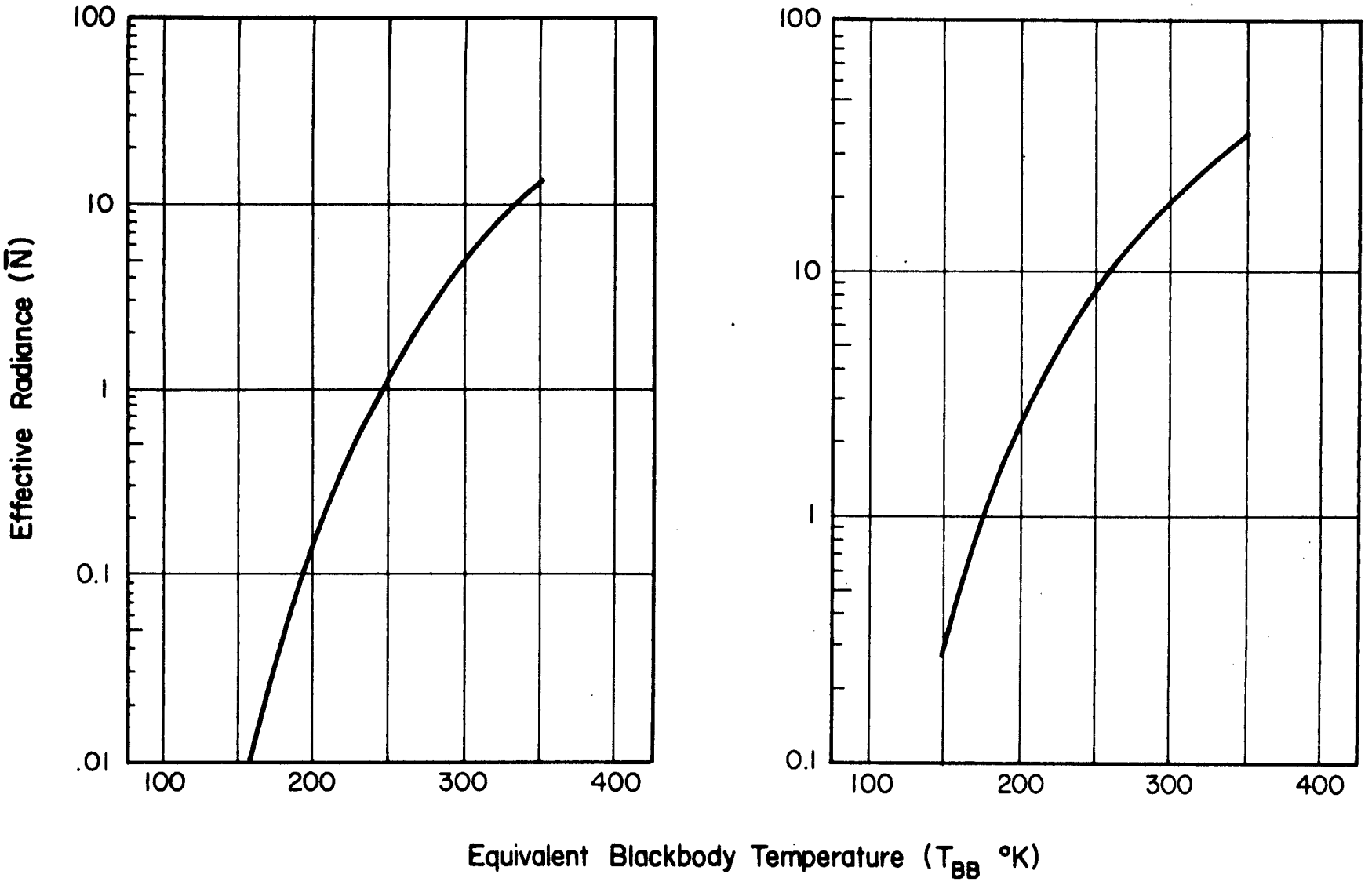

(a) Effective Radiance versus Equivalent Blackbody Temp. For 6.7 μm Channel

(b) Effective Radiance versus Equivalent Blackbody Temp. For 11.5 μm Channel

Figure 3-3 Calibration Curves for the THIR of NIMBUS IV

4. INFRARED ANALYSIS

The computations presented in this section are meant simply to demonstrate the spatial variability of radiometric parameters introduced by the use of the MSFC 4-D Model atmospheres. The radiometric model by Anding used in this study can provide good simulation of the spectral radiance at any of the specified wavelengths. However, given the finite spectral band widths of specific radiometer systems, as defined by their effective spectral response functions, there is no clear and unambiguous approach to the simulation of the radiometric quantities actually measured by a real system. The approach adopted in this study (that of using the effective spectral response function to simulate the effective radiance, and using this computed value to derive the effective blackbody temperature from a calibration chart) is subject to a number of interpolation errors. Consequently, the computation results in Section 4 should not be used to construct absolute correction factors for the specific sensors discussed. More appropriately, the data should only be used to interpret the relative spatial variability of the radiometric quantities anticipated in simulation results using the MSFC 4-D Models.

4.1 Introduction

The MSFC 4-D atmospheric model showed marked differences in temperature, water vapor and pressure across its 45 homogeneous moisture regions. In fact, the analysis of Section 2 indicated significant climatic differences within latitudinal belts that are represented by only one atmosphere in the U. S. Standard Atmosphere Supplements. This section will look at the radiometric parameters derived from these same atmospheres to see if the significant atmospheric differences seen in Section 2 cause significant radiometric differences, or whether the standard atmospheres can provide an adequate representation of global atmospheric attenuation.

Section 3 presented the radiometric model and computation techniques used to determine the blackbody temperatures presented in this section Nine radiometers will be examined: the Nimbus II 3-4 μm (HRIR), 6-7 μm, and 10-11 μm (HRIR) channels and the Nimbus IV 6.7 μm (THIR) and 11.5 μm channels. The 3-4 μm channel, and the 10-12 μm channels are located in atmospheric windows; their values should be relatively independent of

atmospheric structure and composition, and highly dependent on surface temperature. The other two channels are located in the water vapor absorption band; the variations in their values should show a high correlation with the atmospheric variations seen in the moisture regions.

The blackbody temperatures will be presented for all the regions and standard atmospheres to permit a summary of global variability. They will then be examined for differences within the same latitudinal belts analyzed in Section 2 to determine the sensitivity of infrared transmission to atmospheric differences. Last, the radiometric values will be given for two typical suborbital tracks to allow an estimate of the actual variations encountered within one orbit.

4.2 Overview of the Regional Radiometric Data

Figure 4-1 presents the surface temperatures for the 45 regions for winter and for summer. It should be noted that the data for the Southern Hemisphere regions 37 to 45 for July appears with the Northern Hemisphere January regions and that the corresponding data for January is grouped with July. In the radiometric model, the earth was assumed to have an emissivity of 1; these temperatures are thus the effective blackbody temperatures at the earth's surface. The precipitable water values for these regions are the same as those discussed in Section 2; reference to those values, and to the plots of atmospheric structure, will be made throughout this section.

4.2.1 The Window Channels

The computed effective blackbody temperatures for the three "window" channels are presented in Figures 4-2 and 4-3. It is immediately clear that some attenuation has occurred in all channels, even though they are located in atmospheric "windows". None of the temperatures given should be taken as precise values of effective blackbody temperature due to approximations in the calibration and conversion from spectral radiance to blackbody temperature (this is especially true for the 3-4 μm channel); however, the errors are consistent for each channel permitting comparisons between the regions and some evaluation of the atmospheric effects.

The blackbody temperatures measured by 3-4 μm channel, and the two 10-11 μm channels, are highly dependent on the surface temperatures beneath the atmosphere. A glance at the figures show that the radiometric tempera-

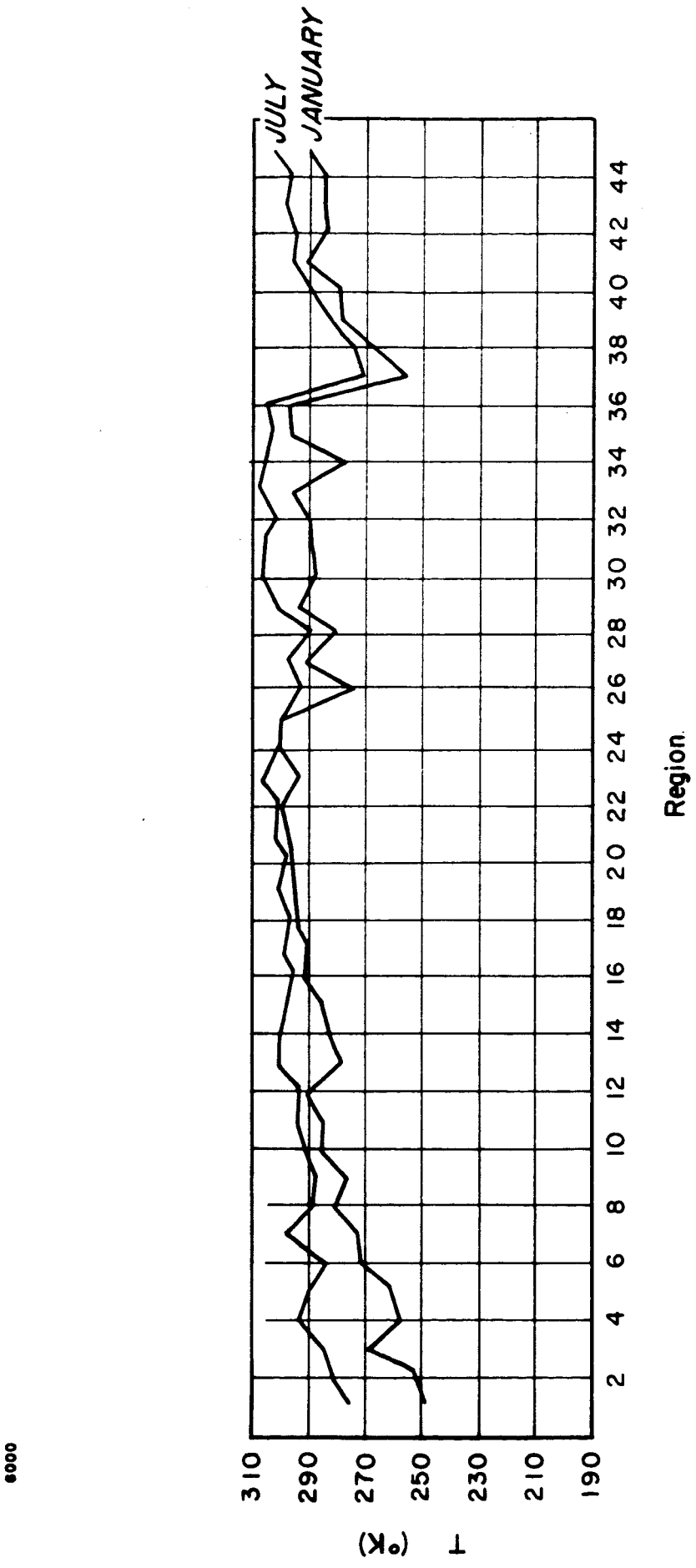

Figure 4-1 Region Surface Temperatures

6027

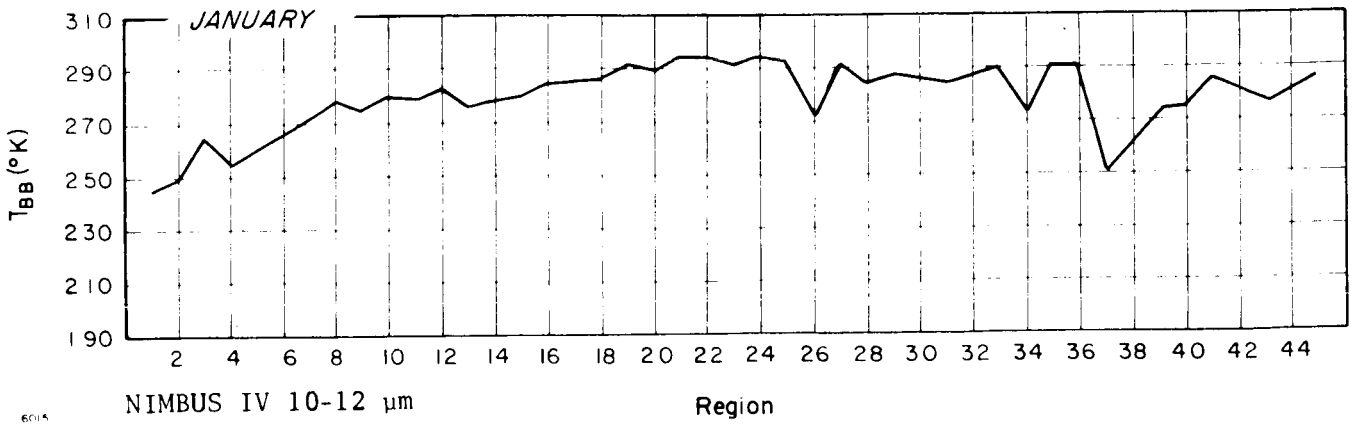

6015

NIMBUS IV 10-12 μm

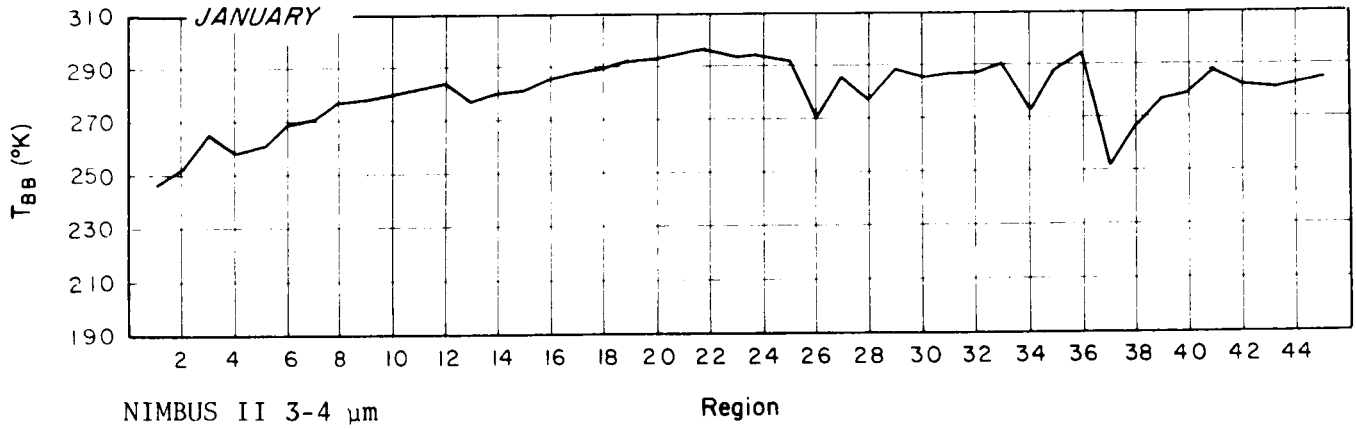

NIMBUS II 3-4 μm

6019

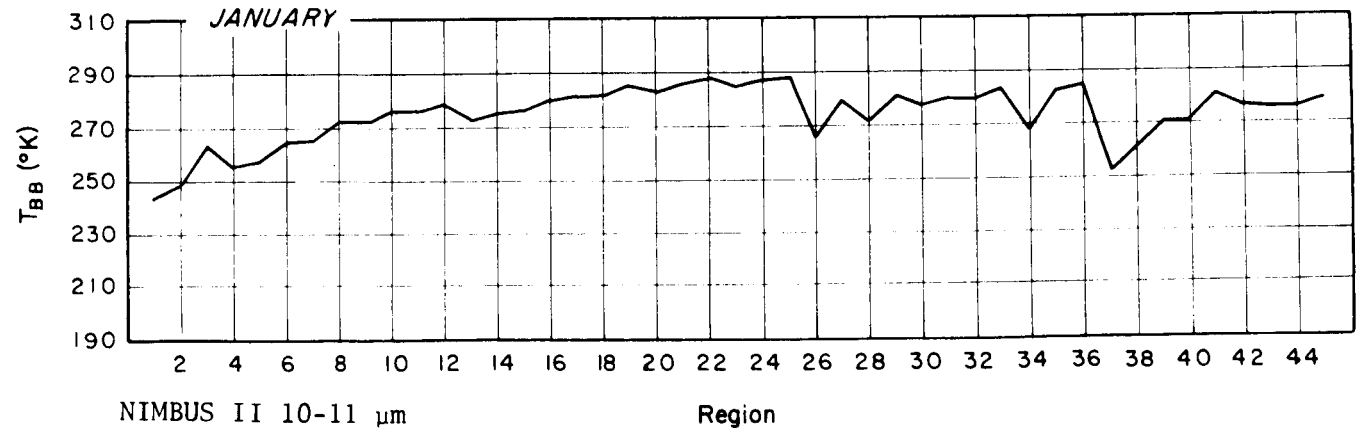

NIMBUS II 10-11 μm

Figure 4-2 "Window" Channel Blackbody Temperatures for the Winter Regions

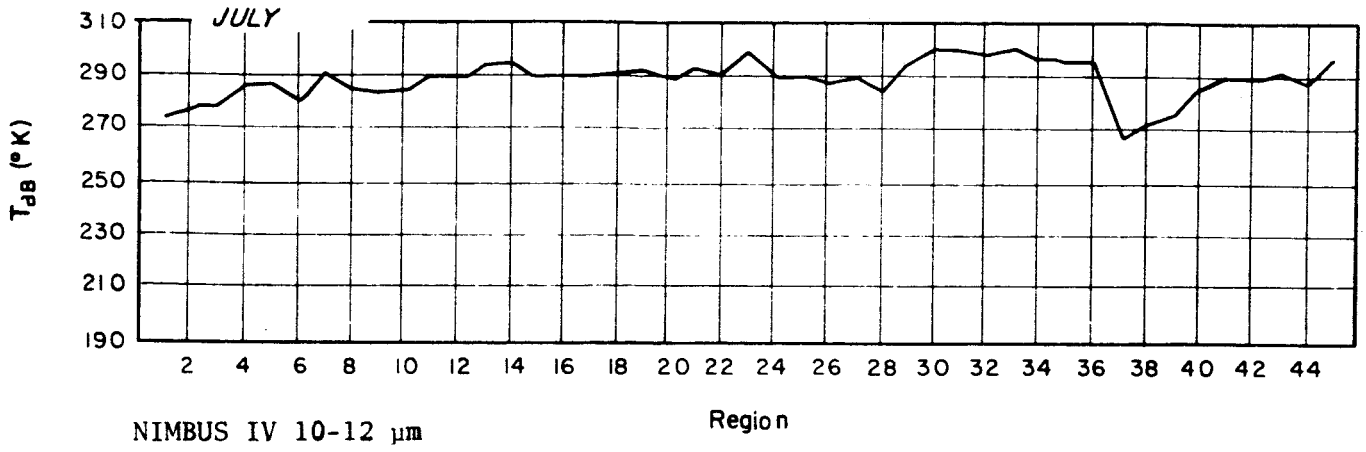

NIMBUS IV 10-12 μm

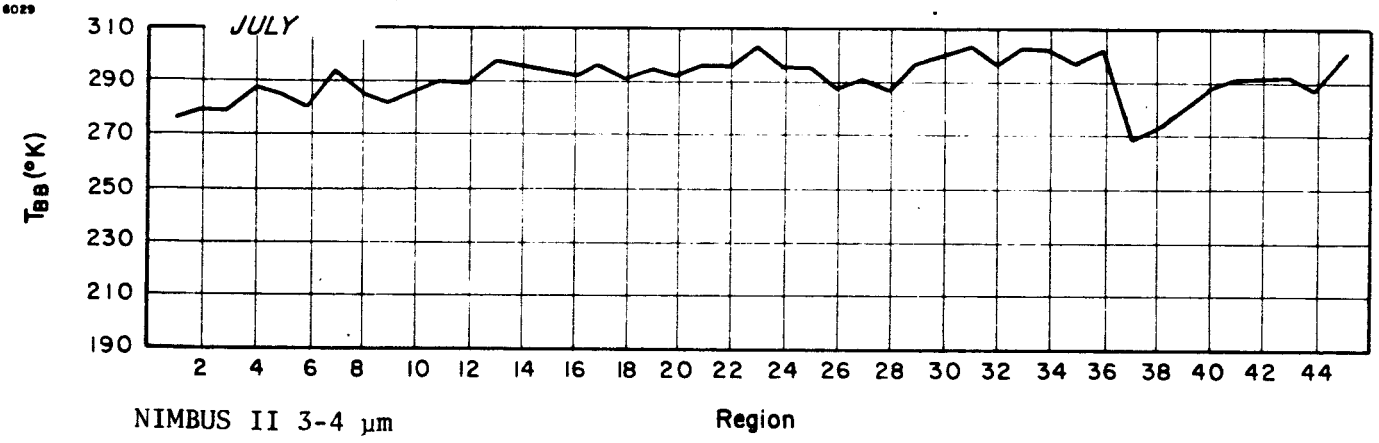

NIMBUS II 3-4 μm

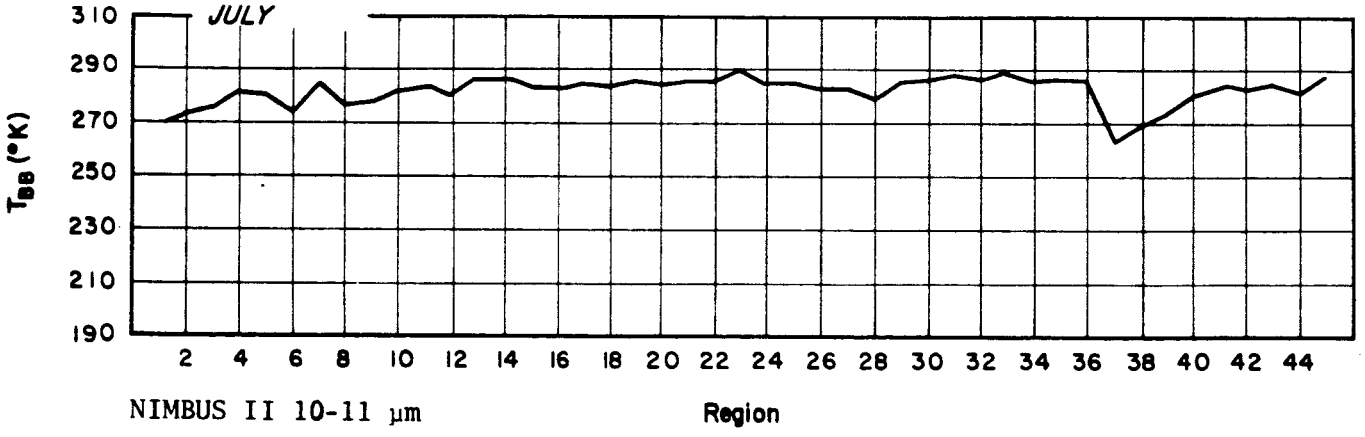

NIMBUS II 10-11 μm

Figure 4-3 "Window" Channel Blackbody Temperatures for the Summer Regions

tures generally increase with increasing surface temperature and decrease with decreasing surface temperature. However, all channels show the atmospheric contamination in that a complete correlation between the surface and radiometric temperatures does not exist; many changes are damped or accentuated by intervening water vapor. The two channels least attenuated - the Nimbus II 3-4 μm and the Nimbus IV 11.5 μm - are very close to the surface temperature in Regions 1, 2, 4, 5 and 37 during the winter. All of these regions have less than 0.5 g cm^{-2} of precipitable water for these seasons. On the other hand, temperature differences of 3°K for the 3-4 μm channel, and from 4 to 6°K for the 11.5 μm channel for Regions 16 to 22 in January show the attenuation due to 2 to 4 g cm^{-2} of precipitable water.

The Nimbus II 10-11 μm channel shows a much greater sensitivity to water vapor than the two channels previously discussed. Even in the driest winter regions the blackbody temperatures are 5°K colder than the surface values; those regions with high moisture content often show a temperature drop of 15° to 20°K. The range of temperatures is decreased from the range of surface temperatures by 6°K in the winter and 8°K in the summer; the most marked changes are in the hot, humid regions where the maximum temperatures recorded are 289° rather than 300°K in the winter and 290° rather than 306°K in the summer. In July Regions 17 through 22 all have blackbody temperatures within 2°K of the one another; yet the surface temperatures increase 4°K and the precipitable water vapor goes from 4 to 5 g cm^{-2}. On the other hand, in January the blackbody temperatures increase 7°K for a surface temperature increase of 8°K; in this season the precipitable water goes from 2 to 4 g cm^{-2}.

4.2.2 The Water Vapor Channels

The two 6-7 μm channels presented in Figures 4-4 and 4-5 exhibit totally different characteristics from those found for the three previously discussed channels. At these wavelengths, the absorbtivity due to water vapor is so high that very large decreases in temperature occur, and the differences in surface temperature are almost totally obscured. The NIMBUS II channel runs 1-2°K colder than the NIMBUS IV with values between 225°K and 255°K in the winter, and between 235°K and 255°K in the summer. Comparison of these blackbody temperatures with the precipitable water for the same regions reveals, as expected, a very high inverse correlation. To

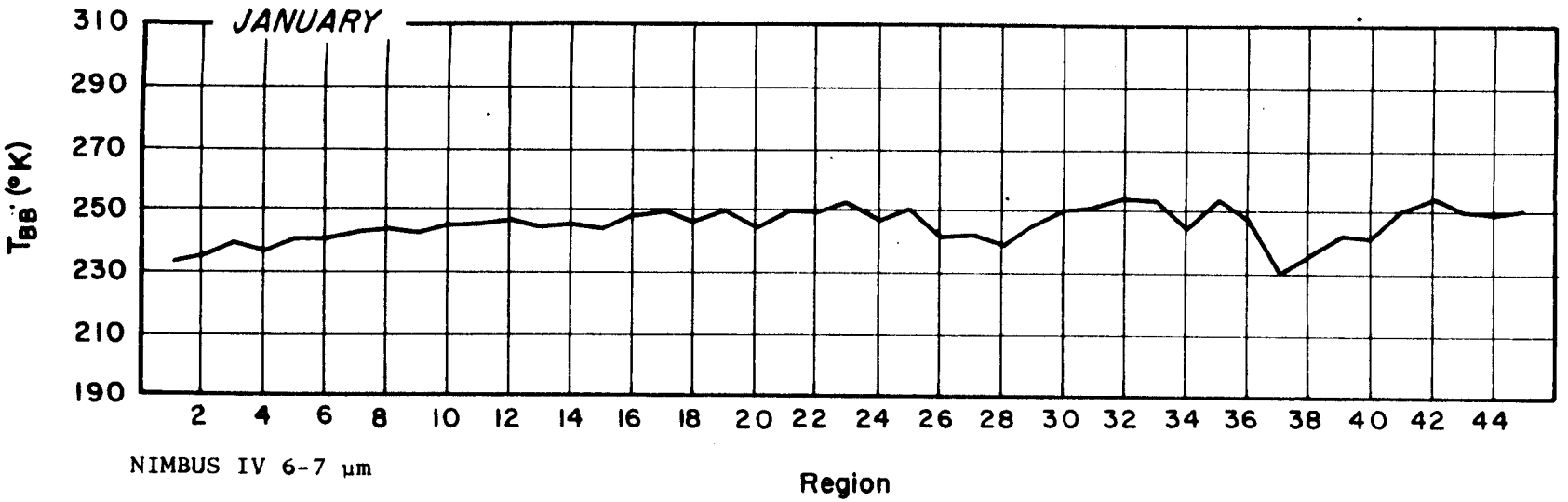

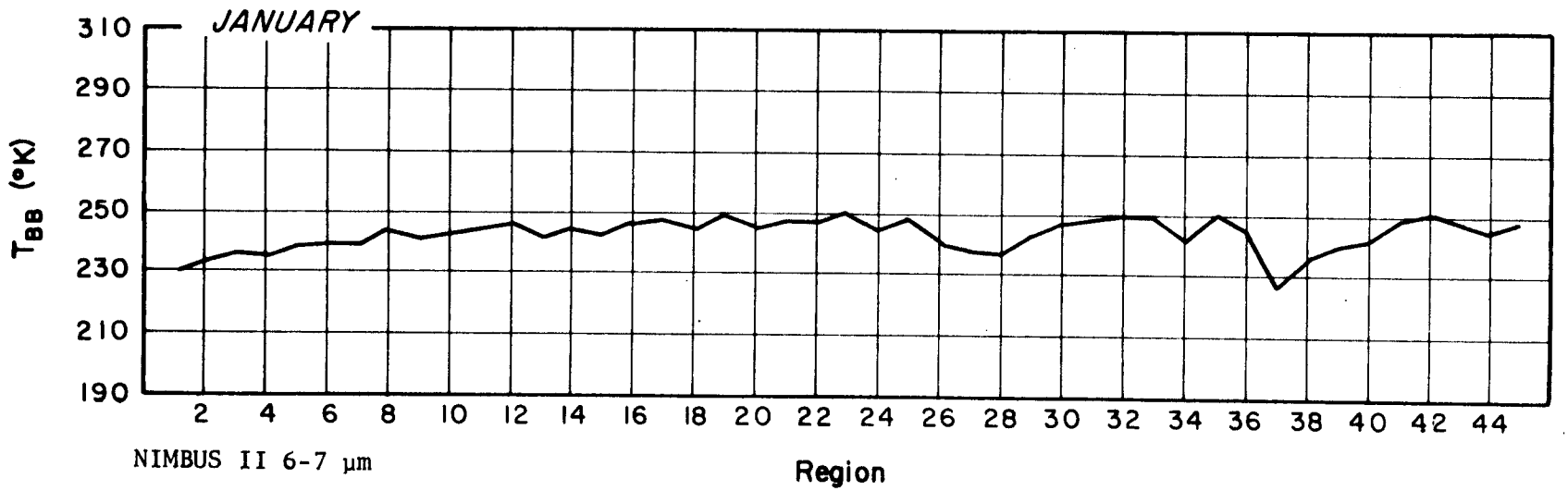

Figure 4-4 "Water Vapor" Channel Blackbody Temperatures for the Winter Region

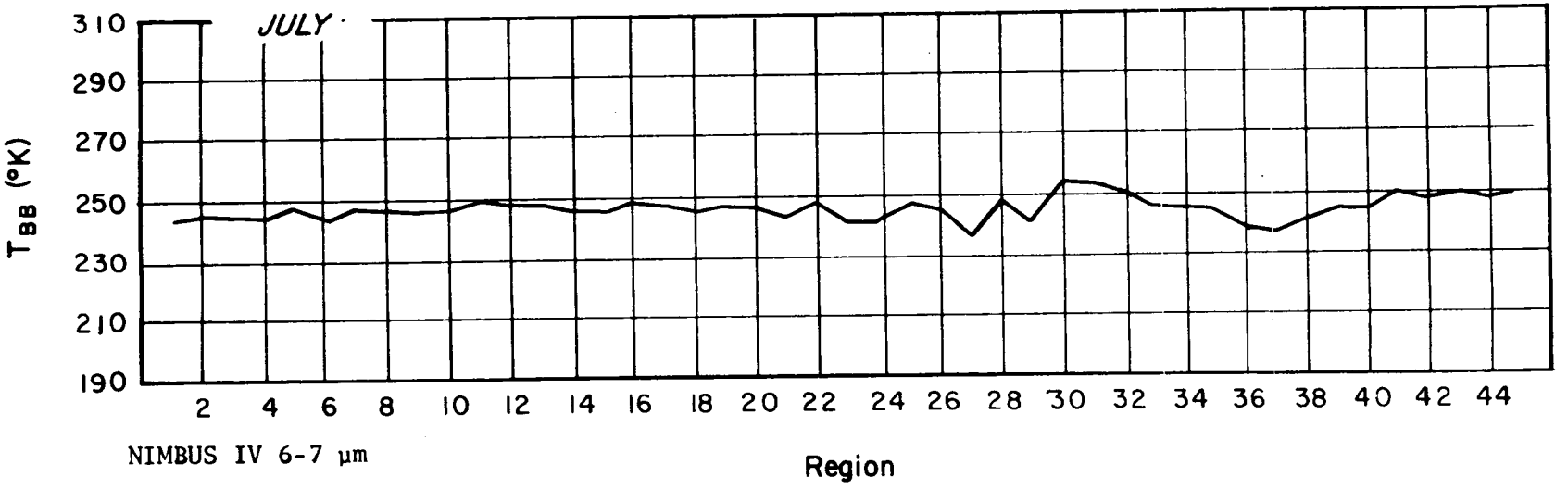

NIMBUS IV 6-7 μm

6030

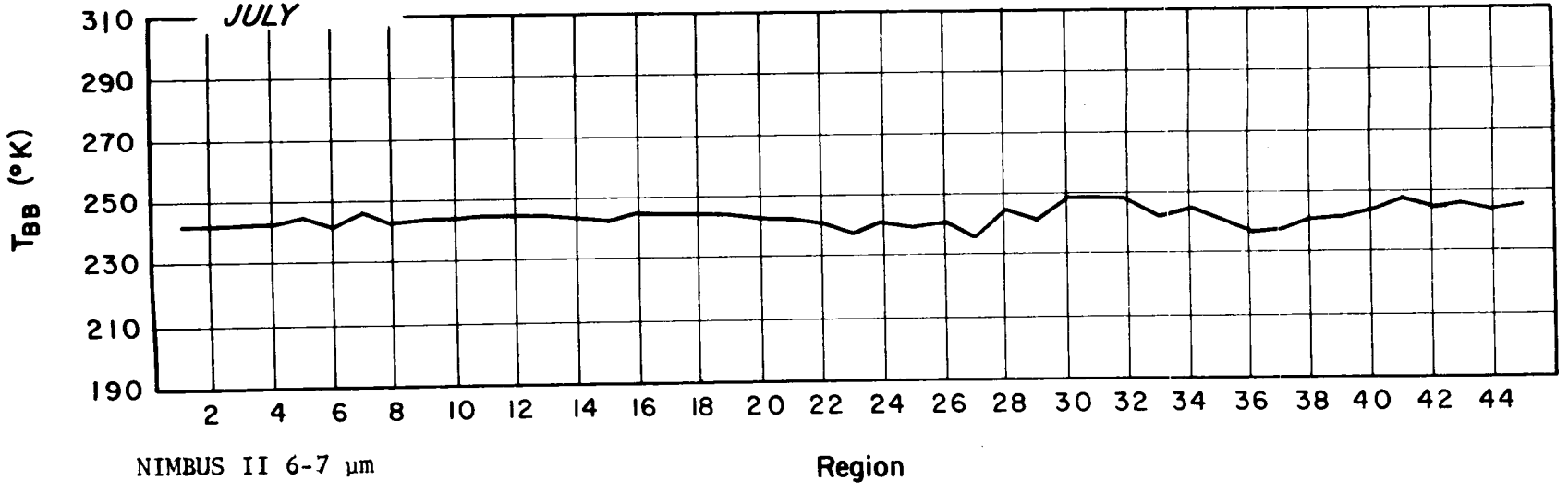

NIMBUS II 6-7 μm

Figure 4-5 "Water Vapor" Channel Blackbody Temperatures for the Summer Region

obtain the fairly smooth blackbody temperature plots, some influence of the surface temperature is clearly evident; since the temperature differences increase from 15°K in the Arctic to 50°K in the tropics (and to 66°K in the monsoon season of Region 36), a compensatory increase of 39° to 50°K in surface temperature is necessary to maintain most of the blackbody temperatures in the 240° to 250°K temperature range. It is intuitively clear that the higher moisture values are usually associated with the higher surface temperatures; where this is not so (e.g., Regions 33-35 July), significant changes in these blackbody temperatures do occur.

4.3 Comparison with the Standard Atmospheres

The blackbody temperatures computed for the standard atmospheres are given in Figures 4-6 and 4-7. Since only nine values represent all latitudinal belts for both seasons, both January and July appear together in the plot of each channel. For clarity, a plot of the standard atmosphere surface temperatures is given in Figure 4-7.

The range of blackbody temperatures computed from the standard atmospheres duplicates well the range computed from the 4-D atmospheres; only the extremely hot values in the "window" channels corresponding to the summer deserts, and the extremely cold values in the "water vapor" channels corresponding to the Antarctic winter, are not reproduced. To permit comparisons between the two data sets, all blackbody temperatures computed from the region data were regrouped by latitudinal belts and appear in Figures 4-8 through 4-17. Since surface temperatures vary greatly within each zone, and since the differences between the surface temperatures and the blackbody temperatures are the values most representative of atmospheric attenuation, Figures 4-18 through 4-27 present the "window channel" temperature differences applicable to each latitudinal belt. On the temperature difference plots, the value computed from the appropriate standard atmosphere appears as a constant across the graph; both sets of figures may be easily compared with the precipitable water plots given in Figures 2-14 through 2-23.

4.3.1 The Arctic and Antarctic Zones

The actual blackbody temperatures computed from the standard atmospheres for 75°N (Figures 4-8 and 4-9) correspond well to the values computed from

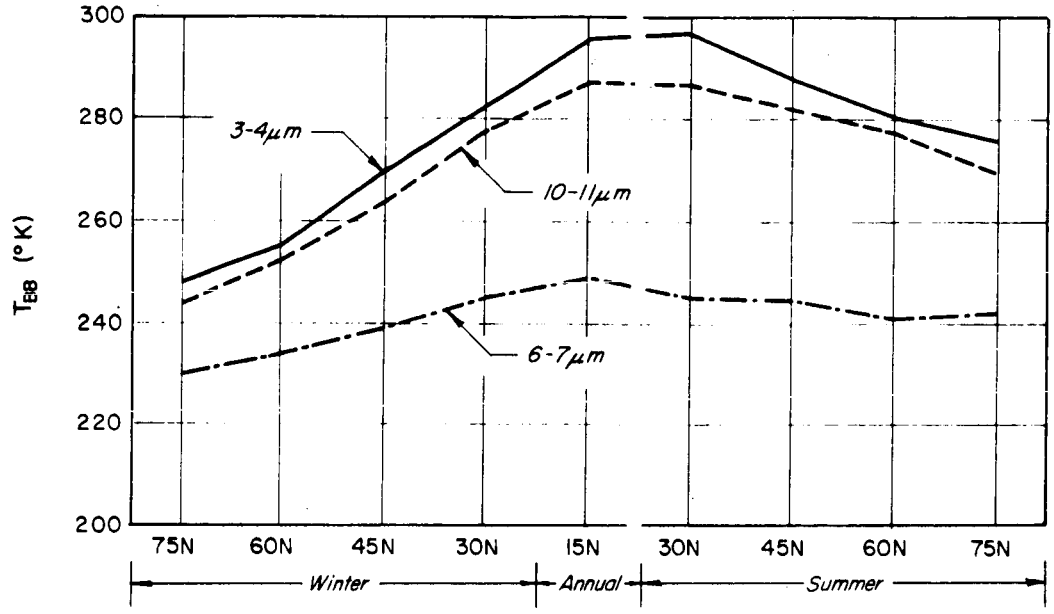

Figure 4-6 NIMBUS II Blackbody Temperatures for the Standard Atmospheres

6087

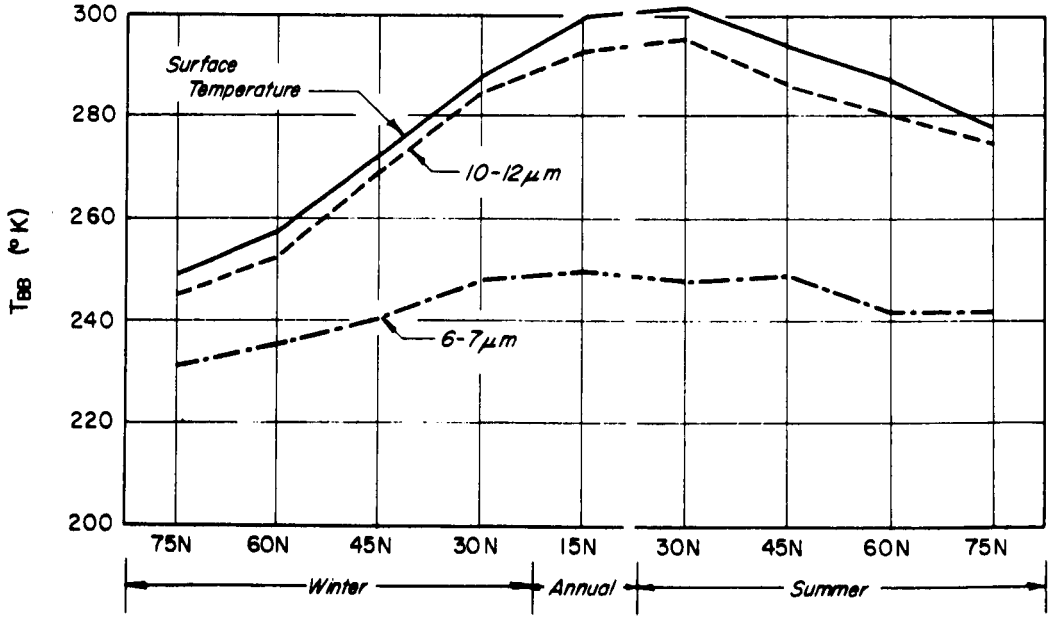

Figure 4-7 Surface Temperatures and NIMBUS IV Blackbody Temperatures for the Standard Atmospheres

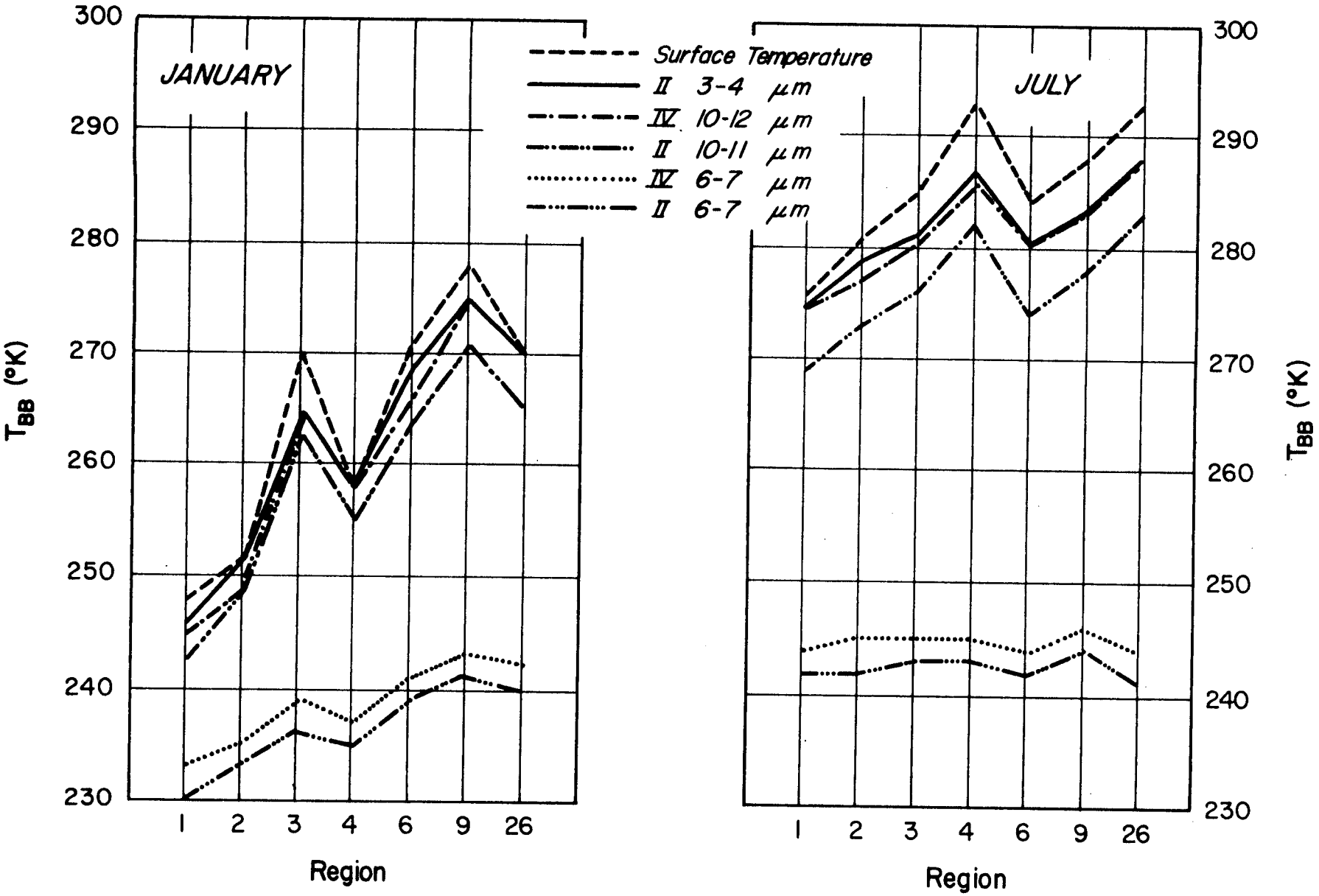

Figure 4-8 Blackbody Temperatures 60.75° -90°N

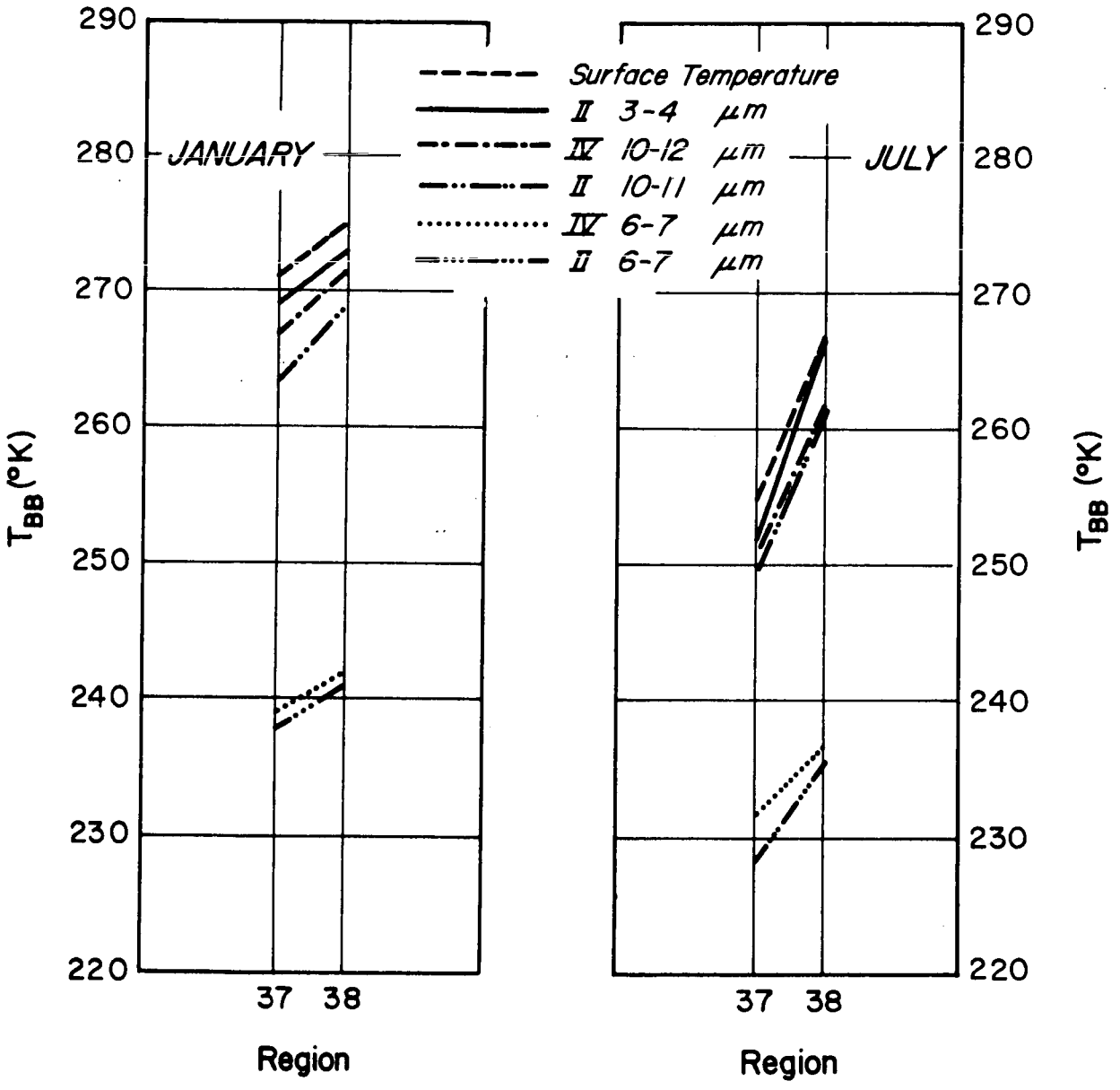

Figure 4-9 Blackbody Temperatures 60.75° -90°S

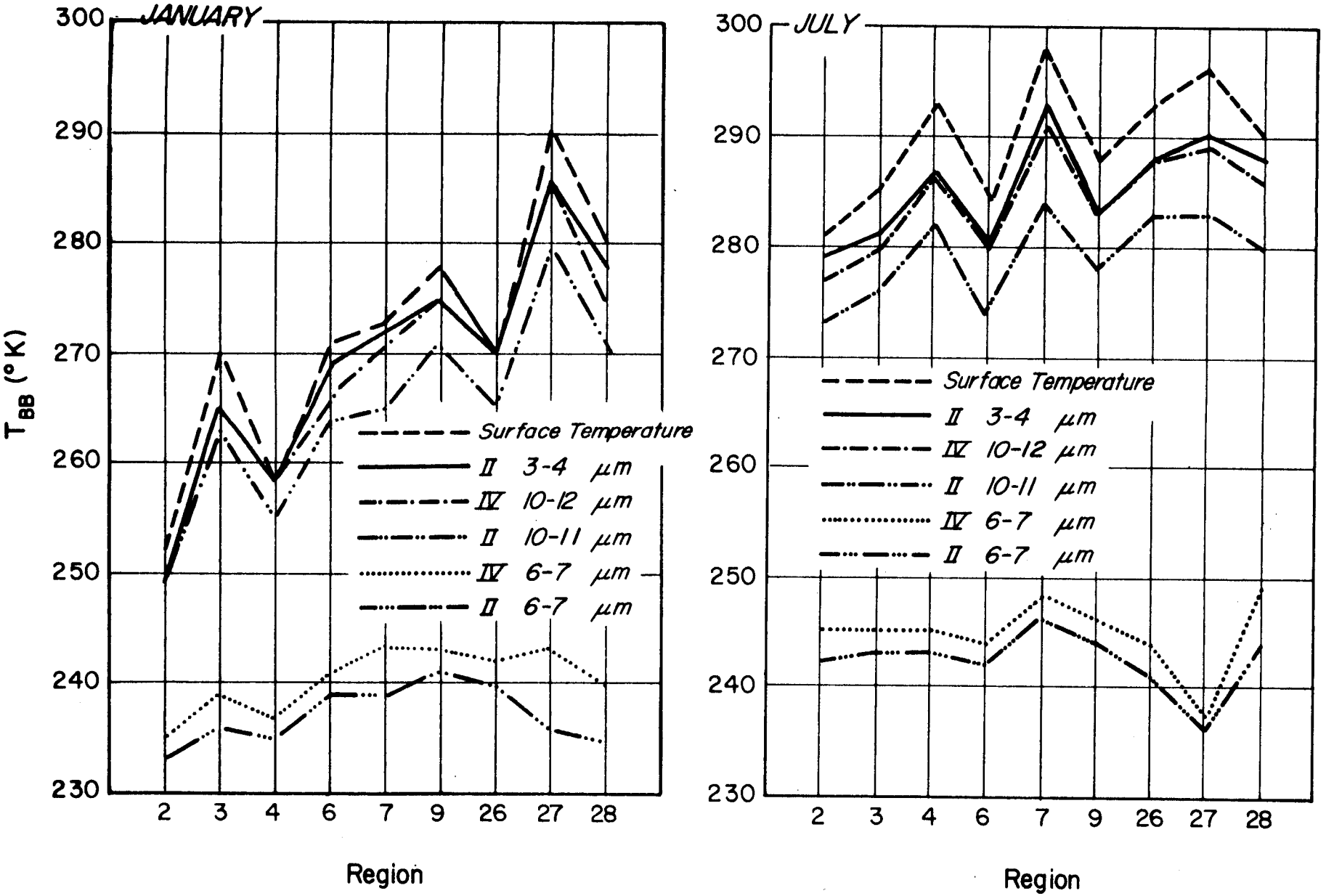

Figure 4-10 Blackbody Temperatures 50.25° -60.75°N

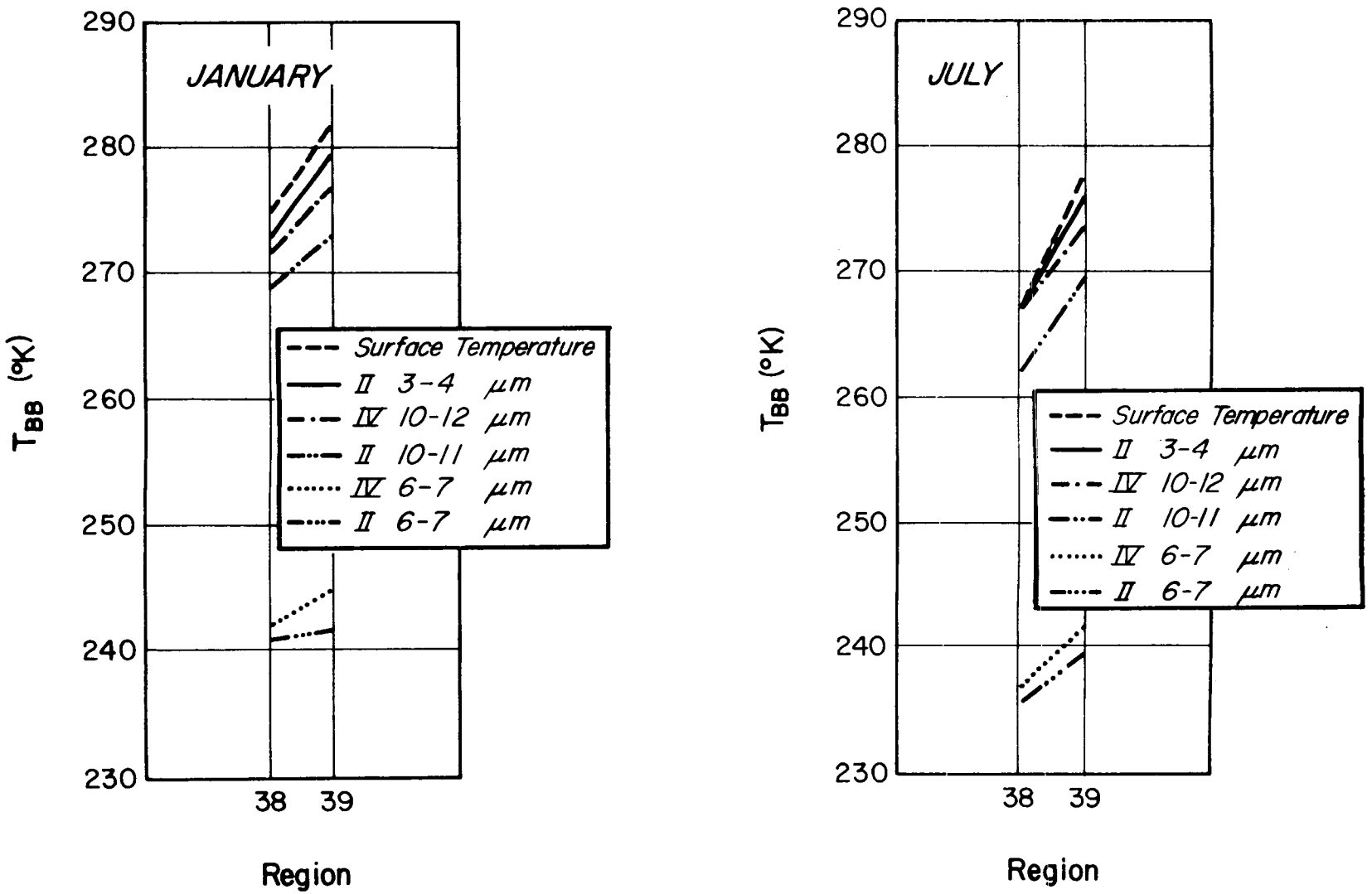

Figure 4-11 Blackbody Temperatures 50.25° -60.75°S

6102

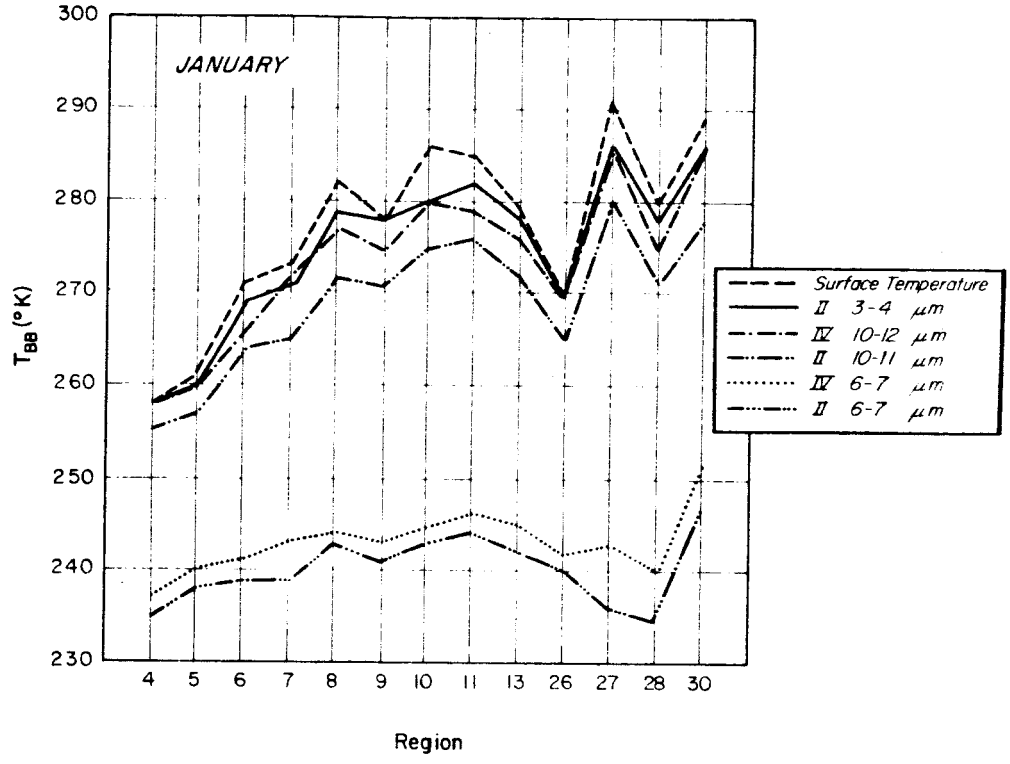

6103

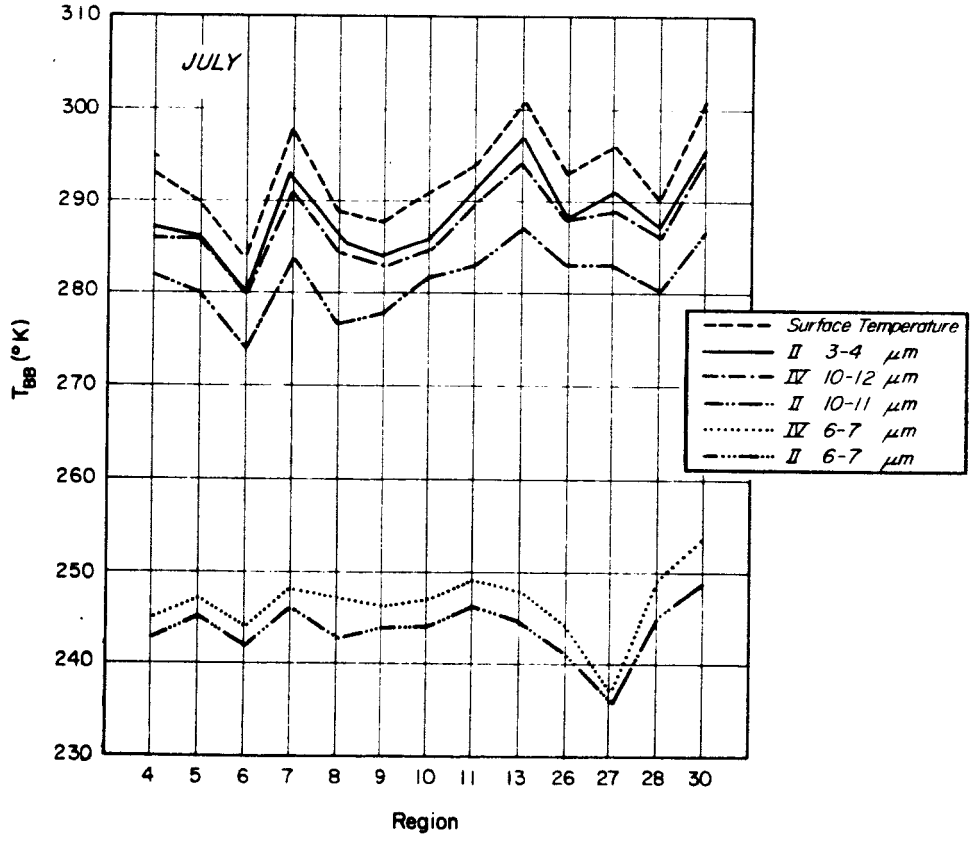

Figure 4-12 Blackbody Temperatures 37.5° -50.25°N

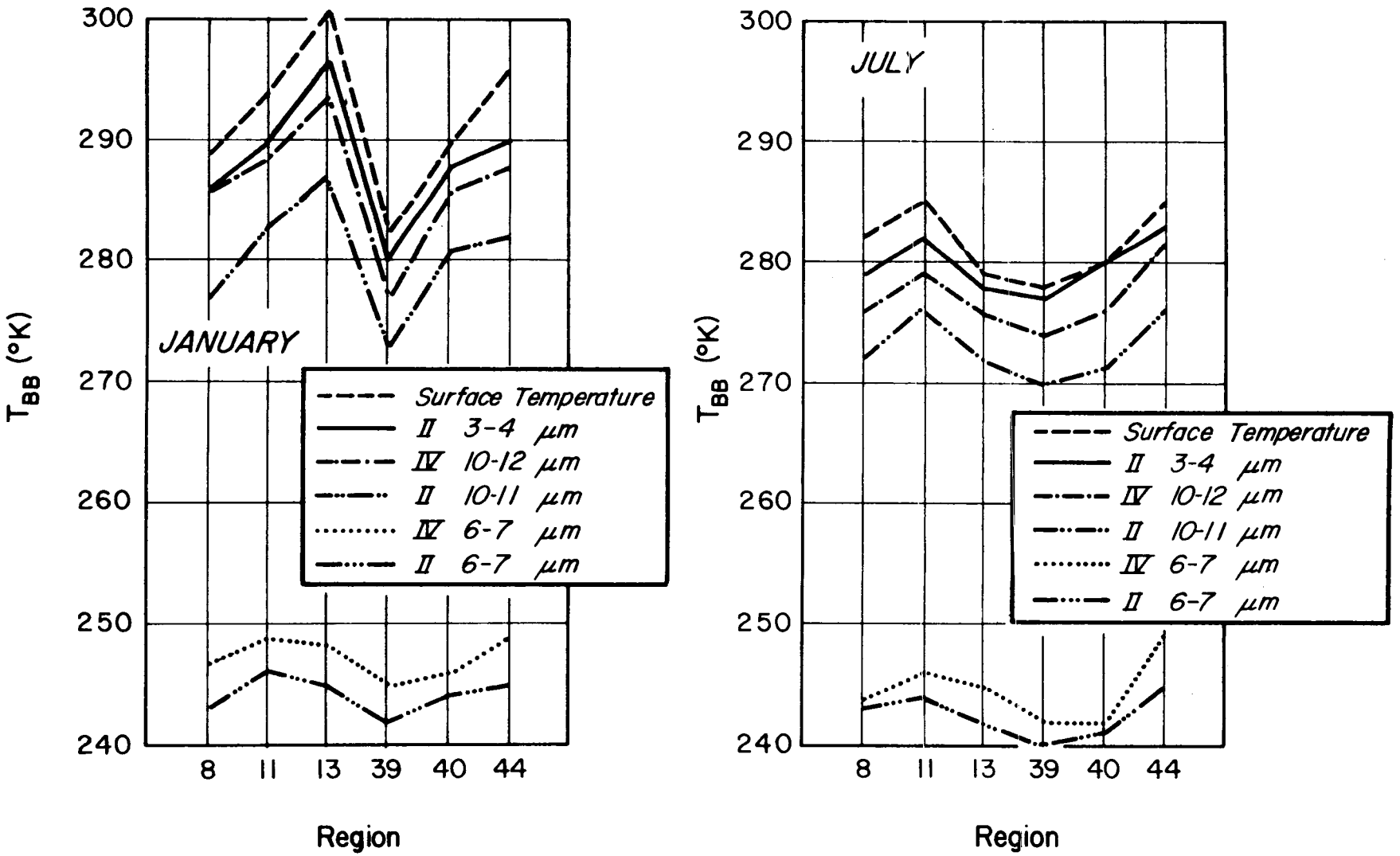

Figure 4-13 Blackbody Temperatures 37.5° -50.25°S

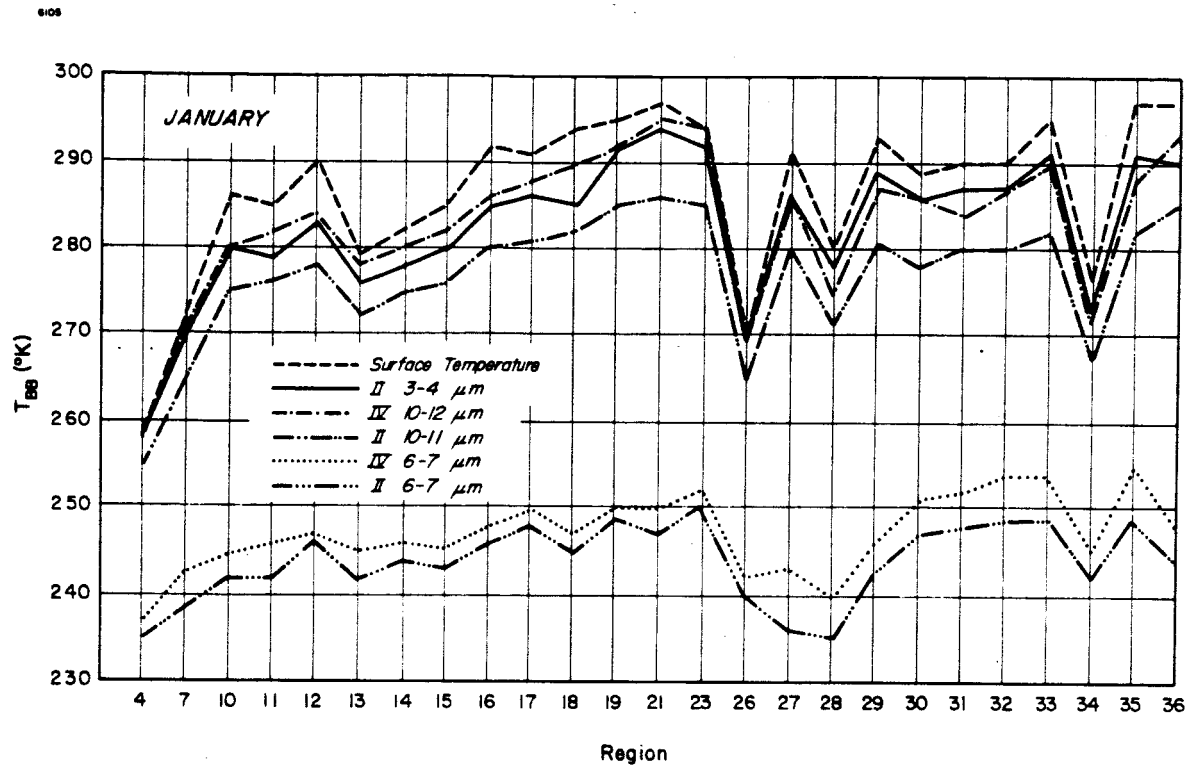

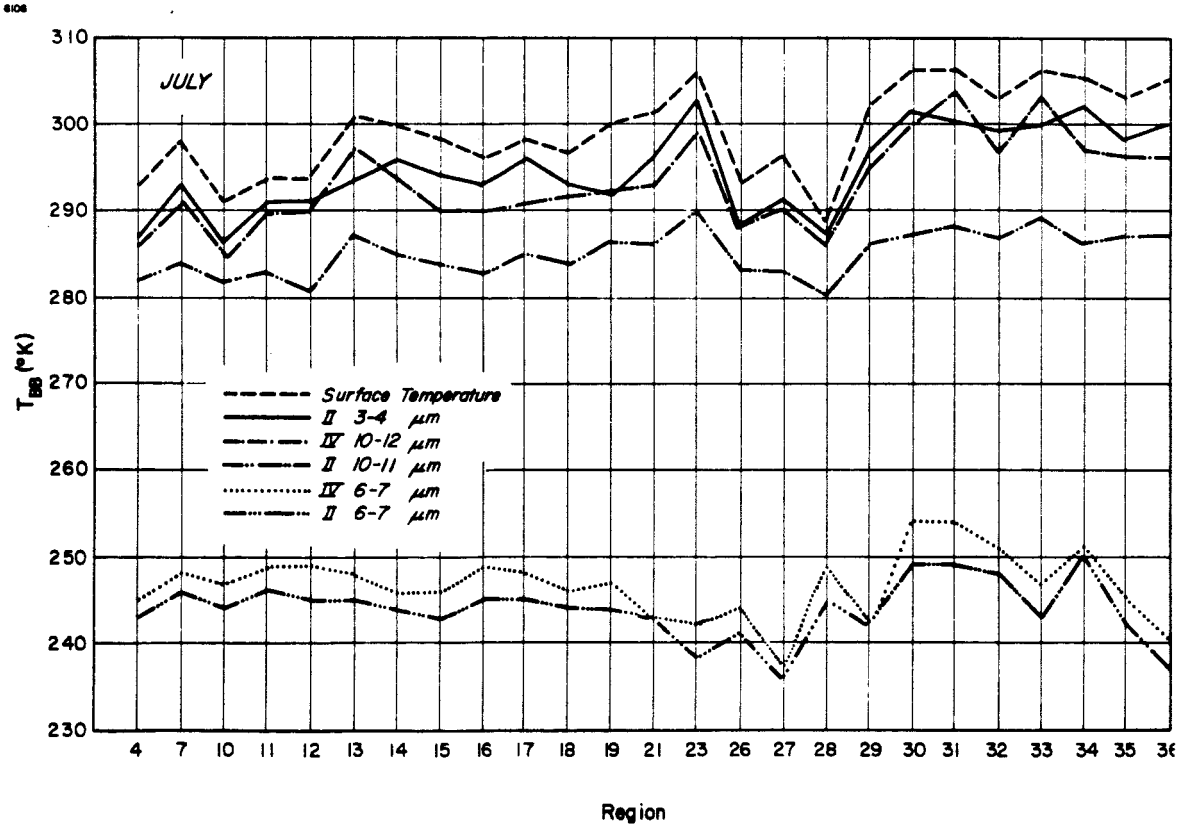

Figure 4-14 Blackbody Temperatures 22.5° -37.5°N

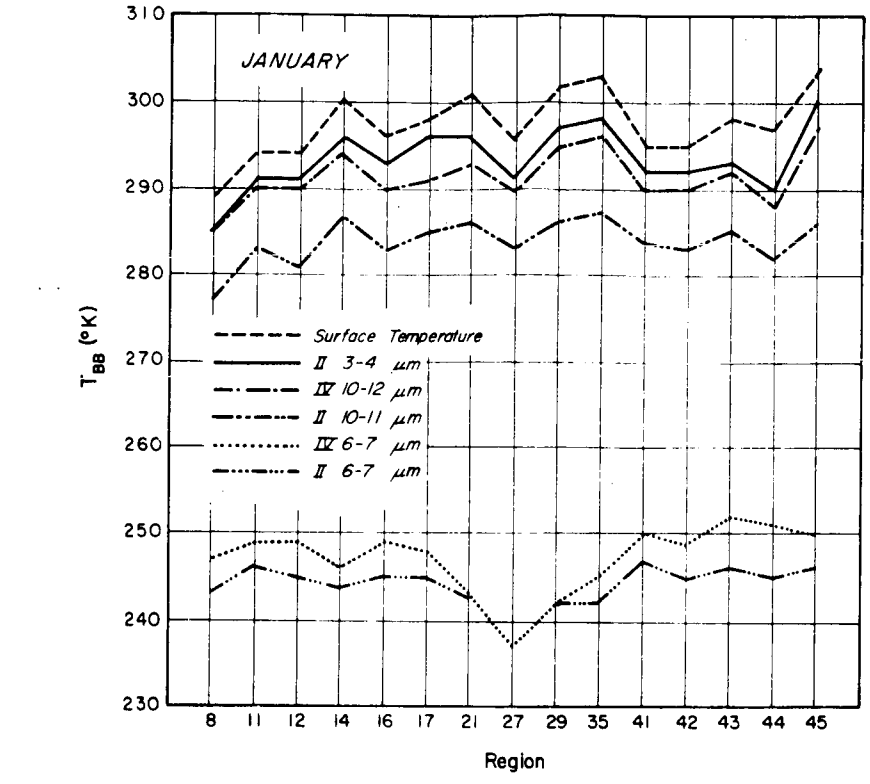

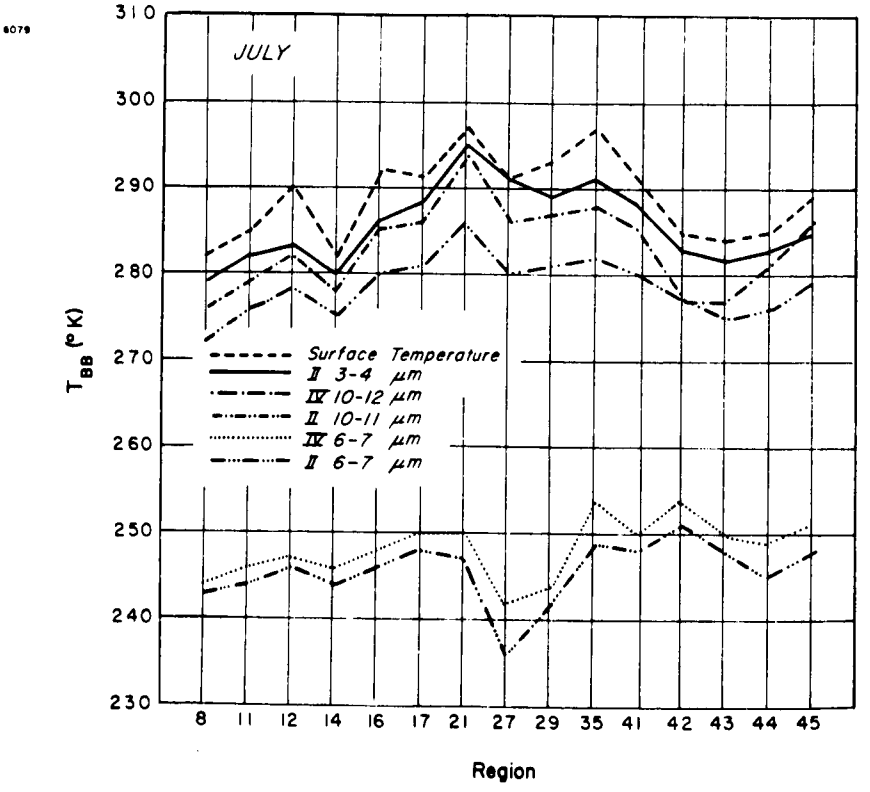

Figure 4-15 Blackbody Temperatures 22.5° -37.5°S

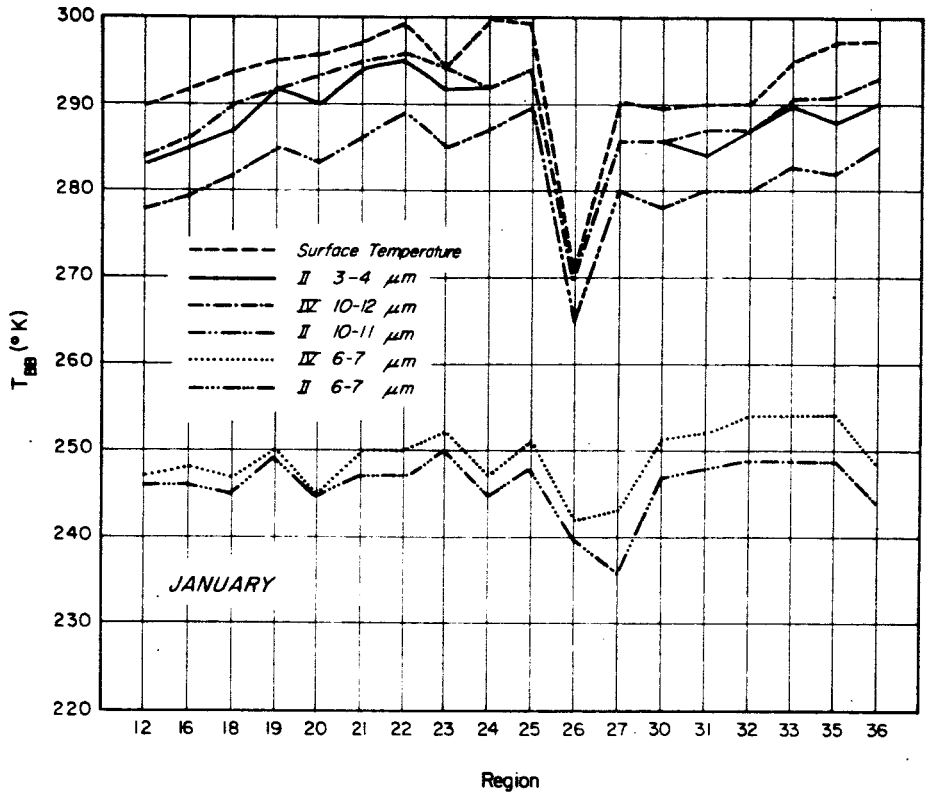

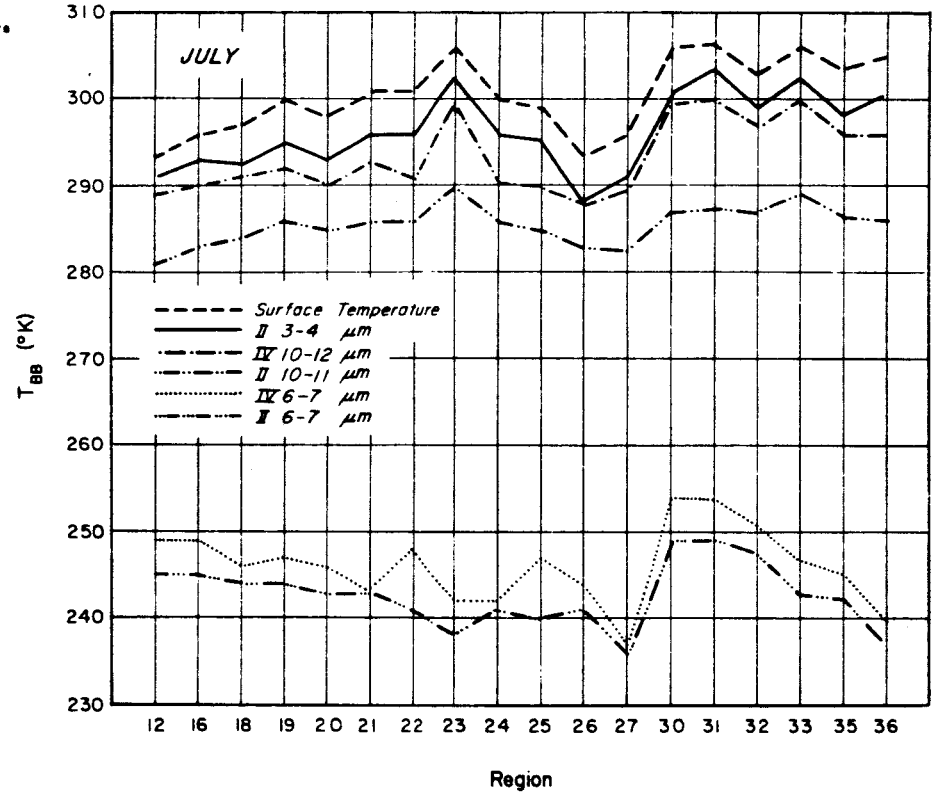

Figure 4-16 Blackbody Temperatures 0^{o} -22.5^{o}N

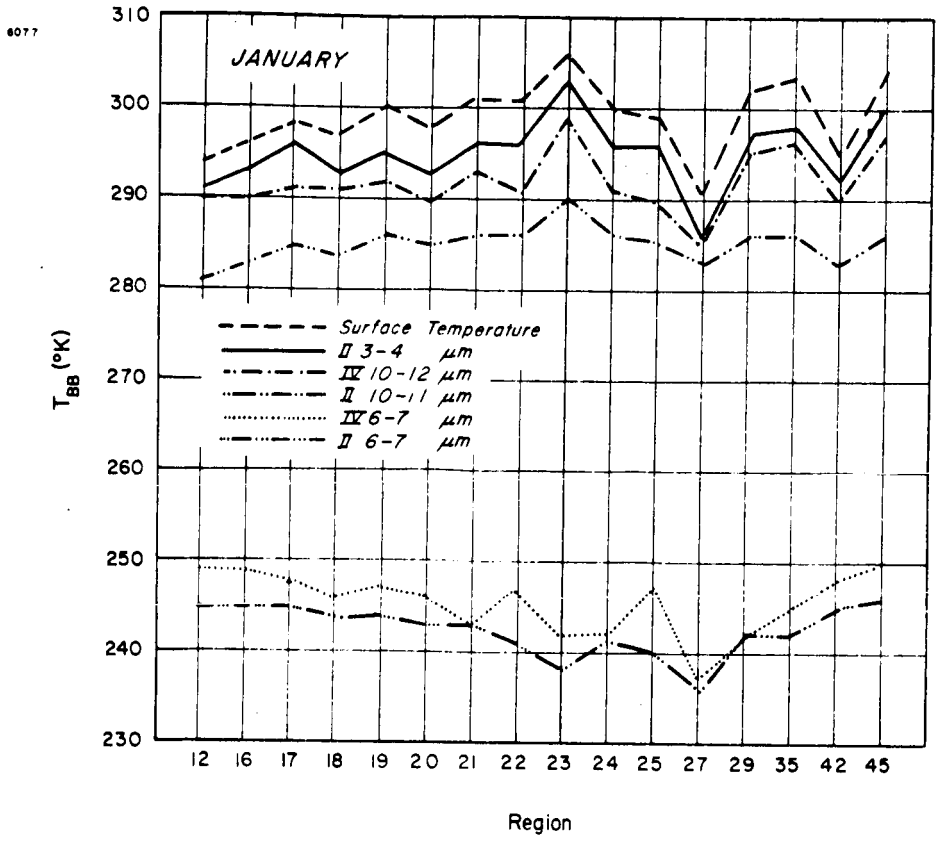

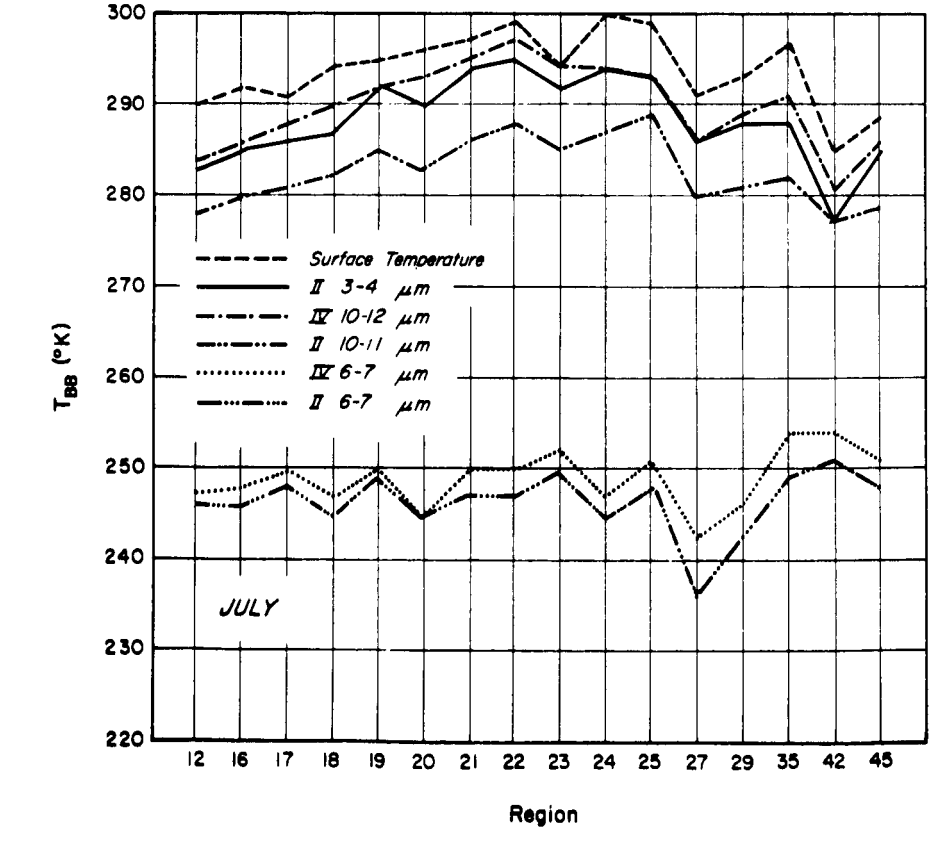

Figure 4-17 Blackbody Temperatures 0^{o} -22.5^{o}S

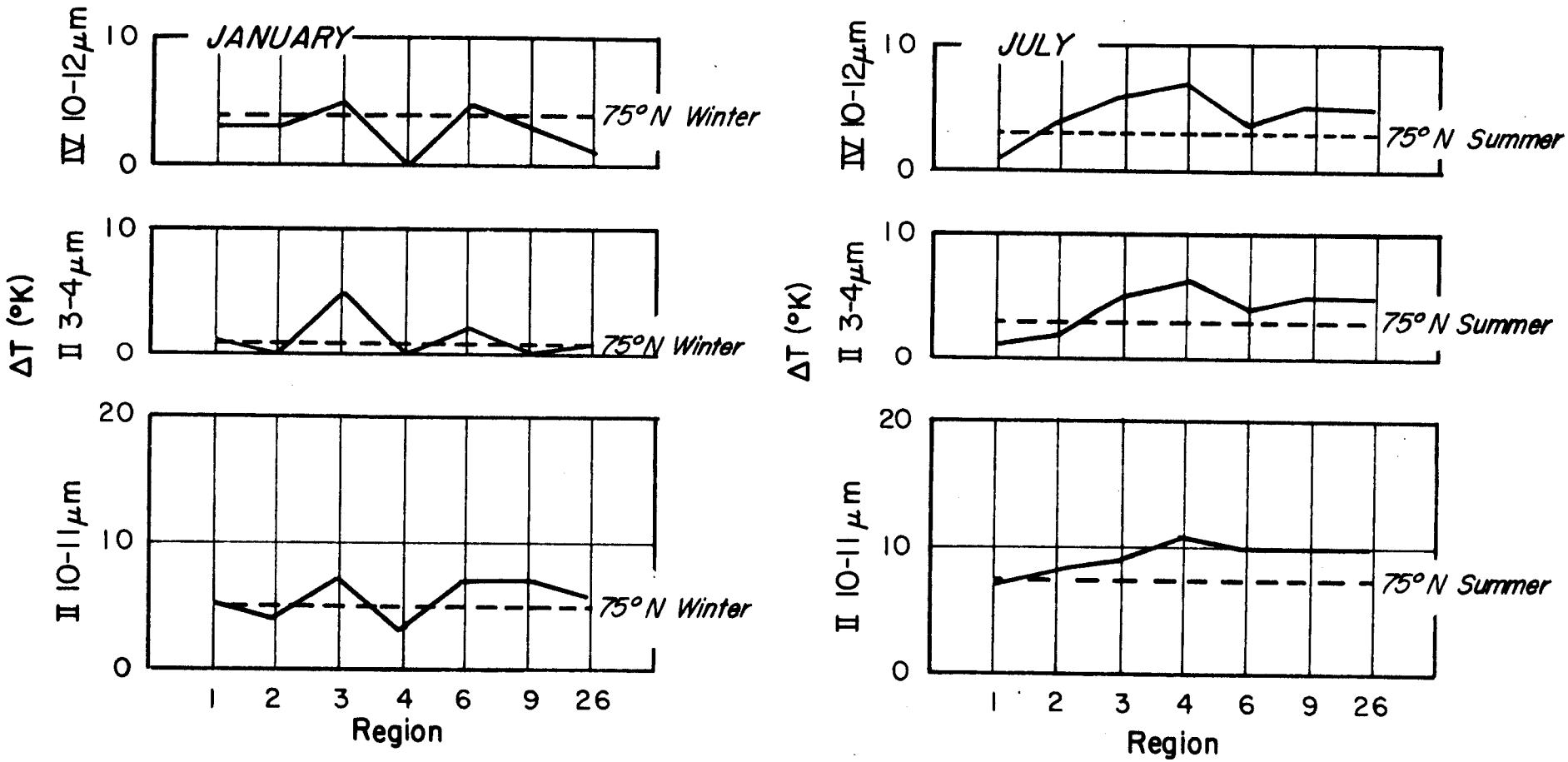

Figure 4-18 "Window" Channel Blackbody Temperature Decrease 60.75° -90°N

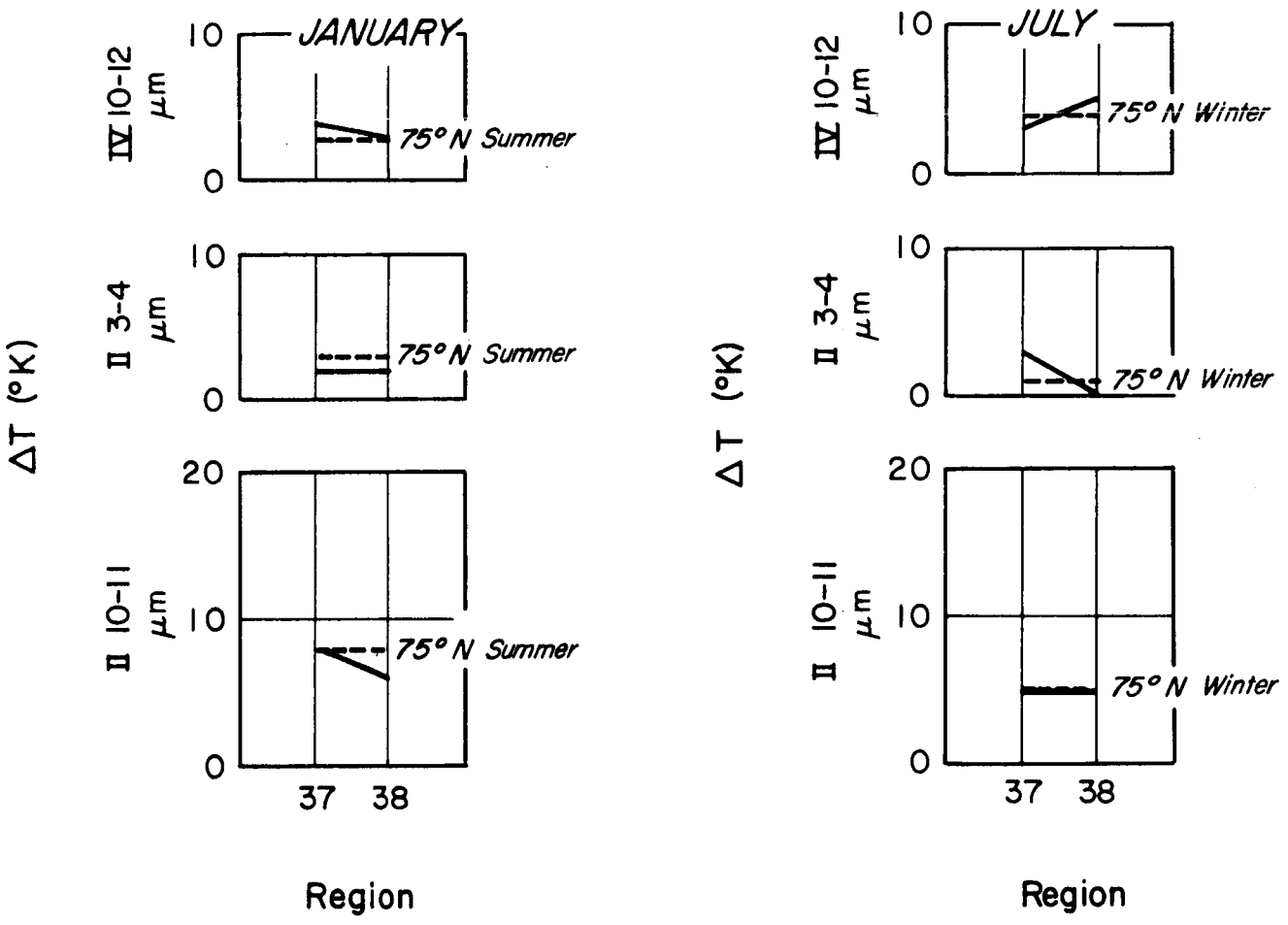

Figure 4-19 "Window" Channel Blackbody Temperature Decrease 60.75° -90°S

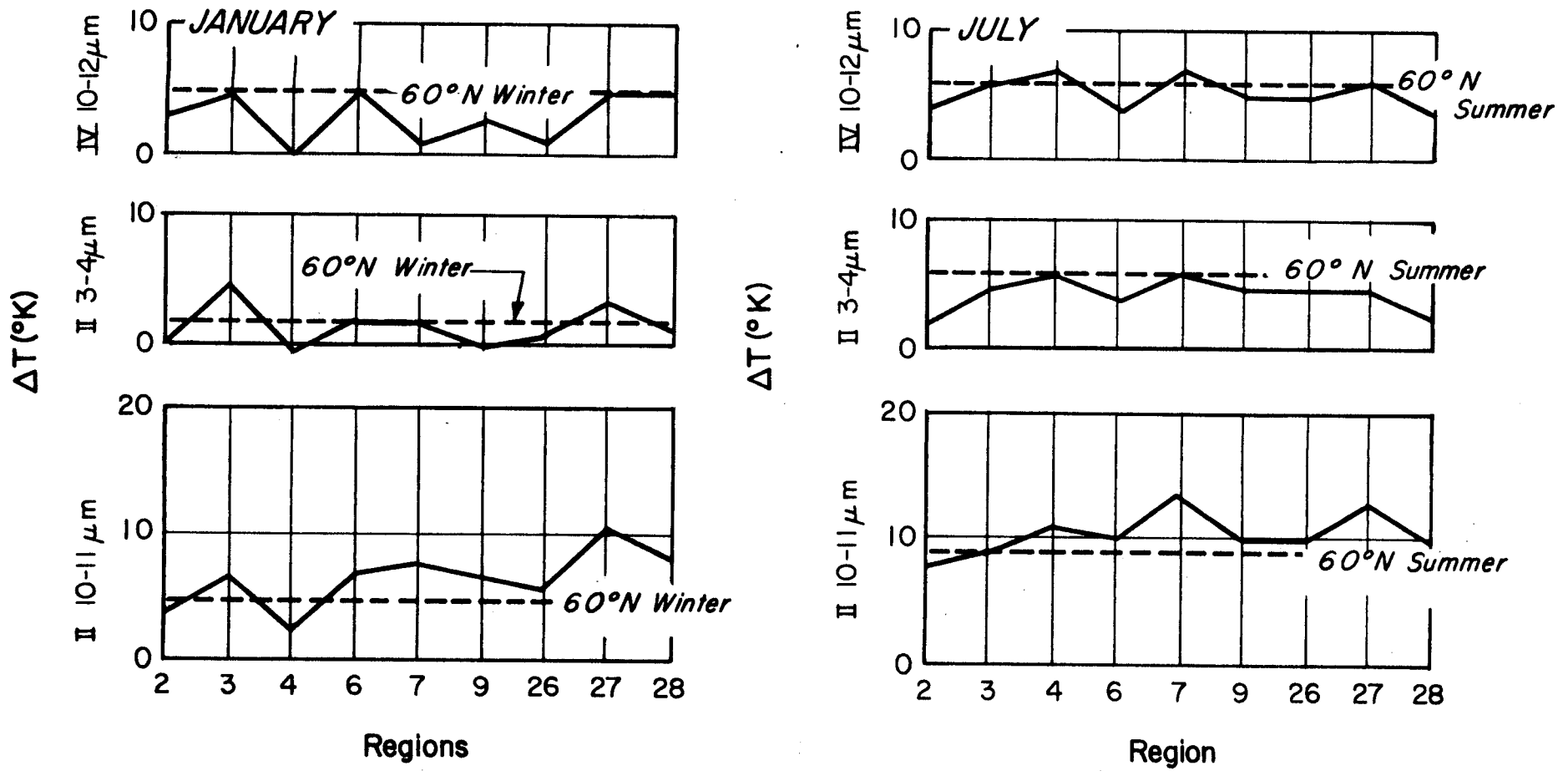

Figure 4-20 "Window" Channel Blackbody Temperature Decrease 50.25° -60.75°N

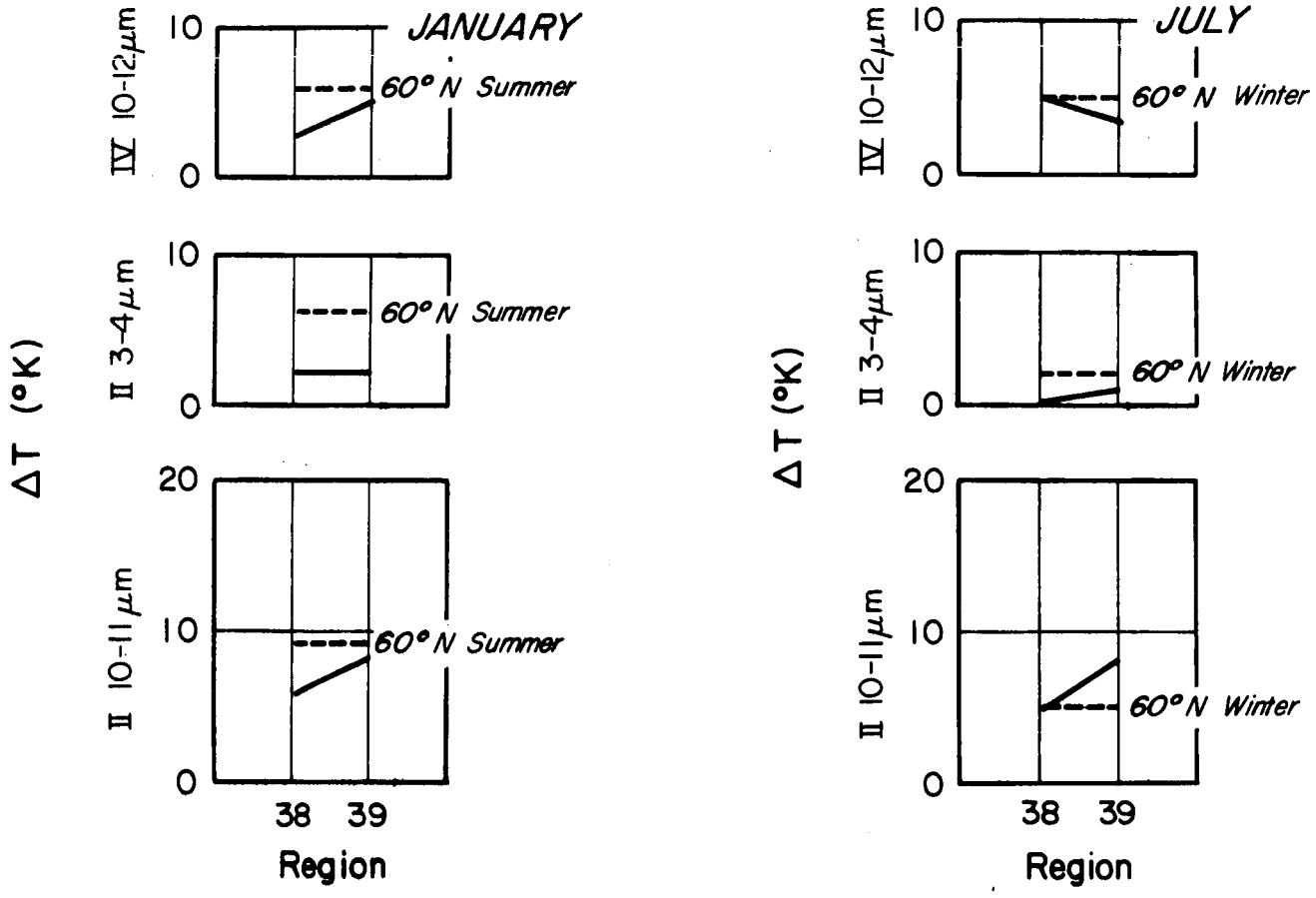

Figure 4-21 "Window" Channel Blackbody Temperature Decrease 50.25° -60.75°S

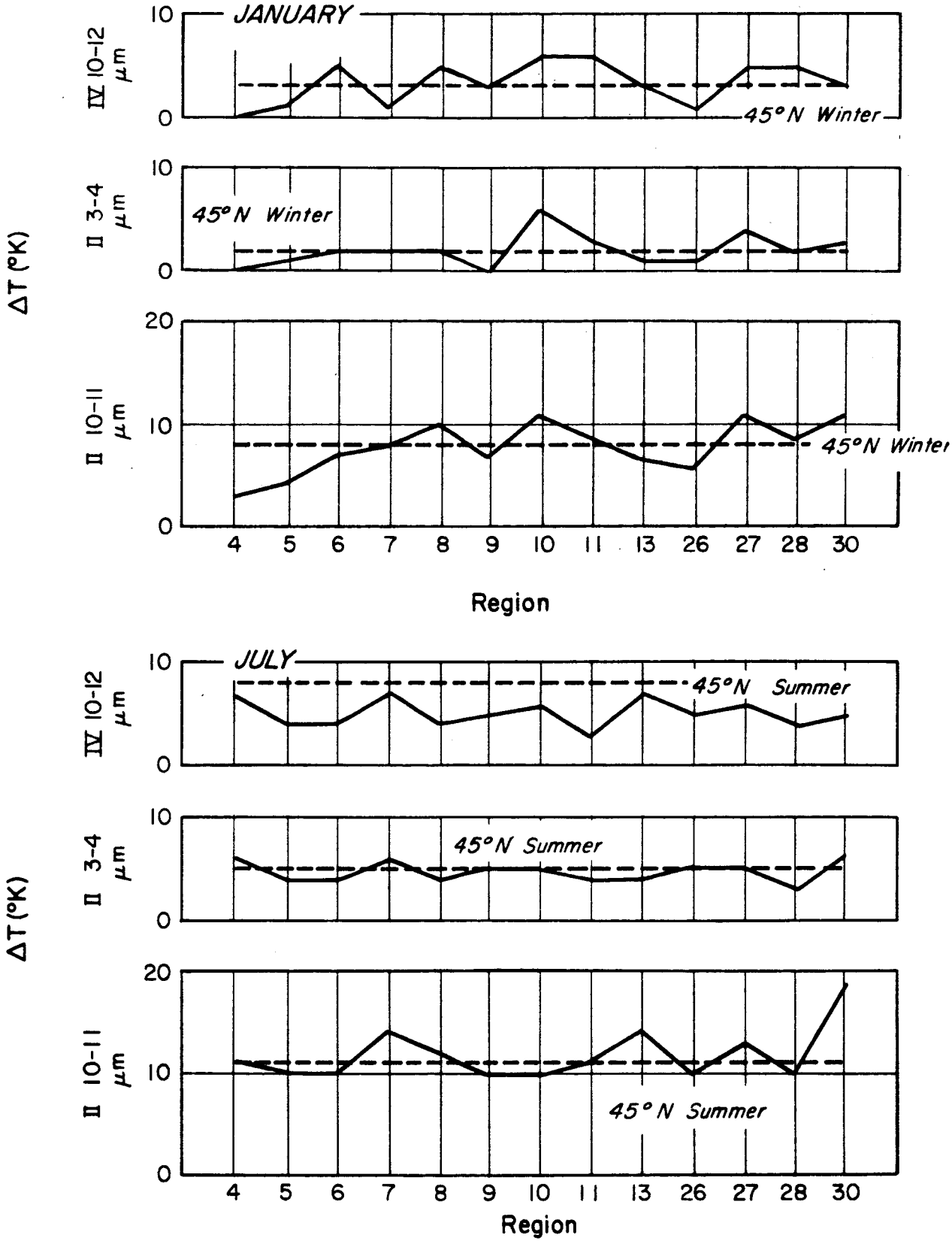

Figure 4-22 "Window" Channel Blackbody Temperature Decrease 37.5° -50.25°N

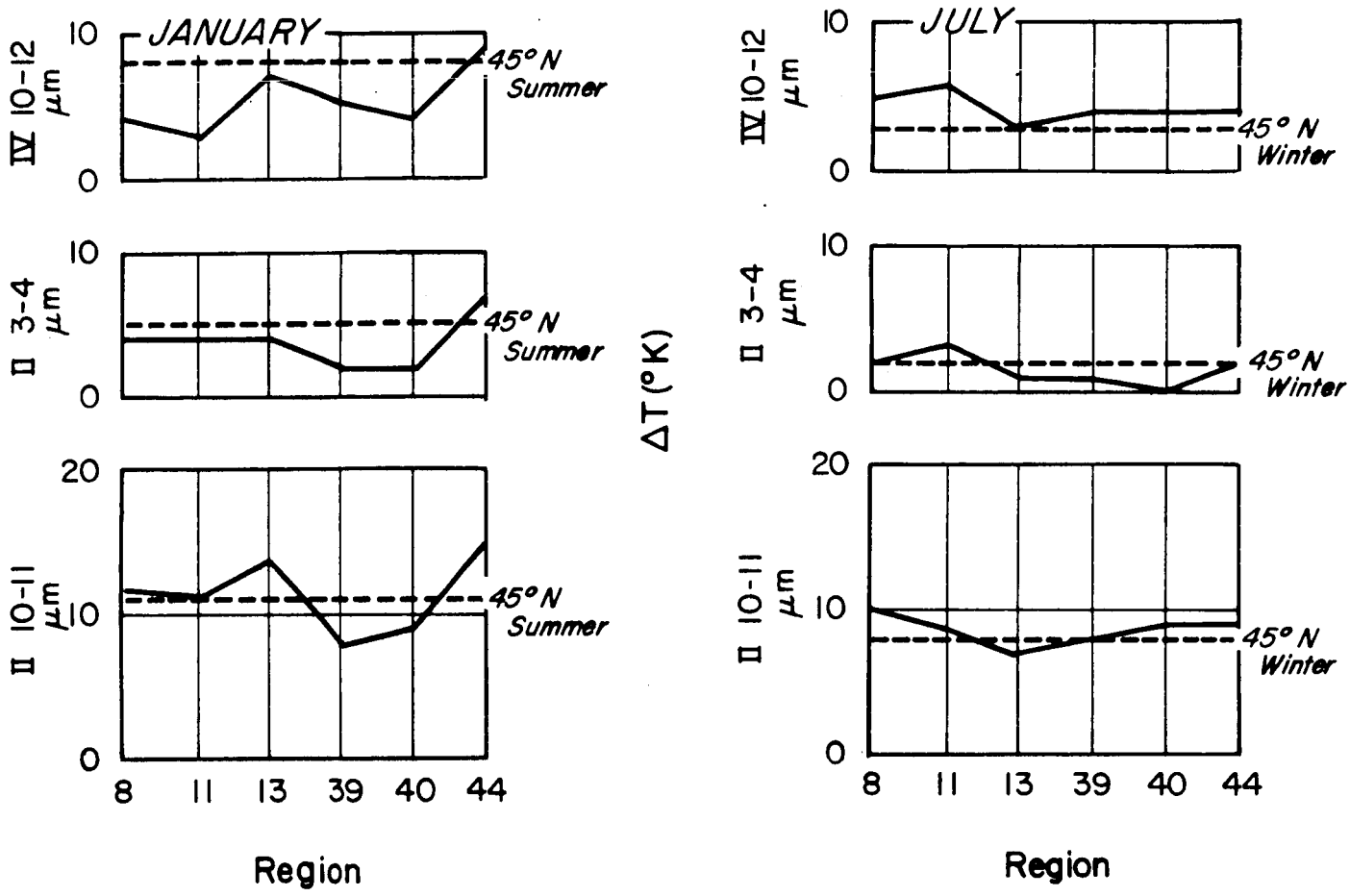

Figure 4-23 "Window" Channel Blackbody Temperature Decrease 37.5° -50.25°S

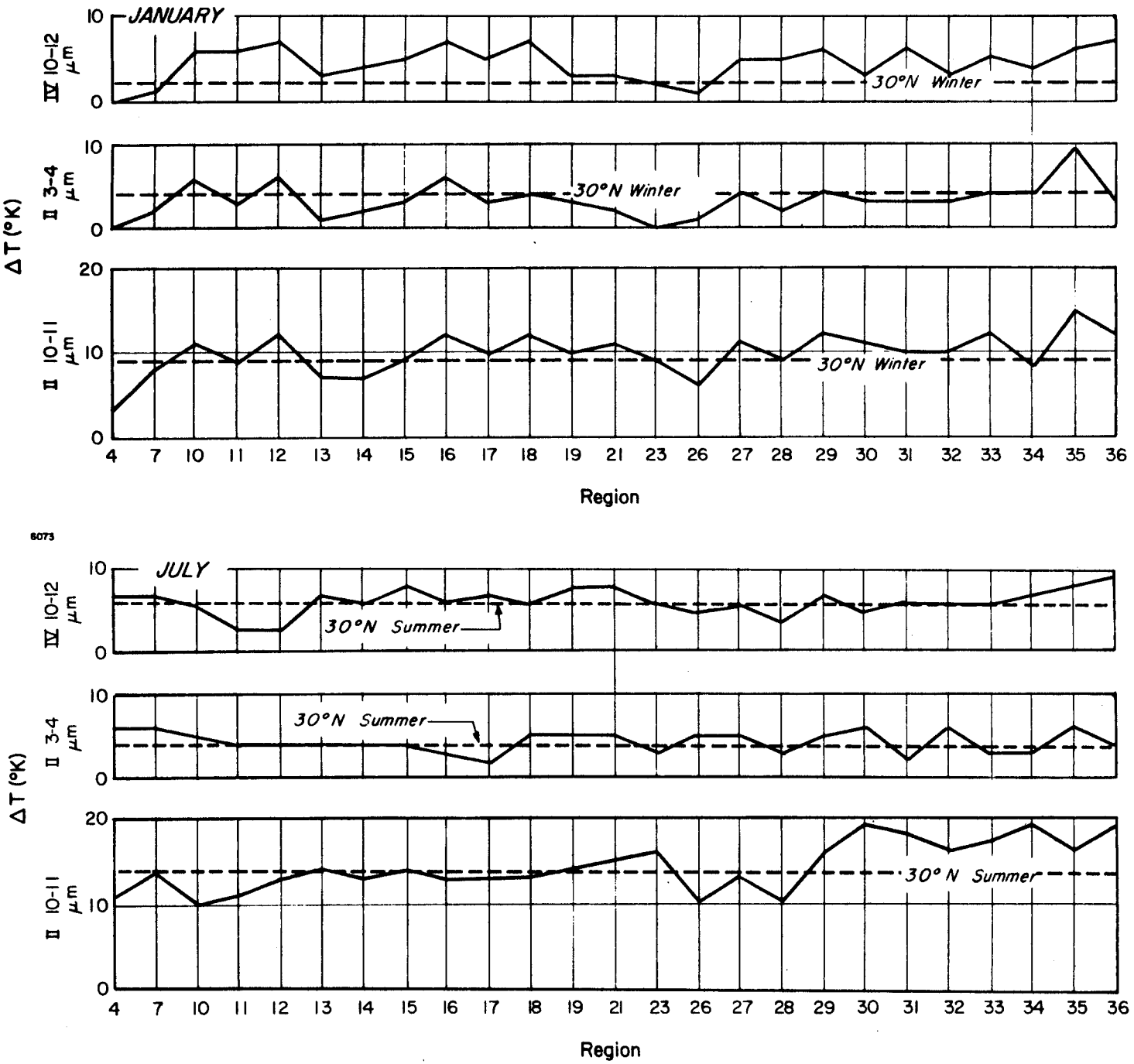

Figure 4-24 "Window" Channel Blackbody Temperature Decrease 22.5° -37.5°N

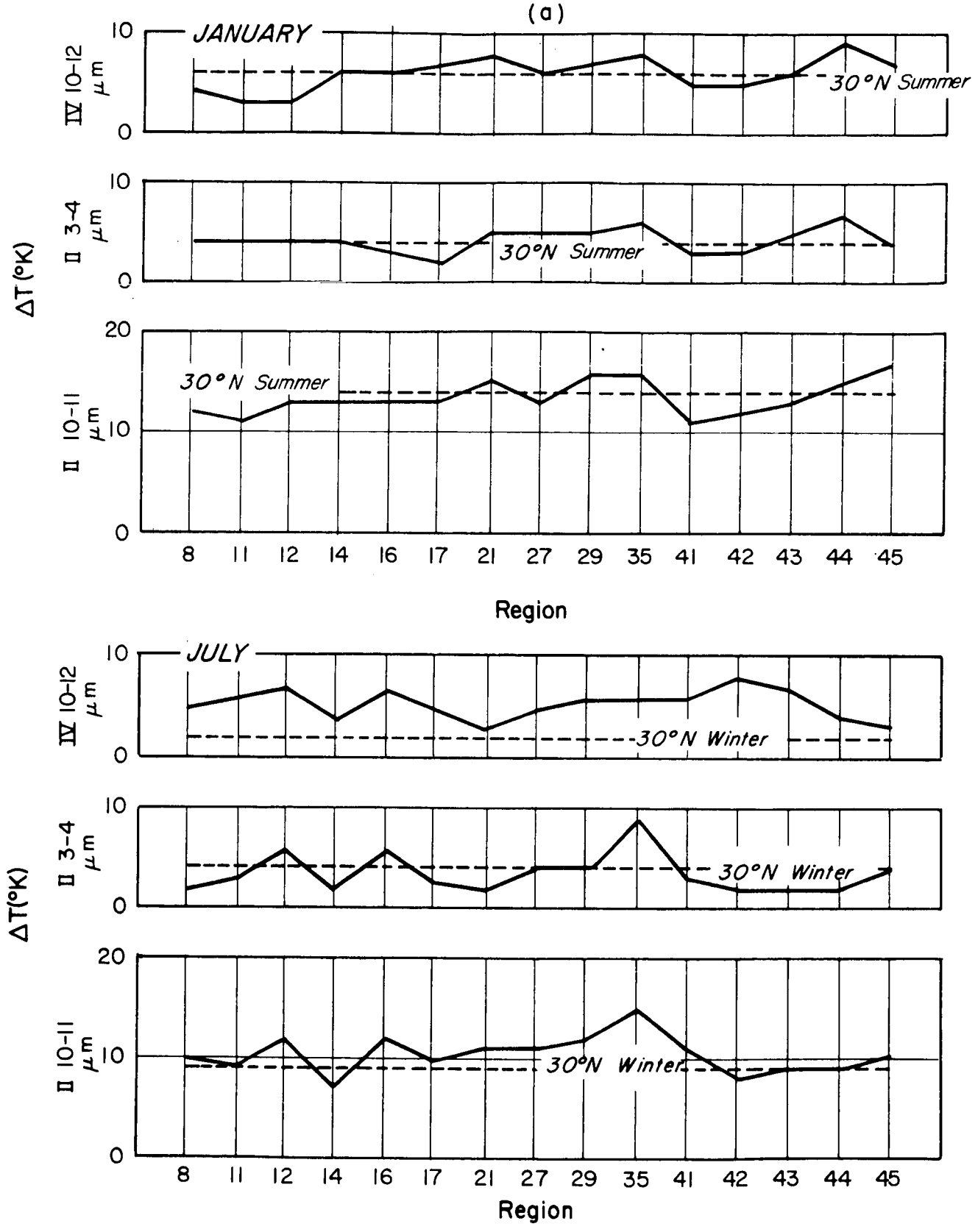

Figure 4-25 "Window" Channel Blackbody Temperature Decrease 22.5° -37.5°S

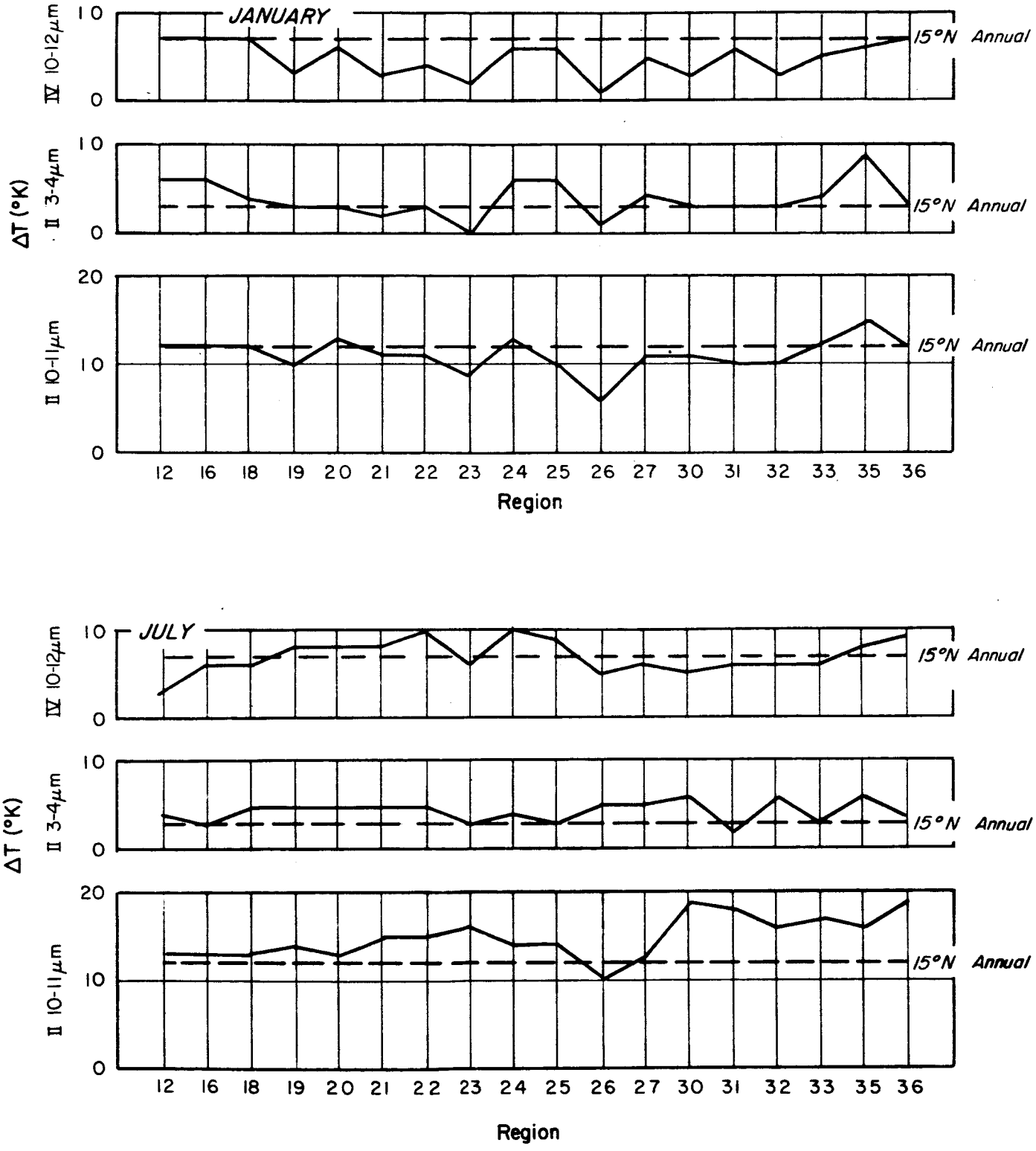

Figure 4-26 "Window" Channel Blackbody Temperature Decrease 0^{o} -22.5^{o}N

6098

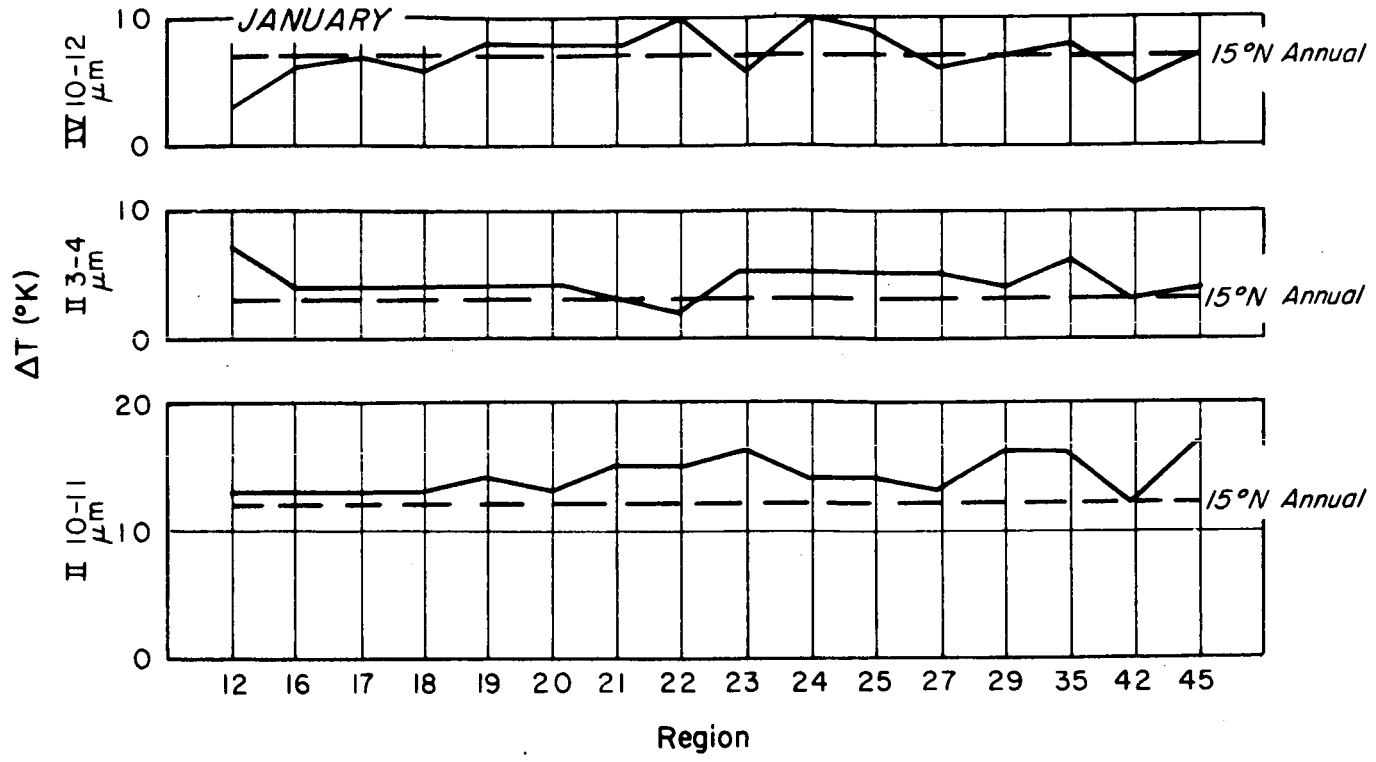

6609

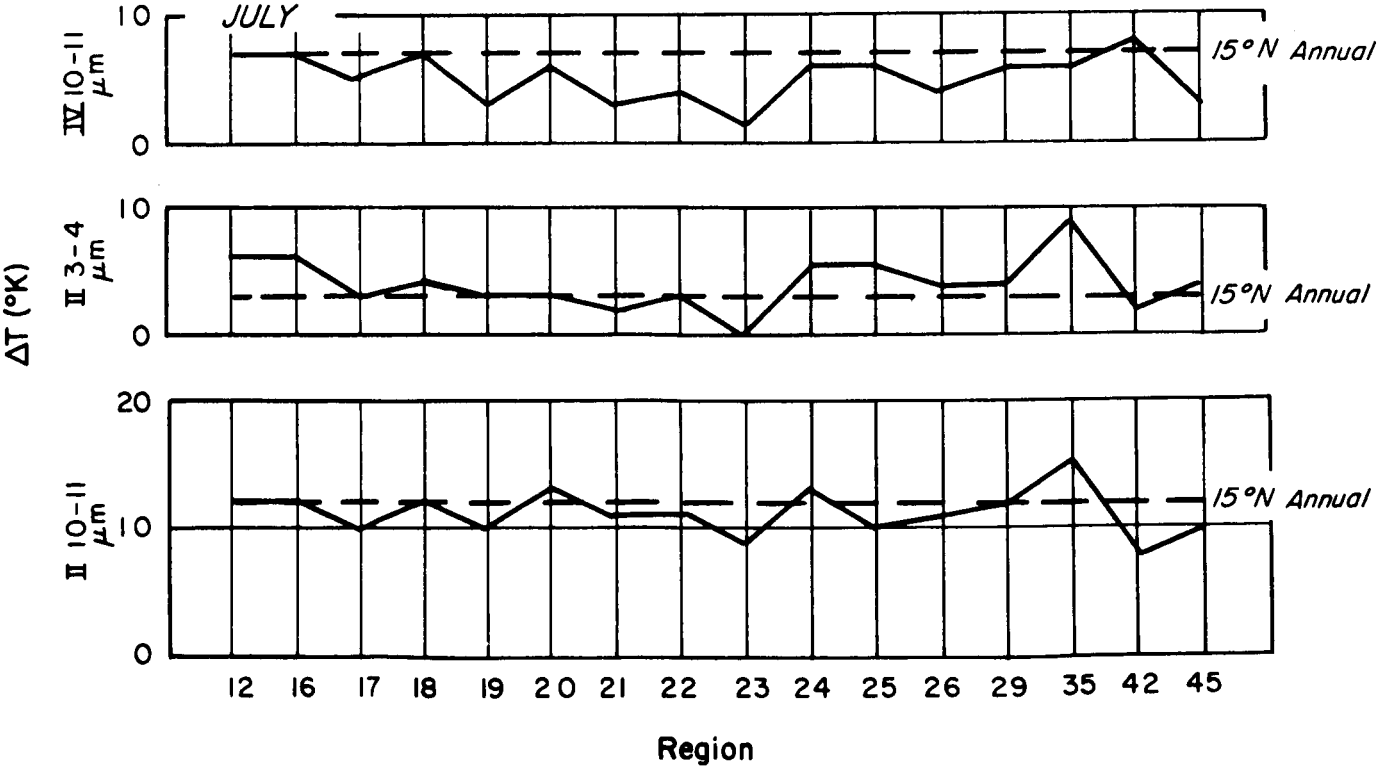

Figure 4-27 "Window" Channel Blackbody Temperature Decrease 0^{o} -22.5^{o}S

the Region 1 atmosphere and, accordingly, are too low for the values computed from the other regions north of 60.75°N. As expected from the atmospheric analysis in Section 2, the standard atmosphere gives radiometric values too cold for the Antarctic winter and too warm for the Antarctic summer (Regions 37 and 38).

Figures 4-18 and 4-19 show that all regions north of 60.75°, with the exception of the warm, moist Region 3, show a temperature decrease of 0-2°K in the 3-4 μm channel. The 75°N standard atmosphere's value of 1°K thus represents this channel very well in these latitudes. Regions 37 and 38 show a temperature decrease of 3°K; the standard atmosphere is slightly more in error here.

The Nimbus II 10-11 μm channel shows temperature differences of 3 to 7°K; the value of 5°K computed for 75°N is a good median and accurately represents the Antarctic. The Nimbus IV 10-12 μm channel is not so well behaved; there the differences between the surface temperatures and the radiometric temperatures range from 0 to 6°K, and the standard atmosphere's value of 4°K overestimates the attenuation for all but the ocean regions, Regions 6, 9 and 38. Less attenuation is predicted for Region 4 than for the drier and colder Regions 1 and 2; this reflects, in part, the error in measuring small differences in large numbers and, in part, the effects of atmospheric density and vertical temperature distribution. The standard atmosphere for July provides a good estimate of the attenuation expected for Regions 1, 2, 37, and 38 during the summer; however, the other regions in this zone are clearly subarctic in this season and are not well represented by the values for 75°N.

4.3.2 The Subarctic Zone

In the computed blackbody temperatures for the "window" channels (Figures 4-10, 4-11), the 60°N standard atmosphere resembles Regions 3 and 6 during July, and no regions during January. As was seen in Figures 2-6, the standard atmosphere surface temperature is colder than any region surface temperature between 50.25 and 60.75° during the winter season.

The predicted attenuation is far more representative of this latitudinal belt than are the predicted blackbody temperatures. No one region is accurately represented for all channels but many region values do not depart significantly from those predicted by the standard atmosphere (Figures 4-20,

4-21). This is especially true for the Nimbus IV 10-12 μm channel in July; the temperature loss indicated by the regions ranges from 4° to 7°K; the value of 6°K computed from the standard atmosphere is excellent. The same expected temperature decrease is given for the 3-4 μm channel for the same month; since 6 of the 9 regions have expected losses of 5 to 6°K, this value is also quite good. The standard atmosphere's 2°K temperature drop computed for January represents a good estimate as it is both a mean and a mode of the region values. For both seasons, the standard atmosphere slightly underestimates the attenuation found in the NIMBUS II 10-11μm channel; in January just the opposite occurs in the Nimbus IV 10-12 μm channel where attenuation is overestimated for all but Regions 3, 6, 27, and 28.

In keeping with the water vapor amounts shown in Figures 2-16 and 2-17, the standard atmosphere does not predict enough attenuation in the water vapor channels for any of the January regions but Regions 2 and 4; in July its values are much more typical. Since this is a transition zone, which shows an increase of 8°K in the January "water vapor" blackbody temperature from Regions 2 to 9, it is important that the region data be retained to provide adequate radiometric information.

4.3.3 The Mid-Latitude Zone

Most of the regions between 37.5 and 50.25°N have already been presented in the previous section. However, the additional regions match well with the regions already in evidence, and a glance at Figures 4-22 and 4-23 make it immediately clear that the attenuation predicted by the standard atmosphere for 45°N is representative for all channels but the NIMBUS IV 11.5 μm channel in July. There the estimated amount of attenuation is too large. The actual radiometric values are misleading because this, like the sub-arctic zone, is an area of highly variable surface temperatures (Figures 4-12 and 4-13); a detailed breakdown of surface temperatures is necessary to obtain the blackbody temperatures. However, if an estimate of temperature loss is desired, the standard atmosphere would rarely be off by 3° K.

4.3.4 The Subtropics

Because of the large climatic variability in the latitudes between 22.5° and 37.5°, two-thirds of the 4-D moisture regions are represented in these zones. This leads, of course, to very large variations in the blackbody temperatures; the NIMBUS II 3-4 μm channel varies 45°K in temperature during the Northern Hemisphere winter (Figure 4-24). The summer values in the "window" channels are much more stable (the surface temperatures only vary by 25°K) but the high variability in moisture content, coupled with the varying surface temperature seen in both seasons (Figure 2-20), causes a 30°K range in the values of the water vapor channel. Normally, increased temperatures are matched with increased water vapor and thus to increased attenuation; in this latitudinal belt, the very hot, dry deserts are a clear exception to the rule. The Southern Hemisphere is much less variable at these latitudes; it is not, however, homogeneous (Figure 4-25).

In light of the significant differences in temperature and moisture seen in these latitudinal belts, the plots of temperature decrease for the "window" channels (Figures 4-24 and 4-25) seem quite smooth. As expected, the winter values show a greater variability than the summer ones; yet the majority of the values lie within 3°K of the 30°N standard atmospheres. A notable exception is the Southern Hemisphere July NIMBUS IV 10-12 μm channel; here the standard atmosphere underestimates the attenuation in all regions. It is also slightly low for this channel during the northern hemisphere winter. Since the standard atmosphere overestimates the moisture for most of these regions, this result clearly illustrates the complex relationship between the atmosphere's structure and composition, and its attenuating effect on infrared radiation. The standard atmosphere also underestimates the attenuation in Regions 35 and 36 for all channels; these regions have a higher moisture content than that given by the standard atmosphere.

4.3.5 The Tropics

The tropics show less variability than the subtropics with a 30°K range of blackbody temperatures in the "window" channels indicating a greater similarity in surface values (Figures 4-16 and 4-17). The "water vapor" channels are more variable; this reflects the fact that the water vapor at

these latitudes varies more substantially than do the surface temperatures. Figures 4-26 and 4-27 show, however, that the annual standard atmosphere for 15°N is not truly a representative value. It overestimates the attenuation for two of the three winter channels and underestimates it for two of the three summer channels. On the other hand, the variability in attenuation is so small that only the winter values for the Nimbus IV 10-12 μm channel, and the summer desert values for the Nimbus II 10-11 μm channel, consistently diverge from the standard atmosphere by more than 3°K. It would seem, though, that this zone might be better represented by separate atmospheres for summer and winter.

4.4 Simulated Orbital Tracks

4.4.1 Selection of Simulated Values

The value of the atmospheric models in predicting the infrared temperatures sensed by satellites can be summarized by a simulation of typical orbital tracks. Since most satellites have a pole-to-pole orbit, two longitudes were selected for analysis, 90°W and 180°. The 90°W longitude approximates the center of the North American continent; in contrast the 180° longitude intercepts land only at the tip of Siberia. This facilitates a comparison between oceanic and continental conditions while permitting a survey of differences (or similarities) across the latitudinal belts in both hemispheres.

For this analysis, the regions appropriate to each longitude were selected, and their radiometric values plotted by latitude for each of the five channels (Nimbus II 3-4 μm, 6-7 μm, 10-11 μm, Nimbus IV 6-7 μm, 10-12 μm). These values appear as line drawings in Figures 4-28 through 4-32. To show the blackbody temperatures that would be predicted by the standard atmospheres for the same tracks, the computed radiometric values were plotted as dots at the appropriate latitudes on the same figures.

4.4.2 Analysis of Simulations

The northern hemisphere is predominantly covered by land at 90°W longitude and is thus represented by the regions which most closely resembled the standard atmospheres (Section 2). This similarity reappears here; the standard atmosphere blackbody temperatures agree well with the 4-D tempera-

6035

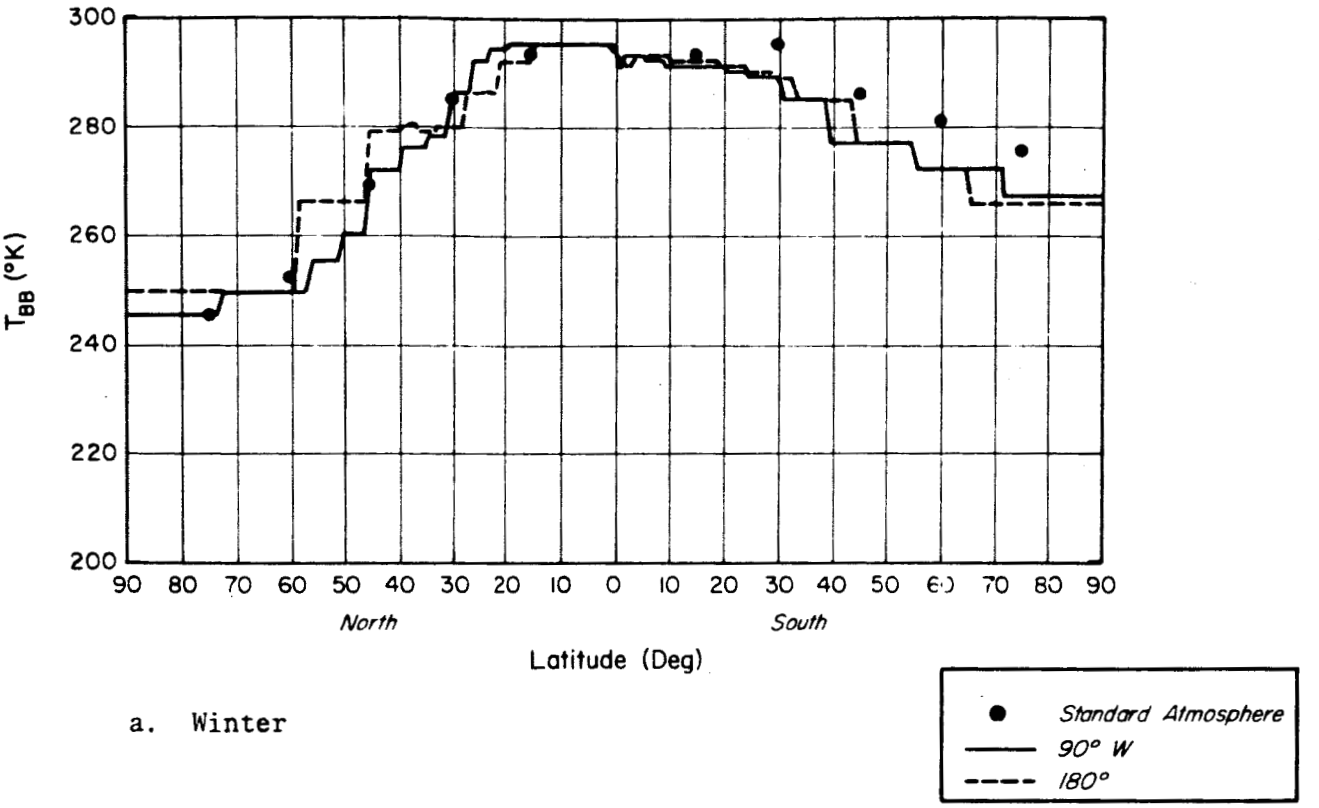

a. Winter

6034

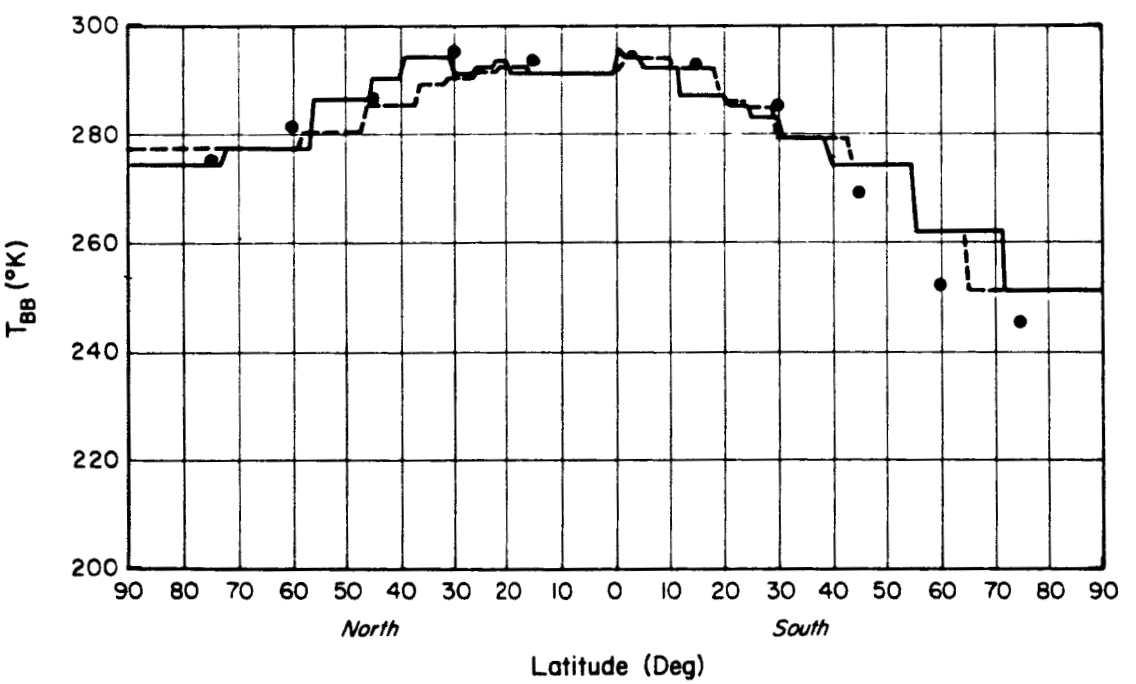

b. Summer

Figure 4-28 NIMBUS IV 10-12 μm Blackbody Temperatures at 90°W and 180° Longitude

6042

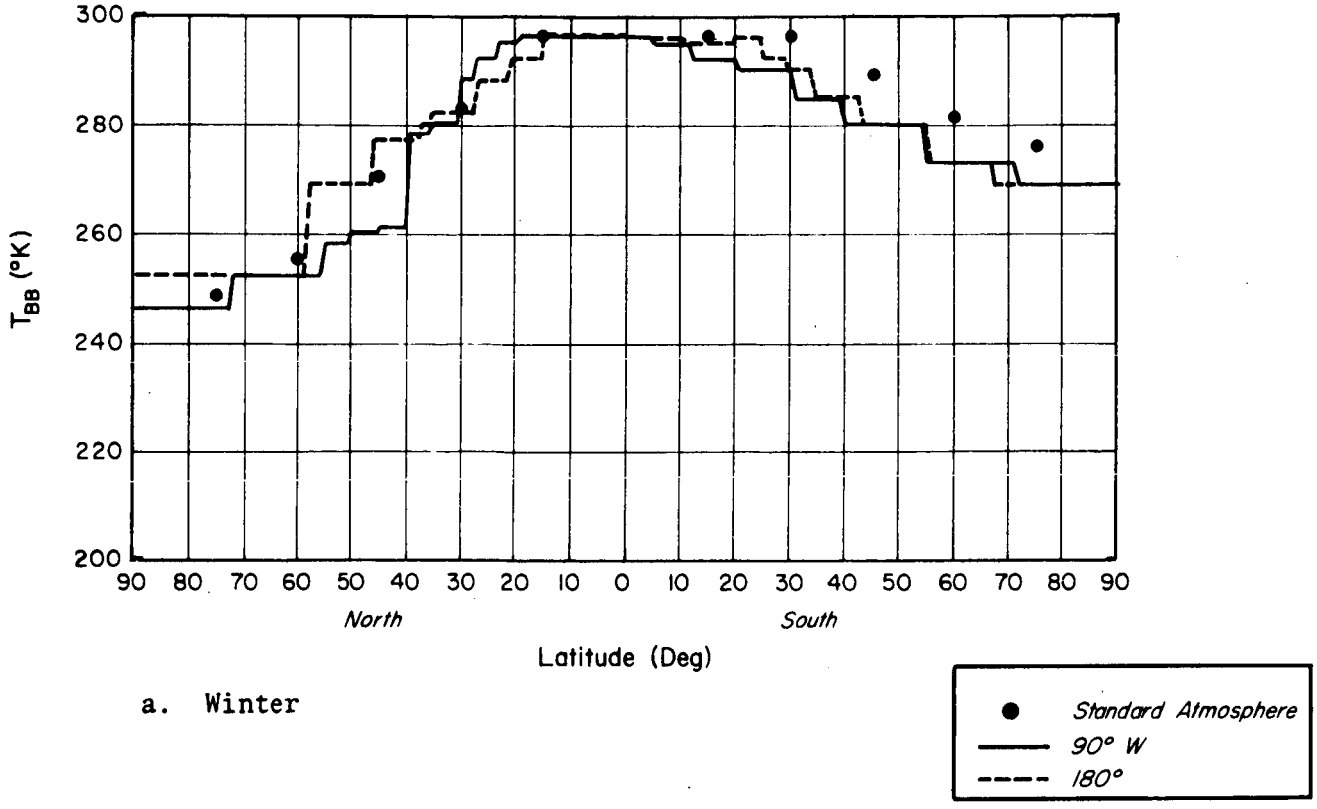

a. Winter

6043

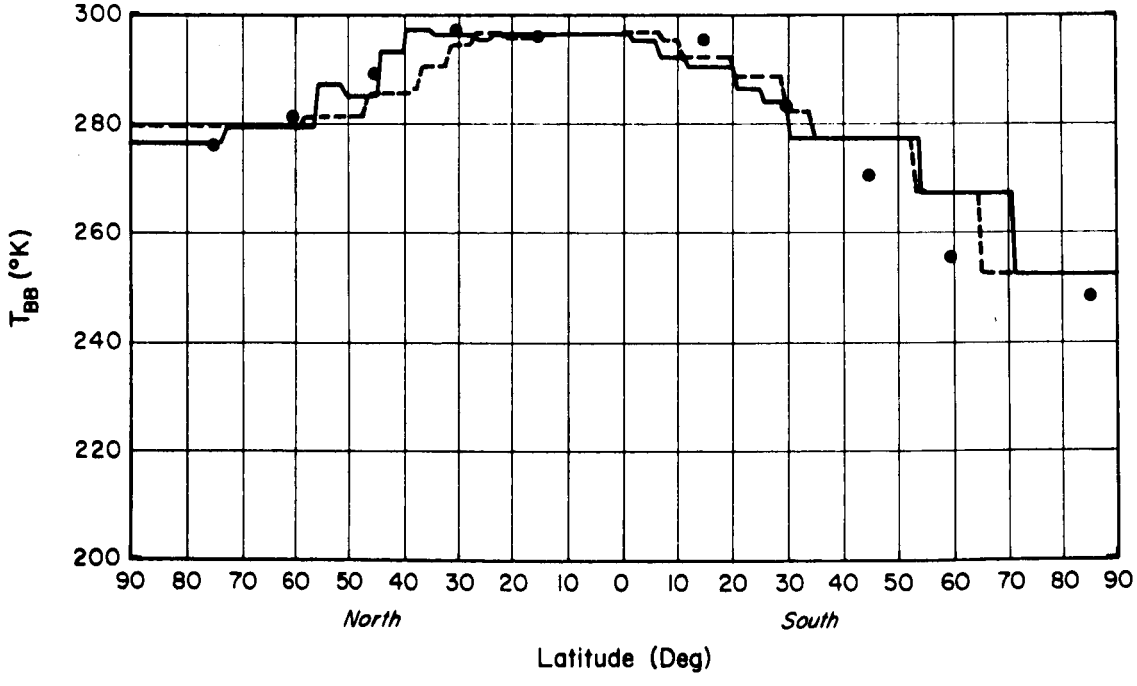

b. Summer

Figure 4-29 NIMBUS II 3-4 μm Blackbody Temperatures at 90°W and 180° Longitude

6038

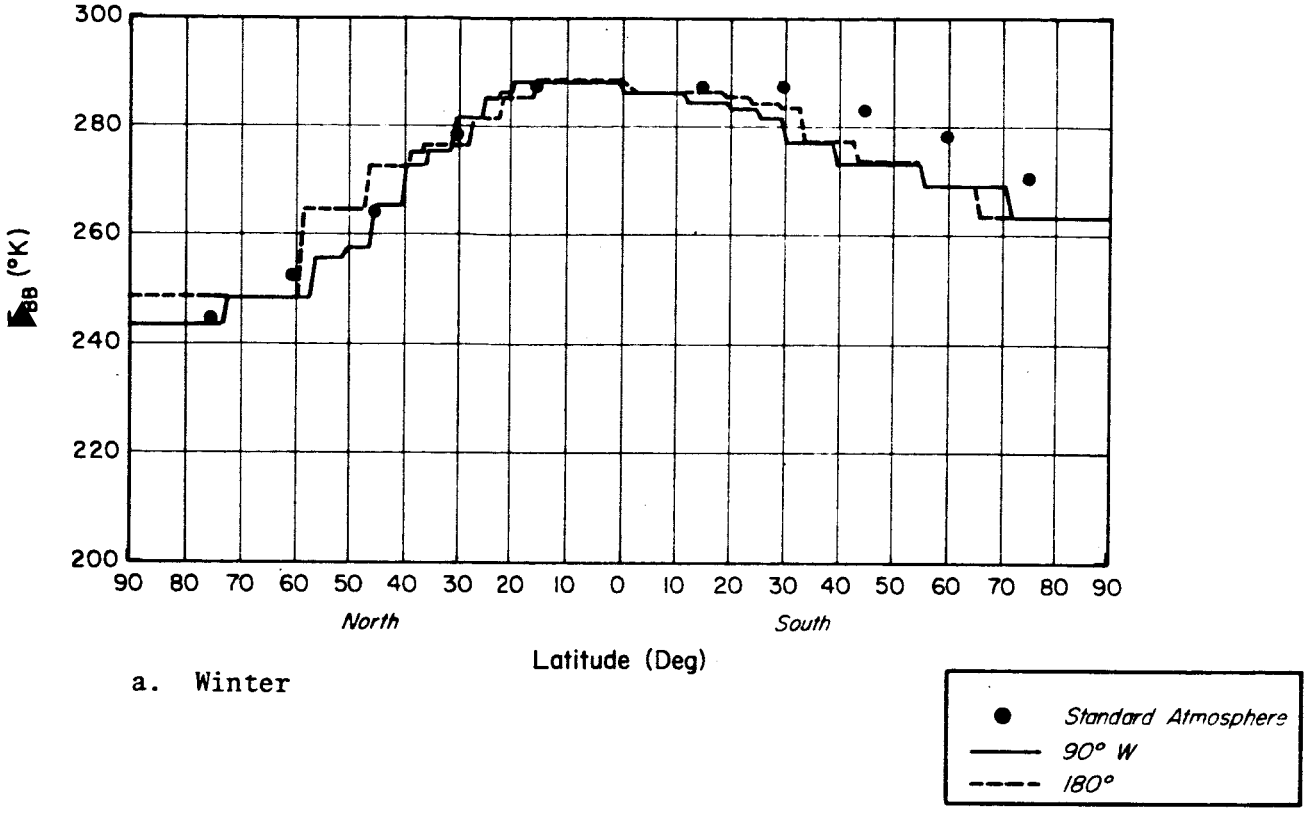

a. Winter

6039

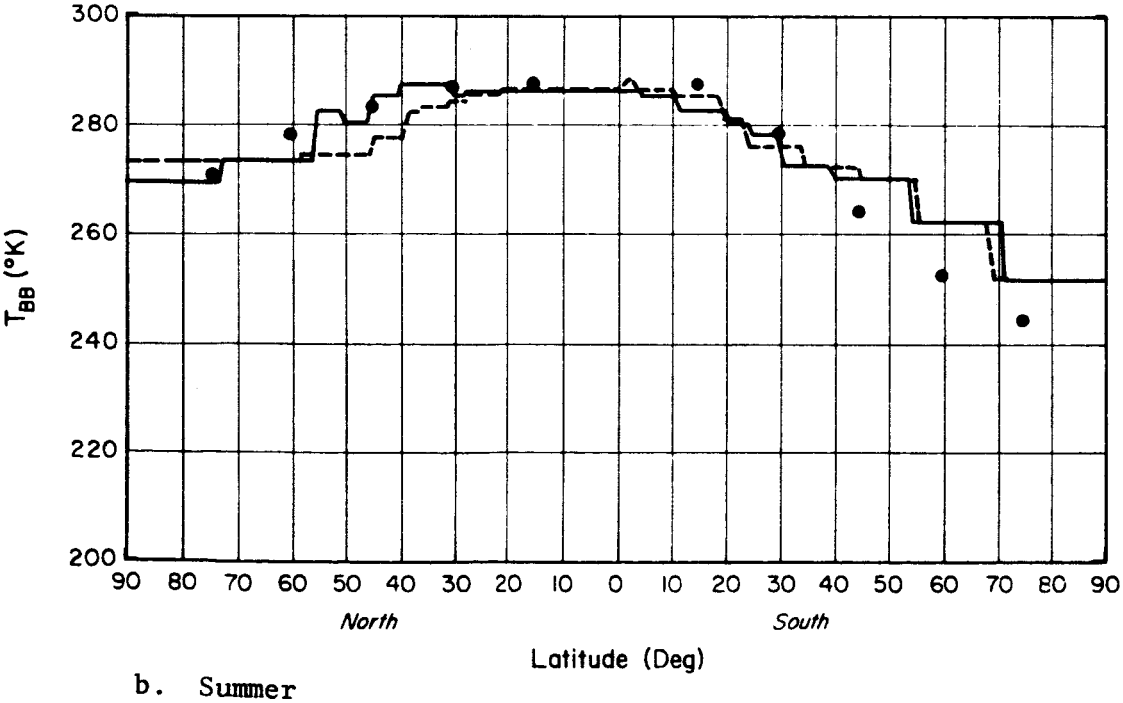

b. Summer

Figure 4-30 NIMBUS II 10-11 μm Blackbody Temperatures at 90°W and 180° Longitude

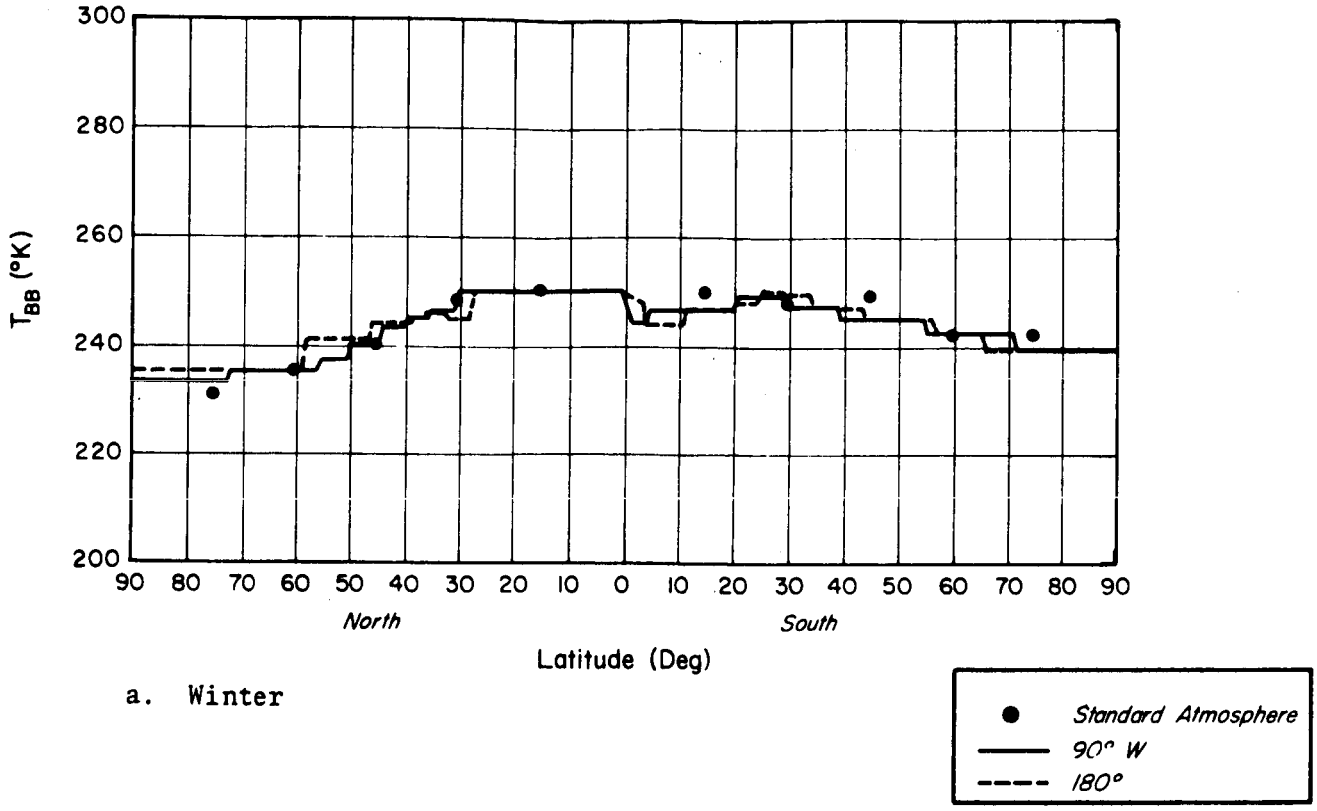

a. Winter

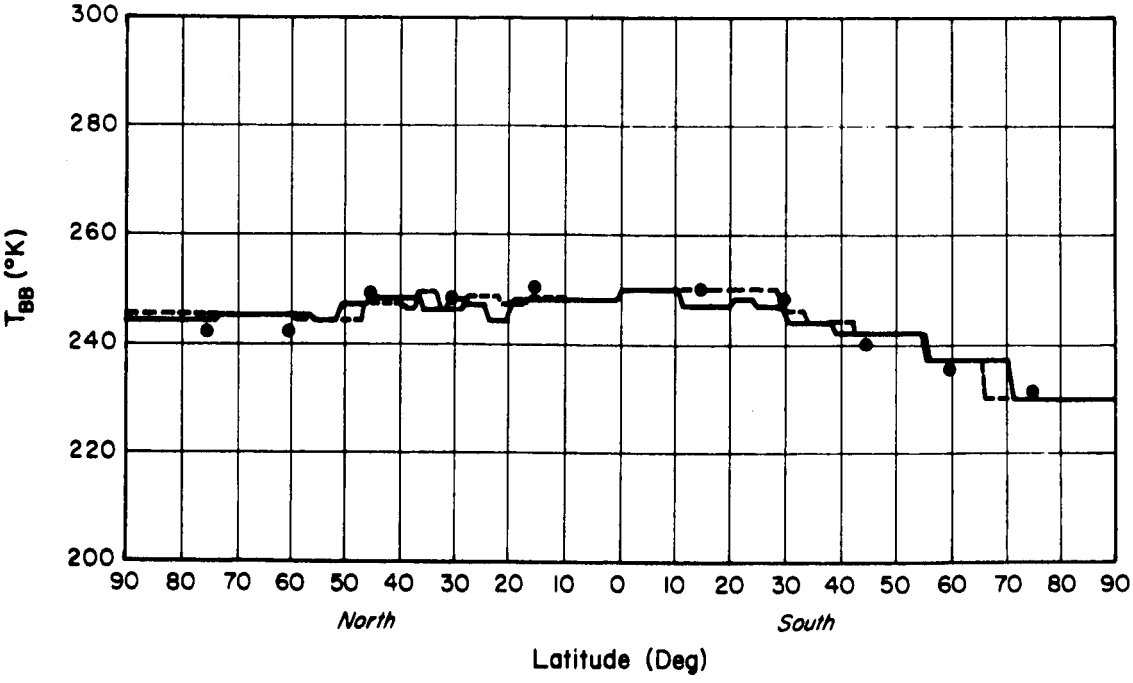

b. Summer

Figure 4-31 NIMBUS IV 6-7 μm Blackbody Temperatures at 90°W and 180° Longitude

6046

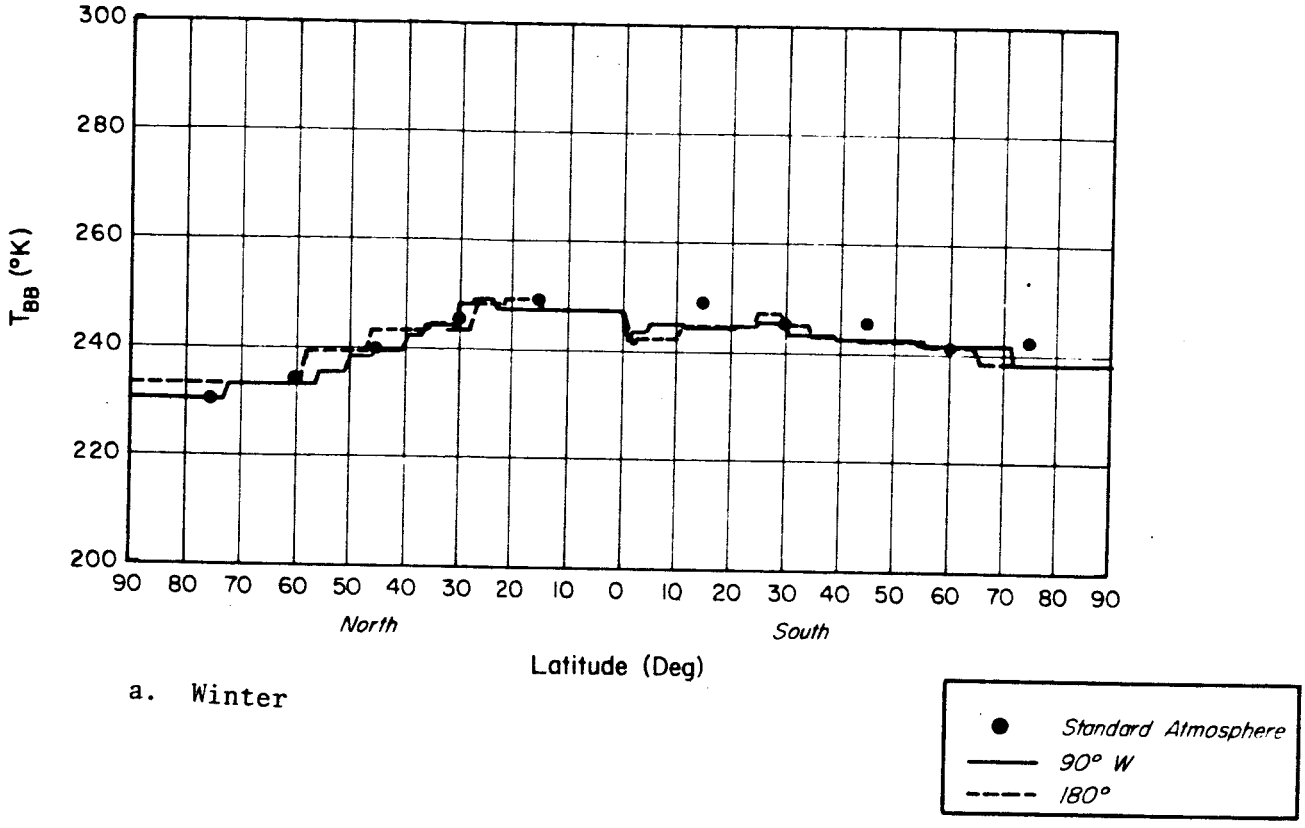

a. Winter

6047

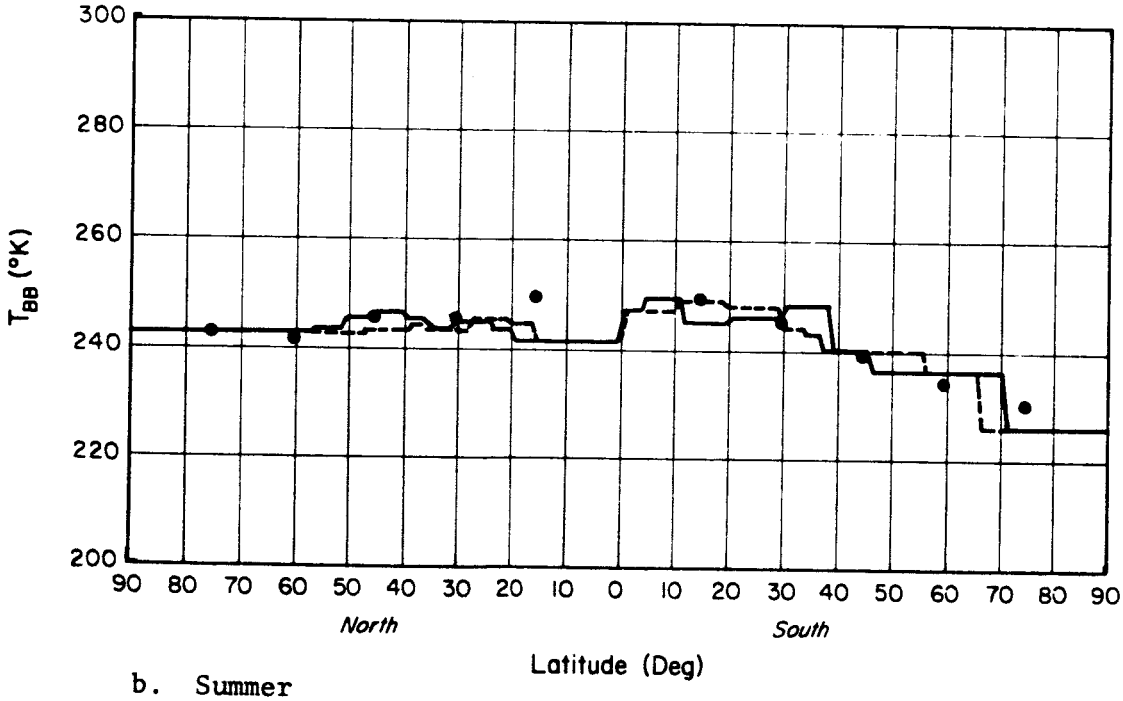

b. Summer

Figure 4-32 NIMBUS II 6-7 μm Blackbody Temperatures at 90°W and 180° Longitude

tures for all latitudes except the tropics in the July Nimbus II μm channel. The radiometric values at this meridian also show the expected atmospheric differences; that is, the latitudes from 50° to 30°N show a temperature increase of 30°K in the "window" channel as the sensor travels south during January, and less than a 15°K increase during July. The blackbody temperatures for the tropics differ but little for the two seasons in the "window" channels; more of a change is visible in the "water vapor" channels emphasizing that the seasonal variability of water vapor here is greater than the seasonal variability of temperature.

The blackbody temperatures drawn from the two sets of atmospheres for 180° agree within 2°K throughout the Northern Hemisphere. However, the standard atmospheres do seem slightly less representative at this longitude since the predicted temperatures are generally too warm for the July "window" channels, and too cold for the more northerly latitudes in the January "water vapor" channels. The only really significant difference between the two longitudes occurs in the latitudinal zone of 50° to 40°N; there the winter ocean blackbody temperatures run warmer than the land values, and the summer ocean temperatures run colder. This agrees well with the analysis of the temperature and moisture parameters done earlier.

The standard atmospheres do not represent the southern hemisphere at either longitude except at 30°S in July or, possibly, in the water vapor channels. During the winter a smaller range of temperatures is found than was seen in the northern hemisphere, and the transition from very cold to moderate warm temperatures is much more pronounced between 50° and 90°S than between 30° and 50°S. The summer range of temperatures is slightly greater than that indicated by the standard atmospheres but all temperatures are colder. This is partly due to the dominance of ocean regions on this half of the orbital subtrack; it is more due to the different climatic patterns of this hemisphere.

5. DISCUSSION OF RESULTS

5.1 Comparison with Other Model Computations

To demonstrate the validity of the computations made with Anding's model, the results for Supplementary Atmospheres were compared with computations made by other authors. Salomonson (1970) used the same Supplementary Atmospheres to calculate the expected effective blackbody temperature for the HRIR (with spectral response in the 3.4 μm region). The radiometric model used, however, was one developed by Kunde (1967). The results of his calculations are shown in Table 5-1, together with the corresponding value obtained in this study. The table shows that the present computations, with the exception of the tropical results, appear to be systematically colder than the results obtained by Salomonson. This might be due to a systematic error in the interpolation of the effective spectral response functions at specific wavelengths. However, the differences of 1°K and 2°K for the tropics are certainly within acceptable limits. Apart from agreement in absolute values, the more important aspect of the comparison in Table 5-1 is the trend in the data. In both sets of computations, the seasonal and regional variability is maintained.

Another set of computations useful as comparison with the results presented in this study are the ones recently reported by Stevenson and Miller (1972). In this study, preliminary computations using Kunde's technique were performed of the expected values of ΔT corresponding to four meteorological conditions. The results for the downward looking case are shown in Table 5-2.

The importance of these results is that the computed temperature differences are within the limits shown in Section 4 of this study, and that the expected atmospheric effect is greater for the MRIR than for the HRIR, a result clearly brought out in the data shown in Section 4. Perhaps more important is the fact that the data shown illustrates that even diurnal effects can produce very significant differences in the expected radiometric values, a factor which must be considered in the simulation of such values. With the variance statistics built-in the MSFC 4-D data, these small scale effects can be effectively simulated by a properly designed Monte Carlo scheme.

TABLE 5-1

COMPARISON OF SIMULATED EFFECTIVE BLACKBODY TEMPERATURES FOR THE HRIR USING SUPPLEMENTARY ATMOSPHERES

Atmosphere	Temperature Surface (^{o}K)	Effective Blackbody Temperature, T_{bb} (^{o}K)	
		"Salomonson"	"Anding"
1) Tropical	299.65	294.37	296
2) Subtropical Summer	301.15	295	297
3) Subtropical Winter	287.15	284	283
4) Mid-Latitude Summer	294.15	290	289
5) Mid-Latitude Winter	272.59	271	270
6) Sub-Arctic Summer	287.15	283	282
7) Sub-Arctic Winter (Cold)	257.28	257	256
8) Arctic Summer	278.15	275	276
9) Arctic Winter (Mean)	249.22	249	248

TABLE 5-2

$\Delta T=(T_s - T_{bb})$ VALUES DERIVED FROM STEVENSON & MILLER (1972)

Time / Sensor	"Dry" (<2pr-cm of water vapor)		"Wet" (>2pr-cm of water vapor)	
	0000 Local	1200 Local	0000 Local	1200 Local
HRIR	2.5°K	2.5°K	3.3°K	3.2°K
10-12 μm MRIR	4.5°K	5.0°K	6.7°K	5.8°K

5.2 Summary

From the detailed analysis of results presented in Sections 2 and 4, the following points are noted:

1. Along latitudinal belts, the effects of "continentality", i.e., the presence of land and water masses, can introduce large variations in moisture content within a latitudinal belt.

2. For each of the latitudinal belts studied, the large spatial differences between regions are found during the summer months, where the range of precipitable water can be in excess of 2 g cm^{-2}. For the winter the range is generally less than 1 g cm^{-2}.

3. As expected, the most pronounced inhomogeneities in precipitable water are found in the July data (both hemispheres) for the latitude belt between the equator and 22.5°N(S). Here the precipitatable water ranges from a low value of about 1.5g cm^{-2} to a high value of about 6.6 g cm^{-2}.

4. For the latitude regions poleward of 37.5°, the values of precipitable water computed from the standard atmosphere appear to be representative of the regional mean for the corresponding latitude belts. Equatorward from 37.5°, the supplementary atmosphere appears to be systematically too high to be representative of the mean for the corresponding latitude belt.

5. These differences in moisture between the supplementary atmospheres and the 4-D atmosphere are carried through to the radiometric quantities, but to a lesser degree. While the range of precipitable water for a given latitude belt often exceeds 50% of the mean value, the corresponding radiometric temperature seldom exceed 1/30 of the mean values of the effective blackbody temperatures for the latitude belt.

5.3 Conclusions

The analysis in this study shows that the supplementary atmospheres as given in the Handbook of Geophysics are probably more representative of the temperature structure of the regimes for which they are designed than they

are of the moisture structure. The most immediate difficulty using the Supplementary Atmospheres is the high differentiation in the moisture field between land and water, a characteristic not included in the supplementary atmospheres. This differentiation is most pronounced in the tropical belts with their wet equatorial forests and extremely dry deserts.

These regional differences in moisture field are reflected, although to a lesser degree, in the differences in simulated effective blackbody temperatures. The use of the supplementary atmospheres alone, especially in the mid- and low-latitude regions, fails to bring out the significant patterns in expected effective blackbody temperatures in a given latitude belt. It is clear, therefore, that the limitations of atmospheric effect correction tables such as those presented by Salomonson (1970) and others must be recognized. For more precise corrections (to be used for local regions), detailed correction tables should be computed using the 4-D Model corresponding to that region. Thus, the correction factors can be made to reflect the true variability of the real atmosphere.

6. REFERENCES

Anding, D., R. Kauth, and R. Turner, 1971: Atmospheric Effects on Infrared Multispectral Sensing of Sea-Surface Temperature from Space, NASA CR-1858.

Handbook of Geophysics and Space Environment (S. C. Valley, Editor), 1965: Air Force Cambridge Research Laboratories, Office of Aerospace Research, U.S.A.F.

Kunde, V.G., 1967: Theoretical Computations of the Outgoing Infrared Radiance from a Planetary Atmosphere, NASA TND - 4045.

NIMBUS Project: The NIMBUS II User's Guide (R.R. Sabatini, Editor), Goddard Space Flight Center, NASA.

NIMBUS Project: The NIMBUS IV User's Guide (R.R. Sabatini, Editor), Goddard Space Flight Center, NASA.

Salomonson, V., 1971: Private Communication (as reported in: Sabatini, R. R., G.A. Rabchevsky and J.E. Sissala, 1971; NIMBUS Earth Resource Observation, Tech. Report No. 2, Allied Research Associates. Inc., Concord, Ma.)

Spiegler,D. B. and M.G. Fowler, 1972: Four-Dimensional Atmospheric Models (Surface to 25 km Altitude), NASA CR-20820.

Spiegler, D. B. and J.R. Greaves, 1971: Development of Four-Dimensional Atmospheric Models (Worldwide), NASA CR-61362.

Stevenson, M. R., and F.R. Miller, 1972: Application of High Resolution Infrared and Visual Data to Investigate Changes in and the Relationship Between Sea-Surface Temperature and Cloud Patterns Over the Eastern Tropical Pacific, Final Report, Contract No. N62306 - 71 - C- 0120, Inter-American Tropical Tuna Commission, La Jolla, Calif, 92037.

U. S. Standard Atmosphere Supplement, 1966. Superintendent of Documents, U. S. Government Printing Office, Washington, D. C., 289 pp.

APPENDIX A

A DISCUSSION OF WATER VAPOR PARAMETERS AND THEIR RELATIONSHIPS

A.1 Mathematical Relationships

Considerable confusion has arisen due to the varying definitions and expressions of water vapor. The form used in the MFSC 4-D model is absolute humidity, ρ_ω, also known as water vapor density, and is expressed in units of g m^{-3}. A more commonly used unit is mixing ratio, w, a dimensionless term usually expressed in g kg^{-1}. To facilitate conversion, the relationship between the two terms is given here as:

$$W = (\rho_\omega / \rho_d) * 10^3 \qquad \text{(A-1)}$$

where

W is the mixing ratio, g kg^{-1},

ρ_ω is the water vapor density, g m^{-3},

ρ_d is the density of the dry air, g m^{-3}

In the 4-D model, ρ_d is referred to simply as the atmospheric density; thus the mean mixing ratio is simply the ratio of the water vapor density to the atmospheric density.

The dew point can be found from the mixing ratio graphically by plotting on the standard pseudo-adiabatic charts. When the atmospheric density is less than 1000 g m^{-3}, and the absolute humidity is small, the dew point can also be approximated by using the absolute humidity value in place of the mixing ratio. This does, however, cause grave errors near the surface. There the density is greater than 1000 g m^{-3} and the moisture is relatively high; use of the absolute humidity in such circumstances can overestimate the dew point by 3-4°K and lead to an erroneous indication of supersaturation or atmospheric instability.

Computational means are necessary to obtain the dew point directly from the absolute humidity value. The equation requires knowledge of the atmospheric temperature, and is:

$$T_D = 237.3/(7.5 - \log_{10} (\frac{T * \rho_\omega}{1324.037})) \quad \text{(A-2)}$$

where T_D is the dew point temperature, ^oC,

T is the atmospheric temperature, ^oK,

ρ_ω is the absolute humidity, g m^{-3}

If it is desired to express the water vapor of the 4-D model in dew point temperatures, this is the most direct and accurate approach.

A.2 Example of Error in Dew Point Approximation

Region 11, January, was selected to illustrate the dew point error caused by using the absolute humidity value for the mixing ratio value. The following mean values were given for the surface:

Temperature	284.65 °K
Pressure	1014.24 mb
Absolute Humidity	8.38 g m^{-3}
Density	1241.33 g m^{-3}

The last two terms gave a mixing ratio of 6.75 g kg^{-1}. When the absolute humidity and the mixing ratio were plotted on a pseudoadiabatic chart, they gave the following results:

Dew Point (from absolute humidity)	284.8 ^oK
Dew Point (from mixing ratio)	281.6 ^oK

The use of the absolute humidity value not only overestimates the dew point by more than 3^oK; it indicates that this region is supersaturated. Although supersaturation is not impossible for an ocean region, an average state of supersaturation for a five-year period is totally unreasonable.

APPENDIX B

MODIFICATIONS TO THE PROGRAMS OF DR. DAVID ANDING

Two programs were received from Dr. David Anding, CATM and RADST. The details of these programs are given in the report by Dr. Anding and are generally appropriate here, as no changes were made to the computations or theories given. It was necessary, however, to change the control cards to make the programs run on the 360/75 available to ERT.

The major modifications were in the input and output portions of the programs. The program to set up the atmospheric models needed for the radiation calculations, CATM, acquired new keywords and subroutines which input data from the 4-D region coefficients or from the ERT-NWRC disk files. These routines greatly increased the flexibility of the program and significantly minimized the time and effort needed to input these data sets. The program to compute infrared attenuation due to atmospheric absorption, RADST, was altered to print out vertical profiles of the weighting function for selected wavelengths, and to write on disk (or tape) values of total transmission as well as spectral radiance.

All other changes were minor. For example, CATM was changed to interpolate starting at the given surface height, if the initial level requested was below the surface height. This was important to retain the surface layer; previously, the output atmosphere would commence at the next highest level, i.e. 500 m, often losing a significant amount of moisture.

APPENDIX C
AN EVALUATION ON THE EFFECTS OF CLOUDS ON STATISTICS OF PRECIPITABLE WATER

C.1 Introduction

The statistics of atmospheric parameters which make up the 4-D Model Atmospheres were compiled independent of cloud cover conditions. For most climatological applications such cloud-cover-independent statistics are appropriate. Yet there exists a class of applications in which subsets of these statistics, those describing clear sky conditions only, are useful. One important area where such statistics are useful is the simulation of earth viewing missions by aircraft or spacecraft-borne visible and infrared sensors. In such an application the presence of clouds automatically precludes further consideration of atmospheric attenuation effects. The statistics of atmospheric temperature and moisture become important only when there are no clouds.

Intuitively it can be argued that there should be differences in the structure of the atmosphere, i.e., its vertical temperature and moisture distributions, between clear sky and cloudy conditions. This is especially true in the case of the moisture field where the presence of clouds is an indication of saturation at certain levels. With the limited variance in the temperature fields for a given climatic regime, the saturation in turn is an indication of an atmosphere more moist (in terms of absolute moisture parameters such as precipitable water or absolute humidity) than one without clouds. The means of precipitable water computed for all days would in fact overestimate the mean of precipitable water for clear sky days only.

From the analysis presented in the report, it is clear that while the effective blackbody temperature or atmospheric transmissivity is not a simple function of any of the moisture parameters, the precipitable water determines to a large extent the degree of atmospheric interference in a cloudless atmosphere. Given this consideration, it becomes important to evaluate the degree to which the 4-D model moisture statistics are overestimates of those for clear sky days. In the following paragraphs, the results of some analyses directed towards this problem are presented. These results are compared with some findings by other investigators.

C.2 Analysis

Data from three stations were selected for analysis. San Diego (03131) and San Francisco (23230) from moisture Region 18, and Tucson (23160) from moisture Region 30 were selected as being representative of regions with "moderate to high" and "low" annual mean moisture content. The period of record used in the analysis was the two year period between 1 January 1965 and 31 December 1966. Daily values of precipitable water at each of the stations were computed using the rawinsonde data on magnetic tape. These values were then grouped by season (with winter being defined as December, January and February) and stratified by cloud cover conditions. To do this, use was made of the daily surface observation reports at 12Z made at each of the stations. Seasonal and annual statistics of the means and variances of precipitable water were then compiled for the following cloud cover conditions, some of which are overlapping (in tenths): 0-1, 2-3, 4-9, 10, 0-3, 4-10, 2-10, 0-10, and "Precipitation". Results of these calculations are shown in Tables C-1, C-2, and C-3. Using these results, computations of the seasonal and annual values of the following ratios were computed: $R_1 \equiv \overline{W}(0\text{-}1)/\overline{W}(0\text{-}10)$ and $R_2 \equiv \sigma_w(0\text{-}1)/\sigma_w(0\text{-}10)$ where $\overline{W}(0\text{-}1)$ and $\sigma_w(0\text{-}1)$ are the mean and variance of precipitable water for days with cloud cover less than one tenth; and $\overline{W}(0\text{-}10)$ and $\sigma_w(0\text{-}10)$ are the corresponding values computed for all days. These ratios are shown in Table C-4.

C.3 Discussion

Statistics of seasonal mean values of precipitable water for all sky conditions (cloud cover category 0-10) for the three stations show characteristically high values during the summer and low values in winter. The lowest seasonal values of precipitable water are found in Tucson during the winter months. The ratio of clear sky days to all days is approximately 1/2 for Tucson while the same ratio for San Diego and San Francisco is less than 1/3, reflecting the differences in climatic regimes.

The annual and seasonal mean values of the ratios R_1 and R_2 shown in Table C-4 do not indicate any significant differences between individual stations or climatic regimes. R_1, the ratio corresponding to the seasonal mean values of precipitable water, ranges from a low value of 0.705 (Tucson/

Table C-1

MEANS ($\bar{W}$) AND VARIANCES (σ_w) OF PRECIPITABLE WATER (IN CM) FOR STATION 03131 (SAN DIEGO)

Season	Cloud Cover (Tenths)																	
	0 - 1		2 - 3		4 - 9		10		0 - 3		4 - 10		2 - 10		0 - 10		Rain	
	$\bar{W}$	σ_w	$\bar{W}$	σ_w	$\bar{W}$	σ_w	$\bar{W}$	σ_w	$\bar{W}$	σ_w	$\bar{W}$	σ_w	$\bar{W}$	σ_w	$\bar{W}$	σ_w	$\bar{W}$	σ_w
Winter	0.847 (74)	0.071	1.118 (16)	0.085	1.222 (45)	0.087	1.409 (42)	0.267	0.895 (90)	0.084	1.313 (87)	0.181	1.282 (103)	0.170	1.100 (177)	0.175	1.659 (5)	0.195
Spring	1.299 (41)	0.180	1.355 (18)	0.144	1.488 (48)	0.079	1.550 (74)	0.080	1.316 (59)	0.167	1.526 (123)	0.080	1.504 (140)	0.090	1.457 (181)	0.117	1.277 (5)	0.069
Summer	2.174 (42)	0.413	2.399 (17)	0.641	2.551 (51)	0.656	2.093 (67)	0.460	2.239 (53)	0.479	2.291 (118)	0.592	2.304 (135)	0.595	2.273 (177)	0.552	0.0 (0)	0.0
Fall	1.554 (66)	0.342	1.474 (13)	0.365	1.805 (38)	0.340	1.968 (59)	0.277	1.541 (79)	0.342	1.904 (97)	0.305	1.853 (110)	0.328	1.741 (176)	0.353	2.762 (7)	0.139
Annual	1.389 (223)	0.456	1.597 (64)	0.543	1.786 (182)	0.560	1.778 (242)	0.339	1.435 (287)	0.481	1.781 (424)	0.433	1.757 (488)	0.450	1.642 (711)	0.481	2.001 (17)	0.572

( ) indicate sample size

Table C-3

MEANS ($\bar{W}$) AND VARIANCES (σ_w) OF PRECIPITABLE WATER (IN CM) FOR STATION 23160 (TUCSON)

Season	Cloud Cover (Tenths)																	
	0 - 1		2 - 3		4 - 9		10		0 - 3		4 - 10		2 - 10		0 - 10		Rain	
	$\bar{W}$	σ_w	$\bar{W}$	σ_w	$\bar{W}$	σ_w	$\bar{W}$	σ_w	$\bar{W}$	σ_w	$\bar{W}$	σ_w	$\bar{W}$	σ_w	$\bar{W}$	σ_w	$\bar{W}$	σ_w
Winter	0.683 (85)	0.060	0.805 (25)	0.054	1.037 (31)	0.200	1.126 (37)	0.141	0.711 (110)	0.061	1.085 (68)	0.167	1.010 (93)	0.152	0.854 (178)	0.134	1.134 (10)	0.253
Spring	0.889 (98)	0.080	0.953 (37)	0.128	1.086 (35)	0.167	1.133 (13)	0.188	0.906 (135)	0.093	1.090 (48)	0.169	1.035 (85)	0.155	0.957 (183)	0.120	0.199 (1)	0.0
Summer	1.735 (54)	0.469	2.475 (42)	0.673	2.797 (36)	0.483	2.989 (50)	0.487	2.059 (95)	0.688	2.908 (86)	0.489	2.766 (128)	0.586	2.460 (182)	0.772	3.332 (10)	0.214
Fall	1.301 (91)	0.265	1.733 (30)	0.453	1.916 (34)	0.798	1.858 (25)	1.007	1.408 (121)	0.343	1.892 (59)	0.871	1.838 (89)	0.729	1.556 (180)	0.564	3.472 (1)	0.0
Annual	1.089 (328)	0.325	1.577 (134)	0.831	1.735 (136)	0.937	2.018 (125)	1.151	1.231 (462)	0.519	1.871 (261)	1.056	1.771 (395)	0.997	1.462 (723)	0.806	2.242 (22)	1.474

( ) indicate sample size.

Table C-2

MEANS ($\bar{W}$) AND VARIANCES (σ_w) OF PRECIPITABLE WATER (IN CM) FOR STATION 23230 (SAN FRANCISCO)

Season	Cloud Cover (tenths)																	
	0 - 1		2 - 3		4 - 9		10		0 - 3		4 - 10		2 - 10		0 - 10		Rain	
	$\bar{W}$	σ_w	$\bar{W}$	σ_w	$\bar{W}$	σ_w	$\bar{W}$	σ_w	$\bar{W}$	σ_w	$\bar{W}$	σ_w	$\bar{W}$	σ_w	$\bar{W}$	σ_w	$\bar{W}$	σ_w
Winter	0.953 (54)	0.121	1.210 (37)	0.068	1.273 (42)	0.109	1.558 (47)	0.226	1.057 (91)	0.114	1.423 (89)	0.190	1.361 (126)	0.162	1.238 (180)	0.184	1.629 (19)	0.172
Spring	1.162 (31)	0.109	1.425 (61)	0.082	1.370 (40)	0.075	1.569 (51)	0.173	1.337 (92)	0.105	1.482 (91)	0.139	1.459 (152)	0.116	1.409 (183)	0.127	1.541 (16)	0.118
Summer	1.670 (24)	0.091	1.833 (88)	0.171	1.840 (41)	0.235	1.809 (29)	0.322	1.798 (112)	0.157	1.827 (70)	0.267	1.831 (158)	0.212	1.809 (182)	0.199	1.681 (9)	0.141
Fall	1.306 (45)	0.196	1.742 (63)	0.148	1.675 (37)	0.175	1.849 (35)	0.203	1.561 (108)	0.213	1.760 (72)	0.194	1.752 (125)	0.171	1.640 (180)	0.214	1.948 (13)	0.156
Annual	1.210 (154)	0.193	1.618 (249)	0.181	1.536 (160)	0.199	1.669 (162)	0.235	1.462 (403)	0.225	1.603 (322)	0.221	1.609 (571)	0.203	1.524 (725)	0.228	1.685 (57)	0.164

( ) indicate sample size

TABLE C-4

SEASONAL AND ANNUAL VALUES OF R_1 AND R_2

($R_1 = \overline{W}(0\text{-}1)/\overline{W}(0\text{-}10)$; $R_2 = \sigma_w(0\text{-}1)/\sigma_w(0\text{-}10)$)

Season	San Diego		San Francisco		Tucson	
	R_1	R_2	R_1	R_2	R_1	R_2
Winter	0.770	0.405	0.770	0.657	0.800	0.448
Spring	0.892	1.538	0.825	0.858	0.929	0.667
Summer	0.956	0.748	0.923	0.457	0.705	0.608
Fall	0.893	0.969	0.796	0.915	0.831	0.469
Annual	0.846	0.948	0.794	0.846	0.745	0.403

Summer) to a high of 0.929 (Tucson/Spring) with most of the values being between 0.8 and 0.9. The values of R_2, the ratio for the variance, show greater variability. It has a low value of 0.405 (San Diego/Winter) and an anomalously high value 1.53 (San Diego/Spring).

While it is not possible to draw definitive conclusions from results of the limited analysis presented here, it is nonetheless possible to tentatively conclude that:

1. Clear sky days have a mean value precipitable water which is less than that obtained for all days.
2. A "practical" factor to be used to adjust the 4-D mean precipitable water data to obtain the subset of statistics for only clear sky days is most probably between 0.8 and 0.9.
3. The variance of the mean precipitable water for cloudless days is (with minor exceptions) less than the variance for all days.
4. The variability of the variance is sufficiently large as to make it difficult to arrive at an estimated representative factor to use in adjusting the 4-D data. It suffices to say that the 4-D values can greatly overestimate the variance for clear sky cases.

It is perhaps significant to note that the findings in the present study regarding the means of precipitable water are supported by other investigations. Fritz (1949) suggested that the subset of annual mean of precipitable water at continental stations for clear sky days may be obtained from the set of annual means of the same parameter at the corresponding stations by multiplying each value by 0.85. Humphreys (1911), in an earlier study, arrived at a value for the factor of 0.89 using European Stations. These values are certainly in consonance with the findings of this study.

APPENDIX C
REFERENCES

Fritz, S., 1949: The Albedo of the Planet Earth and of Clouds, Journal of Meteorology, Vol.6, pp. 277-282.

Humphreys, W.J., 1911: Physics of the Air, Mc Graw Hill, New York.